SUOMEN GEODEETTISEN LAITOKSEN JULKAISUJA
VERÖFFENTLICHUNGEN DES FINNISCHEN GEODÄTISCHEN INSTITUTES
PUBLICATIONS OF THE FINNISH GEODETIC INSTITUTE

N:o 153

MOBILE LASER SCANNING – SYSTEM DEVELOPMENT, PERFORMANCE AND APPLICATIONS

by

Antero Kukko

SUOMEN GEODEETTISEN LAITOKSEN JULKAISUJA

VERÖFFENTLICHUNGEN DES FINNISCHEN GEODÄTISCHEN INSTITUTES

PUBLICATIONS OF THE FINNISH GEODETIC INSTITUTE

N:o 153

Mobile Laser Scanning – System development, performance and applications

by

Antero Kukko

Doctoral dissertation for the degree of Doctor of Science in Technology to be presented with due permission of the School of Engineering for public examination and debate in Auditorium M1 at the Aalto University School of Engineering (Espoo, Finland) on the 21st of December 2013 at 12 noon.

KIRKKONUMMI 2013

Supervising professor
Professor Henrik Haggrén, Aalto University School of Engineering, Department of Real Estate, Planning and Geoinformatics

Thesis advisors
Professor Juha Hyyppä, Finnish Geodetic Institute, Department of Remote Sensing and Photogrammetry
Docent, PhD Sanna Kaasalainen, Finnish Geodetic Institute, Department of Remote Sensing and Photogrammetry

Preliminary examiners
Professor Jon Mills, Newcastle University, Newcastle upon Tyne, UK

Professor Francois Goulette, MINES ParisTech, France

Opponent
Professor Jonathan Li, University of Waterloo, Waterloo, Ontario, Canada

ISBN (printed): 978-951-711-306-9
ISBN (pdf): 978-951-711-307-6
ISSN: 0085-6932

Juvenes Print –Suomen Yliopistopaino Oy, Tampere 2013

Aalto University
School of Engineering

ABSTRACT

Author
Antero Kukko

Title of the doctoral dissertation
Mobile Laser Scanning – System development, performance and applications

Unit Department of Real Estate, Planning and Geoinformatics

Publisher Finnish Geodetic Institute

Series Publications of the Finnish Geodetic Institute

Field of research Remote Sensing

Manuscript submitted 5 April 2013 **Date of the defence** 21 December 2013

Permission to publish granted (date) 5 November 2013 **Language** English

Article dissertation (summary + original articles)

Laser scanning is a surveying technique used for mapping topography, vegetation, urban areas and infrastructure, ice, and other targets of interest. Its application on a terrestrial mobile platform is a promising method for effectively collecting three-dimensional data for complex environments and for producing model information for location-based services necessitating rapidly collected and up-to-date data.

Development of mobile laser scanning (MLS) systems for such purposes is presented in this study. Different aspects of this technology were analyzed in laboratory experiments, simulations and field tests, in order to understand their effects on the ranging, intensity and point cloud data, especially in terms of point distribution and accuracy. In order to validate the performance of the developed ROAMER and AKHKA MLS systems, various three-dimensional mapping tasks were performed during an international benchmarking test, as well as in the field in numerous projects.

The results showed that the proposed systems can reliably provide accurate data. It has also been shown that the various modalities of the systems allow data acquisition in numerous application scenarios and environments not previously possible. MLS improves the data output compared to terrestrial laser scanning (TLS) and outperforms airborne laser scanning (ALS) in ranging precision and point density. As a result, MLS is well suited to fill the gap between these two previously dominant 3D data acquisition techniques.

Keywords laser scanning, lidar, mobile, mapping, multiplatform, 3D, accuracy, performance, test field, point cloud, GNSS/INS, MLS, TLS, ALS, topography, DEM, urban, geomorphology

ISBN (printed) 978-951-711-306-9 **ISBN (pdf)** 978-951-711-307-6

ISSN 0085-6932

Location of publisher Kirkkonummi **Location of printing** Tampere **Year** 2013

Pages 247 **urn** http://urn.fi/URN:ISBN: 978-951-711-307-6

Aalto-yliopisto
Insinööritieteiden
korkeakoulu

TIIVISTELMÄ

Tekijä
Antero Kukko

Väitöskirjan nimi
Liikkuva laserkeilaus – Järjestelmäkehitys, suorituskyky ja sovellukset

Yksikkö Maankäyttötieteiden laitos
Julkaisija Geodeettinen laitos
Sarja Suomen Geodeettisen laitoksen julkaisuja
Tutkimusala Kaukokartoitus
Käsikirjoituksen pvm 5.4.2013 **Väitöspäivä** 21.12.2013
Julkaisuluvan myöntämispäivä 5.11.2013 **Kieli** Englanti
Yhdistelmäväitöskirja (yhteenveto + artikkelit)

Laserkeilaus on mittaustekniikka, jota käytetään maaston topografian kasvillisuuden, rakennettujen alueiden, infrastruktuurin, jään ja muiden kohteiden kartoitukseen. Tekniikan soveltaminen liikkuvalle alustalle on lupaava menetelmä monimuotoisten ympäristöjen tehokkaaseen kolmiulotteiseen mittaamiseen ja mallinnustiedon tuottamiseen paikkatietopalveluihin, jotka edellyttävät tiedon nopeaa hankintaa ja ajantasaisuutta.

Tässä tutkimuksessa kehitettiin liikkuvia laserkeilausjärjestelmiä (MLS). Eri tekijöiden vaikutuksia etäisyys- ja intensiteettihavaintoihin, pistejakaumaan ja tarkkuuteen selvitettiin laboratoriokokein, simuloimalla ja koetöin. Tutkimuksessa kehitettyjen ROAMER ja AKHKA MLS-järjestelmien suorituskykyä kolmiulotteisen mittaustiedon tuottamiseen erilaisissa kartoitustehtävissä tutkittiin kansainvälisessä vertailututkimuksessa kaupunkitestikentän avulla, mutta lisäksi käytännön sovelluksissa useassa eri projektissa.

Tutkimuksen tulokset osoittavat, että kehitetyt MLS järjestelmät tuottavat tarkkaa tietoa luotettavasti. Järjestelmien monikäyttöisyys mahdollistaa aineistonhankinnan eri sovellustapauksissa ja ympäristöissä tavalla, joka ei ole aikaisemmin ollut mahdollista. Liikkuva laserkeilaus parantaa merkittävästi mittauksen tehokkuutta maalaserkeilaukseen verrattuna, ja ylittää lentolaserkeilauksen suorituskyvyn etäisyysmittauksen tarkkuudessa ja pistetiheydessä. Liikkuva laserkeilaus tarjoaakin näitä kahta aikaisemmin vallitsevaa 3D-mittausteknologiaa hyvin täydentävän kartoitusmenetelmän.

Avainsanat laserkeilaus,, lidar, liikkuva, kartoitus, monialusta, 3D, tarkkuus, suorituskyky, testikenttä, pistepilvi, GNSS/INS, MLS, TLS, ALS, topografia, DEM, rakennettu alue, geomorfologia

ISBN (painettu) 978-951-711-306-9 **ISBN (pdf)** 978-951-711-307-6
ISSN 0085-6932
Julkaisupaikka Kirkkonummi **Painopaikka** Tampere **Vuosi** 2013
Sivumäärä 247 **urn** http://urn.fi/URN:ISBN: 978-951-711-307-6

PREFACE

This thesis wraps up a large portion of work I have carried out at the Finnish Geodetic Institute (FGI) and Aalto University since 2005. The steps taken for the development and evaluation of MLS systems are summarized here. Beyond great advice for this thesis, Professor Juha Hyyppä, Head of the Remote Sensing and Photogrammetry Department (FGI), has provided excellent support for innovation and freedom of conduct. Without your efforts the work would have never been realized. Docent Dr. Sanna Kaasalainen has been advising the thesis and collaborated in the work conducted in the laser laboratory at FGI and in the field. You have been of great help in writing and organizing my thoughts. Professor Henrik Haggrén, Aalto University, provided supervision of the thesis in his gentle way, but I'm also grateful for his support at the early steps of my research career, sheltered in his laboratory at the then Helsinki University of Technology. It has always been encouraging to have discussions with all of you.

Professor Francois Goulette and Professor Jon Mills, the pre-examiners of the thesis, provided valuable criticism towards the manuscript and helped me to widen the view and sharpen the output. Their comments have certainly helped to improve the thesis.

I would like to thank Hannu Hyyppä from Aalto University and Helsinki Metropolia University of Applied Sciences for sharing his ideas and for his enthusiasm towards my work, but also for his invaluable personal support in many ways.

Harri Kaartinen has earned my sincerest gratitude for his endlessly genial fellowship and for sharing my ups and downs. He is also acknowledged for being able to filter out the noise created in my head and to turn them into practice, as well as for organizing the field campaigns with me.

Yuwei Chen has been of great help in system integration from the early stages in developing the synchronization system. Without you the endeavor would have been much more complicated, admitting that it was anyways very complicated. There's further stuff in the pipeline already. Veli-Matti Salminen from Aalto University was the wizard behind the mill and lathe, making my vision into solid metal. Without your effort the diversity in applications would have been much diminished. Also, co-operation with Reinhard Becker and Jürgen Gittinger from FARO Europe and Rolf Berlin from ATS Ab has been productive since the early stages of the system development. Octavian Andrei was the expert of GPS-IMU in the beginning, so thank you for the system testing. Dr. Petteri Alho from University of Turku has provided me a few nice places to visit during the past five years. There have been long and laborious days on many occasions, but they have also given much. Matti Vaaja from Aalto University has contributed in analyzing the data and performance in fluvial studies, and I hope this fruitful co-operation continues also in other fields of application.

There are many others who have contributed to the projects within the topic of this thesis, either in research or managing: Professor Ruizhi Chen, now Texas A&M University, Anttoni Jaakkola, Xinlian Liang, Anssi Krooks, Mika Karjalainen, Matti Lehtomäki, Lauri Markelin, Eetu Puttonen, Lingli Zhu, Pirjo Kivirasi and Matti Pirjetä from FGI; and Marika Ahlavuo and Dr. Iisakki Kosonen from Aalto University. Especially I wish to thank Marika for her help and encouragement, but also for organizing many pleasant events for innovation, and Anttoni for his help in later electronics and power related issues, as well as for lending his equipment for repairs and back-ups. Also, I wish to address my gratitude to Matti for his work on pole detection, Lingli for her dedication to building modeling, and Mr. Robert Guinness for his language revision and detailed suggestions for the manuscript.

The longer I write this, the more I find people who deserve to be mentioned. But I'm running out of space. The "old guard" at FGI has been solicitous towards me, and that is much appreciated: thank you Hannu, Mikko and Risto. Many colleagues have been of great help and comfort, sharing coffee, thoughts, news, jokes and time. Thank you all. I hope somehow to be able to return all the favors I've got from each and every one of you.

Mother, thank you for your caring love and cheering attitude. I wish to thank my brother Ilpo for enormous amounts of support and time for helping in 'the other project' conducted in the meantime of this thesis. I'm fortunate to have you! And the others thank you for your care. Keep on fighting!

My family has carried most of the load. Hanna, you have supported me truly and kept me on the move. There is no word to name your contribution to finishing this odyssey. Thank you for your enduring love. Kids, just keep on running and messing around—your existence is the joy of my life!

To my father who passed away 30 years ago.

Kirkkonummi, November 2013

Antero Kukko

ACKNOWLEDGEMENTS

The development and research presented in this thesis has been funded by:

- Academy of Finland, Centre of Excellence in Laser Scanning Research (CoE-LaSR, 272195).
- Academy of Finland, through projects “Transportation Data Acquisition by Means of ICT-derived 3D Modeling” (jointly with FGI and Aalto), “Improving the Forest Supply Chain by means of Advanced Laser Measurements” (FGI and Univ. Helsinki), “Economy And Technology Of A Global Peer Produced 3D Geographical Information System In Built Environment” (FGI and Aalto), “RivCHANGE” (Univ. Turku), “Science and Technology Towards Precision Forestry” (FGI and Univ.Helsinki), and “Intelligent roadside modeling” (Aalto).
- Finnish Funding Agency for Technology and Innovation, through projects “Development of Automatic, Detailed 3D Model Algorithms for Forests and Built Environment” (FGI), “Developing mapping and modeling approaches as a part of flood risk management business” (FGI, Aalto and Univ. Turku), “Intelligent built environment ÄRY” (FGI), and RYM-SHOK “Energizing Urban Ecosystems” (Aalto, FGI).
- Maj and Tor Nesling Foundation through FLOODAWARE project, and
- Aalto University through project MIDE 4D-Space and Aalto Energy Efficiency Research Programme – Light Energy.

The author also expresses his sincerest gratitude to the Henry Ford Foundation, Jenny and Antti Wihuri Foundation and Tekniikan edistämissäätiö for personal grants towards the research conducted in this thesis.

CONTENTS

ABSTRACT 3

TIIVISTELMÄ 5

PREFACE 7

ACKNOWLEDGEMENTS 9

CONTENTS 10

LIST OF PUBLICATIONS 12

AUTHOR'S CONTRIBUTION 13

LIST OF ABBREVIATIONS 15

1 INTRODUCTION 17

1.1 Background 17

1.2 Motivation 19

1.3 Hypothesis 20

1.4 Aim and objectives of the study 21

1.5 Restrictions to the scope of the thesis 21

1.6 Structure and contribution of the study 21

2 MOBILE LASER SCANNING 24

2.1 Principles 24

2.2 Laser sensor technology 27

2.3 Positioning for mobile laser scanning 33

2.4 MLS Simulation 42

2.5 Laser sensors for MLS 44

2.6 Integrated MLS systems 46

2.7 Summary 47

3 CONDUCT OF THE STUDY 48

3.1 Data and study sites 48
3.2 Methodology 50
3.3 Summary 62
4 RESULTS 63
4.1 Incidence angle effect experiment 63
4.2 Simulation performance 66
4.3 ROAMER 69
4.4 AKHKA 79
4.5 Applications 82
4.6 Summary 94
5 DISCUSSION 96
5.1 Implications of incidence angle effect on LS 96
5.2 Simulations for LS system analysis 97
5.3 Influence of sensor parameters on data characteristics 99
5.4 MLS sensor configuration effects 102
5.5 MLS data characteristics and usability 104
5.6 Future work 107
6 SUMMARY AND CONCLUSIONS 109
6.1 Incidence angle effects 109
6.2 Simulations 109
6.3 MLS systems and performance 110
6.4 Fluvial application remarks 111
6.5 Concluding remarks 112
REFERENCES 115

LIST OF PUBLICATIONS

The thesis is based on the following publications, referred to in the text by the following Roman numerals:

I Kukko, A.; Kaasalainen, S.; Litkey, P. Effect of incidence angle on laser scanner intensity and surface data. Applied Optics **2008**, 47, 7, 986–992.

II Kukko, A.; Hyyppä, J. Small-footprint laser scanning simulator for system validation, error assessment, and algorithm development. Photogrammetric Engineering and Remote Sensing **2009**, 75, 10, 1177–1189.

III Kukko, A.; Andrei, C.-O.; Salminen, V.-M.; Kaartinen, H.; Chen, Y.; Rönnholm, P.; Hyyppä, H.; Hyyppä, J.; Chen, R.; Haggrén, H.; Kosonen, I.; Čapek, K. Road environment mapping system of the Finnish Geodetic Institute – FGI ROAMER. International Archives of Photogrammetry, Remote Sensing and Spatial Information Sciences **2007**, 36, 3/W52, 241–247.

IV Kukko, A.; Kaartinen, H.; Hyyppä, J.; Chen, Y. Multiplatform Mobile Laser Scanning: Usability and Performance. Sensors **2012**, 12, 9, 11712–11733.

V Kaartinen, H.; Hyyppä, J.; Kukko, A.; Jaakkola, A.; Hyyppä, H. Benchmarking the Performance of Mobile Laser Scanning Systems Using a Permanent Test Field. Sensors **2012**, 12, 9, 12814–12835.

VI Alho, P.; Kukko, A.; Hyyppä, H.; Kaartinen, H.; Hyyppä, J.; Jaakkola, A. Application of boat-based laser scanning for river survey. Earth surface processes and landforms **2009**, 34, 1831–1838.

VII Vaaja, M.; Hyyppä, J.; Kukko, A.; Kaartinen, H.; Hyyppä, H.; Alho, P. Mapping Topography Changes and Elevation Accuracies Using a Mobile Laser Scanner. Remote Sensing **2011**, 3, 3, 587–600.

All of the above publications are peer-reviewed journal articles, except publication **III**, which is a peer-reviewed conference article. The original publications have been reprinted with the kind permission of Optical Society of America (**I**), American Society for Photogrammetry and Remote Sensing (**II**), and John Wiley & Sons (**VI**).

Additional papers by the author related to the thesis topic are: Kukko et al., 2013; Kasvi et al., 2012; Lehtomäki et al., 2010; Kaasalainen et al., 2011a; Alho et al., 2011; Holopainen et al., 2011; Holopainen et al., 2013; Jaakkola et al., 2008. They are cited where appropriate within the thesis.

AUTHOR'S CONTRIBUTION

In publication **I**, Kukko was responsible for the experiment design, measurements, data analysis and writing. He also developed some laboratory tools to allow the incidence angle measurements. Dr. S. Kaasalainen took part in the laboratory measurements, data analysis, and writing the paper. P. Litkey assisted in the ALS data analysis.

In publication **II** Kukko defined the laser scanning simulator, implemented it programmatically, developed the artificial forest model, performed the simulations of ALS and MLS scenarios, and performed the data analysis. Kukko wrote the paper, and Prof. J. Hyyppä acted as a supervisor in the study.

In publication **III** Kukko was responsible for the design of the ROAMER platform and acted as an instructor for V.-M. Salminen, who made the technical adaptation and manufacturing of the integration platform. Kukko was responsible for the integration of the sensor systems, specifications, testing and development of the georeferencing solutions for the point data, and he compiled the publication. Mr. H. Kaartinen contributed in the sub-system specifications and sensor selection and assisted in data acquisition. Dr. Y. Chen did the board design and manufacturing of the synchronization electronics, and Dr. O. Andrei took care of the GPS-IMU testing. Dr. I. Kosonen acted as a co-writer and advisor for the project. Dr. H. Hyyppä and Mr. K. Čapek gave valuable advice about the user needs. Prof. J. Hyyppä supervised the development, whereas Prof. H. Haggrén, Prof. R. Chen, and Dr. P. Rönnholm acted as advisors and partners in the project.

In publication **IV** Kukko conducted the AKHKA system design and integration together with H. Kaartinen and designed accuracy assessment. Field data acquisition was undertaken with the help of H. Kaartinen, who also computed the trajectory data; Kukko performed the data calibration, georeferencing and preprocessing of the data in all the studies reported. Kukko wrote the paper, which combines results from various studies. Prof. J. Hyyppä supervised the studies, and Dr. Y. Chen assisted with the electronics.

In publication **V**, Kukko took part in selecting the test field location for mobile laser scanning, scan station design and collecting the reference data together with H. Kaartinen and A. Jaakkola. Kukko also operated the ROAMER system in Stop-and-Go measurements, as well as in the MLS data acquisition. H. Kaartinen was responsible for the quality control of the Stop-and-Go data and performed the trajectory computations. Prof. J. Hyyppä and Dr. H. Hyyppä were the advisors in the study and participated in the planning of the project. Kukko did ROAMER MLS data calibration and

georeferencing. Kukko also participated in the analysis of the results together with H. Kaartinen, Prof. J. Hyyppä and A. Jaakkola, and he was also a co-writer of the paper.

In publication **VI**, Kukko took part in the field campaign planning and implementation and was responsible for the system adaptation to the boat platform. Kukko also operated the ROAMER system during the MLS data acquisition and carried out the data MLS data calibration and georeferencing. He also participated in the analysis of the results together with Dr. P. Alho, Prof. J. Hyyppä and Mr. H. Kaartinen, who were co-writing the paper. Kaartinen also computed the trajectories for the study. Dr. P. Alho acted as the chief officer and navigator of the survey boat. Dr. H. Hyyppä provided his experience as an advisor in the study, and A. Jaakkola assisted in the data analysis.

In publication **VII**, Kukko took part in the field campaign planning and implementation and operated the ROAMER system during the MLS data acquisitions. He also performed out the MLS data calibration, georeferencing, pre-processing, and participated in the analysis of the results together with M.T. Vaaja, Prof. J. Hyyppä and H. Kaartinen. Kaartinen contributed also in trajectory computations and data acquisition. In addition, Kukko took part in the writing of the paper. Dr. H. Hyyppä acted as an advisor in the study. Dr. P. Alho again navigated the survey boat through the shallow waters and brought his fluvial expertise and knowledge of user demands and overall advice to the project.

LIST OF ABBREVIATIONS

2D	two-dimensional
3D	three-dimensional
ALS	Airborne Laser Scanner/Scanning
ATV	All-Terrain Vehicle
AVLN	Automatic Vehicle Location and Navigation
BoMMS	Boat Mobile Mapping System
CoM	Center of Mass
DEM	Digital elevation Model
DIA	Direct Inertial Aiding
DGPS	Differential GPS
DMI	Distance Measurement Indicator
DTG	Dry Tuned Gyro
DTM	Digital Terrain Model
ECI	Earth Centered Inertial
ECEF	Earth Centered Earth Fixed
EPS	Electronic Stabilization Program
FGI	Finnish Geodetic Institute
FOG	Fiber Optic Gyro
FOV	Field of view
GAMS	GPS Azimuth Measurement System
GPRS	General Packet Radio Service
GPS	Global Positioning System
GNSS	Global Navigation Satellite System
HSToF	High Speed Time of Flight

IMU	Inertial Measurement Unit
INS	Inertial Navigation System
ITS	Intelligent Transportation Systems
Laser	Light amplification by stimulated emission of radiation
LiDAR	Light Detection and Ranging
LS	Laser Scanner, Laser Scanning
LSToF	Low Speed Time of Flight
MEMS	Micro Electro Mechanical System
MLS	Mobile Laser Scanning/Scanner
MMS	Mobile Mapping System
PAC	Pulsed Aperture Correlator
PS	Phase Shift
RLG	Ring Laser Gyro
ROAMER	Road Environment Mapper
RTK	Real-Time Kinematic
SPAN	Synchronized Position Attitude Navigation
TLS	Terrestrial Laser Scanner/Scanning
TRF	Terrestrial Reference Frame
ToF	Time of Flight
UHSPS	Ultra High Speed Phase Shift
VRS	Virtual Reference Station
WGS 84	World Geodetic System 1984

1 INTRODUCTION

1.1 Background

Laser scanning (LS) is a surveying technique used for mapping topography, vegetation, urban areas, ice, infrastructure, and other targets of interest (Garvin et al., 1996; Kraus and Pfeifer, 1998; Haala, Brenner and Anders, 1998; Maas and Vosselman, 1999; Naesset, 1997; Hyyppä et al., 2001). More precisely, ALS is a method based on Light Detection and Ranging (LiDAR) measurements from an aircraft, where the precise location and orientation of the sensor and the direction of the transmitted LiDAR beam is observed, and therefore the 3D coordinates of the objects reflecting the laser beam can be determined (Wehr and Lohr, 1999). In addition to ALS, there is burgeoning activity in Terrestrial Laser Scanning (TLS), where the laser scanner is mounted on a tripod (Aschoff, Thies and Spiecker, 2004; Henning and Radtke, 2006; Liang and Hyyppä, 2013) or on a kinematic (i.e., moving while mapping) platform for conducting Mobile Laser Scanning (MLS), e.g. for civil engineering (Talaya et al., 2004; Kremer and Hunter, 2007; Gräfe, 2007ab; Jochem, Höfle and Rutzinger, 2011; Ibrahim and Lichti, 2012; **III**; **IV**; **V**) and for the field of autonomous vehicle guidance systems (e.g., Montemerlo et al., 2006; Brenner, 2009). LS is sometimes referred to as LiDAR because of its central role in the data generation.

The emergence of LS is rooted in the history of LiDAR technology. In 1975, NASA and other organizations developed an airborne oceanographic LiDAR system for measuring chlorophyll concentration and other biological and chemical substances. Non-scanning (profiling) LiDAR was used for bathymetry, forestry and other applications in the 1970s and 1980s (e.g., Solodukhin 1978; Nelson et al. 1984; Schreier et al. 1985), which established the basic principles of using lasers for remote sensing purposes. LS has benefited from the development of Global Navigation Satellite Systems (GNSS) and inertial sensors for precise positioning and orientation measurements, of which King (1998) gives an overview. The first experiments with modern LS instruments were conducted in the early 1990s, and in 1993 the first prototype of a commercial ALS dedicated to topographic mapping was introduced. For the development of ALS and LS, thorough background can be found in Bufton (1989), Lohr and Eibert (1995), Flood and Gutelius (1997), and Hyyppä et al. (2008).

A typical LS system consists of (1) a laser ranging unit (i.e., LiDAR) (2) an opto-mechanical scanner, (3) a position and orientation unit, and (4) a control, processing, and storage unit (Wehr and Lohr, 1999). The laser ranging unit can be subdivided into a transmitter, a receiver, and the optics for both. The basic principle of LiDAR is to use a laser (light amplification by stimulated emission of radiation) to illuminate an object and then a photodiode to register the backscatter radiation (Schawlow and

Townes, 1958). The range is then determined by signal processing, making use of the fact that the speed of light is constant. The receiver optics collects the backscattered light and focuses it onto a photodiode detector, which converts the incident power of photons to electrical pulses (Wehr and Lohr, 1999). The opto-mechanical scanning unit controls the deflection of the transmitted laser beams towards the target. The design of the deflection unit defines the scan pattern on the ground. The position of the laser ranging unit is determined using observations from Differential Global Navigation Satellite System (DGNSS). The orientation of the scanning unit is determined by the pitch, roll, and heading angles around the three axis of the navigation frame, and are measured by an onboard inertial measurement unit (IMU) (Baltsavias, 1999). The output of the laser scanner is then a georeferenced three-dimensional point cloud of LiDAR measurements, representing the target geometry, complemented with intensity and possibly waveform information of the returned light (Wehr and Lohr, 1999; Hyyppä et al., 2008).

Laser scanning has revolutionized the surveying industry in producing topographic information over the past two decades, proving it to be a valuable method. Its use has contributed to microscale (0.1–5 m) and fine toposcale (5–50 m) mapping of the Earth from satellite and airborne platforms (Garvin et al., 1996; Kraus and Pfeifer, 1998; Haala et al., 1998; Maas and Vosselman, 1999; Naesset, 1997; Hyyppä et al., 2001; Matikainen, Hyyppä and Hyyppä, 2003). Since then the laser scanning technology has been used to produce ever more detailed mapping and modeling of terrestrial systems (Kaartinen and Hyyppä, 2006; Jaakkola et al., 2008; Connor et al., 2009; Heritage and Milan, 2009; Alho et al., 2011; Lehtomäki et al., 2011; Rutzinger et al., 2011b; Zhu et al., 2011; Hyyppä et al., 2012; Kukko et al., 2013; Liang et Hyyppä, 2013) More recent study utilizing the MLS technology in deriving surface roughness parameters for hydraulic modeling is presented in Wang et al., (2013), Vaaja et al., (2013) further extends the performance investigations presented in this thesis of MLS in mapping of fluvial environments, and Saarinen et al., 2013) investigated the vegetation classification from MLS data. Also, a good review and international performance analysis of automated methods for ALS and MLS processing is published by Kaartinen (2013).

Operative ALS data typically provides point densities of 0.5−10 pts/m^2 and beam footprint sizes of a few decimeters and larger (typically 0.3–10 mrad). Using this technique, ground topography and building roofs can be captured, but building façade information is usually not obtained. In contrast to ALS, stationary TLS sensors have a narrow beam width, wide field of view (FOV) and more precise ranging. The most prominent advantage of TLS is its high point density, which can be as high as tens of thousands of points per square meter. This allows detailed 3D modeling of objects and scenes from a terrestrial perspective (Grün and Zhang, 2003; Aschoff, Thies and Spiecker, 2004; Henning and Radtke, 2006; Brenner and Ripperda, 2006; Liang and Hyyppä, 2013). A complication compared to

ALS are the even more massive volumes data and a clear disadvantage the need for a high number of stations to cover the whole scene, due to the relatively short ranges and limited visibility, as well as need for redundant data for successful registration (Zhao and Shibasaki 2003b). This limits the effective data coverage achievable with TLS (**VI**).

MLS provides a means to overcome the shortcomings of both ALS and TLS. To improve the level of detail captured by ALS, MLS is expected to produce similar data cloud point densities as TLS. With onboard positioning sensors MLS provides a huge improvement in effective spatial coverage and distribution of data compared to a TLS survey (Zhao and Shibasaki, 2003b; **IV**; **VI**). In certain conditions, MLS data coverage may approach even the spatial extent provided by ALS but with less mobilization expense. Furthermore, data from objects not visible to ALS can be captured from the ground with MLS. These facts make MLS especially attractive for projects comprising relatively small or limited areas and specific tasks with requirements for high-resolution surface data. In addition, the sensor layout of an MLS system and other surveying arrangements can be adjusted more freely to meet application specific requirements in comparison to tightly regulated airborne platforms (Barber and Mills, 2006; **IV**). A short review of commercial MLS systems was carried out by Puente et al., (2011), where operational layout approaches can be found.

However, the limitations in mobility of vehicle-mounted systems hampers the operability of MLS in rugged or soft terrain and narrow spaces and particularly indoors. For these environments, more sophisticated and lighter platform arrangements are needed, and therefore research and development of a personal backpack MLS has been conducted in **IV** and complemented in this thesis. Also, in areas where the sky view is limited the positioning performance of MLS is challenged on a regular basis, due to poor satellite visibility. This necessitates methodology for control and data processes, but also improvement to the navigation solutions used.

1.2 Motivation

The primary institutional motivation for the development of MLS instruments and methodology was proactive promotion of this particular technology, including data processing methods and applications, to industry, the scientific community and society. Addressing the problems and benefits of the technology will increase the public knowledge of operative mapping agencies and companies, in order to ease the adoption such technologies. Independent system development will provide a research platform for studying data capture effects on the data quality and coverage, and it will also ease development of automated data processing methods. Once the data has been collected, the real added value hides in extraction and refinement of information into useful forms. Moreover, applicability and

feasibility of the particular technology was seen to be demonstrated effectively and completely only by making modality of the systems possible.

Variability in the scanning geometry in MLS applications is more prominent compared to that of ALS. This is the single most significant factor affecting the backscattered light in ultra-small-footprint laser systems. It is further increased by the abruptly moving platform in mobile mapping and thus by rapidly changing measurement geometry. This raises a question of the laser back-scattering effects on the MLS intensity data, especially in applications where the intensity data is to be exploited for object classification. For such approaches, research effort was necessary to find out the effect of incidence angle on laser attenuation for various targets. This will help in the development of intensity calibration procedures not only for MLS, but also for ALS and TLS data, and thus improve the output of laser scanning based data products.

Moreover, issue related to ALS and MLS scanning geometries and echo waveform detection were of great interest, but the data are expensive to acquire, and modality is often limited. In order to analyze the scanning geometry effects on object recognition under controlled conditions, a simulation approach was desired. In conjunction with physical modeling of various scanners, the scattering was to be modeled utilizing the knowledge and data from the incidence angle studies. Simulations were sought to generate ALS and MLS data for sensor layout analysis without needing to have such systems physically.

The need for rapid and cost-effective surveying technologies is ever increasing; better quality and coverage is demanded for managing more and more complex urbanization, transportation and energy distribution systems, as well as natural resources and reserves, in order to use and protect them in sustainable ways. This requires the production of more detailed data faster than ever before. Thus, advanced data acquisition systems and processes are needed, as well as the ability to perform monitoring with reliable detection of critical changes.

1.3 Hypothesis

The hypothesis in this study was that, by applying tactical grade GPS-IMU and an ultra-high-speed phase-shift laser scanner, a high-end mobile laser scanning system can be developed and used for proactive promotion of this particular technology, including data processing methods and applications, to scientific community, industry and society. Appropriate calibration methods and data processing chain could provide accurate and high-resolution three-dimensional data for mapping and modeling applications in different fields of urban, industrial and road environment development, transportation

planning, civil engineering, precision forestry and agriculture, as well as for modeling of geophysical entities and environmental research.

1.4 Aim and objectives of the study

The aim of the study was to develop novel mobile laser scanning systems, analyze their performance and develop new applications.

Objectives of the study were as follows:

1. To develop an experimental setup for measuring the incidence angle effect
2. To develop a laser scanning simulator for system development and analysis
3. To conduct
    - Design and development of integration platforms
    - Sensor integration and testing
    - Development of practical solutions for data georeferencing and quality analysis
    - Development and testing of calibration of the systems
    - Testing of the systems in application scenarios
4. To test the geometric quality of the data acquired with the built MLS systems
    - Determine the performance level of the developed systems
    - Study the data characteristics

1.5 Restrictions to the scope of the thesis

As laser scanning is a versatile technology it is widespread into use in different fields and disciplines. This means that laser scanners are used e.g., in the fields of robotics and autonomous vehicles for motion tracking, localization and mapping. The approach to and requisites for accuracy for mapping of scenes in robotics of is however completely opposite to the scope of and approach taken in this thesis, that deeper literature review and system analysis was confined out.

1.6 Structure and contribution of the study

The thesis consists of a summary and seven original peer-reviewed publications. Following this introductory section, Section 2 presents the literature review describing previous research on topics related to the laser scanning, positioning and MLS development. Materials produced, their purpose of use, and methods used in the study for data analysis are presented in Section 3. Section 4 summarizes the results achieved. Based on the results, the applicability and usability of the developed systems for practical mobile mapping is reflected upon, and the needs and ideas for further research and

development of the systems and data processes are discussed in section 5. Section 6 summarizes and concludes the study.

Considering the objectives of the study, the contribution of the original publications can be summarized as follows:

Paper **I** presents a comprehensive experimental set of data on the dependence of the backscattered laser intensity on the angle of incidence to the target surface. To the authors' knowledge this was the first comprehensive study on these effects in the context of scanning LiDAR.

In publication **II** a simulation approach and methods of small-footprint LiDAR processing were presented and discussed, validated for tree height estimation, and demonstrated for scanning geometry effects analysis for ALS and mobile laser scanning. The simulation method implemented combines for the first time both spatial and radiometric components of a LiDAR observation to produce realistic waveform and point cloud data for system performance analysis, as well as for algorithm development for LiDAR data processing and mapping purposes. As the existing related empirical data were insufficient for effective research and exploitation in mapping applications, the simulated waveform data were needed.

Paper **III** introduced the FGI ROAMER system. The vehicle-borne ROAMER system consists of an integration platform, GPS-IMU positioning and navigation systems, and a wide field-of-view high-speed 3D data acquisition system, having probably the fastest point repetition frequency (PRF) and the widest single scanner field of view in any MLS at the time of its inception.

Paper **IV** summarizes development of multi-platform MLS solutions operated in studies for mapping of different environments. Moreover, a novel backpack version of the MLS equipment was introduced for the first time for surveying applications, where the requirements include precision and mobility in variable rugged terrain conditions.

Paper **V** presents a complete test for studying the performance of various state-of-the-art mobile laser scanning systems on an urban test field established particularly for such purposes. The test was connected to the European Spatial Data Research (EuroSDR) project: "Mobile Mapping-Road Environment Mapping Using Mobile Laser Scanning".

Paper **VI** was the first to introduce a boat-based mobile mapping system (BoMMS) with a laser scanner to allow the derivation of detailed microscale riverine topographical data for applications in fluvial geomorphology.

Paper **VII** demonstrated the change detection possibilities of mobile laser scanning for riverine topography that had previously been lacking. The paper demonstrated the capability of MLS in erosion change mapping on a test site located in the sub-arctic.

2 MOBILE LASER SCANNING

In this chapter different technologies applied to mobile laser scanning are introduced. The general principles and historical background of the MLS is discussed, and techniques and issues related to the scanning Lidar are addressed. Mathematical and physical formulation for direct georeferencing and technologies applied for the determination of MLS trajectory are introduced, and also an overview on the current state-of-practice in commercial MLS operations is given. Research using simulations prior the work presented in **II** is also summarized.

2.1 Principles

Increasing interest has been shown in vehicle-based (mobile) surveying applications of laser scanning since the beginning of the last decade when laser scanners began to be incorporated in mobile mapping systems (MMS) (Talaya et al., 2004; El-Sheimy, 2005). A modern MMS is a ground-operated multi-sensor mapping system that integrates various navigation and data acquisition sensors on a rigid, moving platform for remotely determining the location, dimensions and other characterizing information of the surrounding objects. The key benefits of MMS are (Ellum and El-Sheimy, 2002):

1. Reduced time and cost of field surveys
2. Both spatial and attribute information can be determined from the data
3. Data can be archived and revisited – permitting additional data collection without additional field campaigns.

In general terms a mobile mapping system can be described as a kinematic surveying system utilizing motion tracking and time synchronized data acquisition, regardless of the platform in use. The navigation system typically includes a GNSS receiver(s) with appropriate antenna(s) for positioning and an IMU for platform and sensor attitude determination and high-frequency positioning (Talaya et al., 2004; Hunter, Cox and Kremer, 2006; **III**). GNSS-IMU navigation is often supported with a distance measurement wheel or odometer (often referred as Distance Measurement Indicator (DMI) or Direct Inertial Aiding (DIA)) for constraining the gyro drift, especially during obscured satellite visibility. Other possible data acquisition sensors include digital and video cameras, multi-spectral linear scanners, imaging laser, thermal cameras, ground radars, luminance cameras and ultra-sonic sensors, depending on the media and desired information to be extracted.

Mobile laser scanning, being a sub-category of MMS, is a rapid and flexible method for acquiring three-dimensional topographic data. An MLS system is based on LiDAR sensors, which produce three-dimensional point clouds from the surrounding objects using profiling scanning. However, new types of

scanners are emerging that could provide also simultaneous along-track FOV. In general, the spatial coverage of data in MLS is achieved by the movement of the vehicle and motion-tracking positioning devices, as illustrated in Figure 1. The survey is conducted as the ground vehicle moves around, while the navigation system tracks the vehicle's trajectory and sensor attitude, used to produce a 3D point cloud from the range data collected by the onboard scanners.

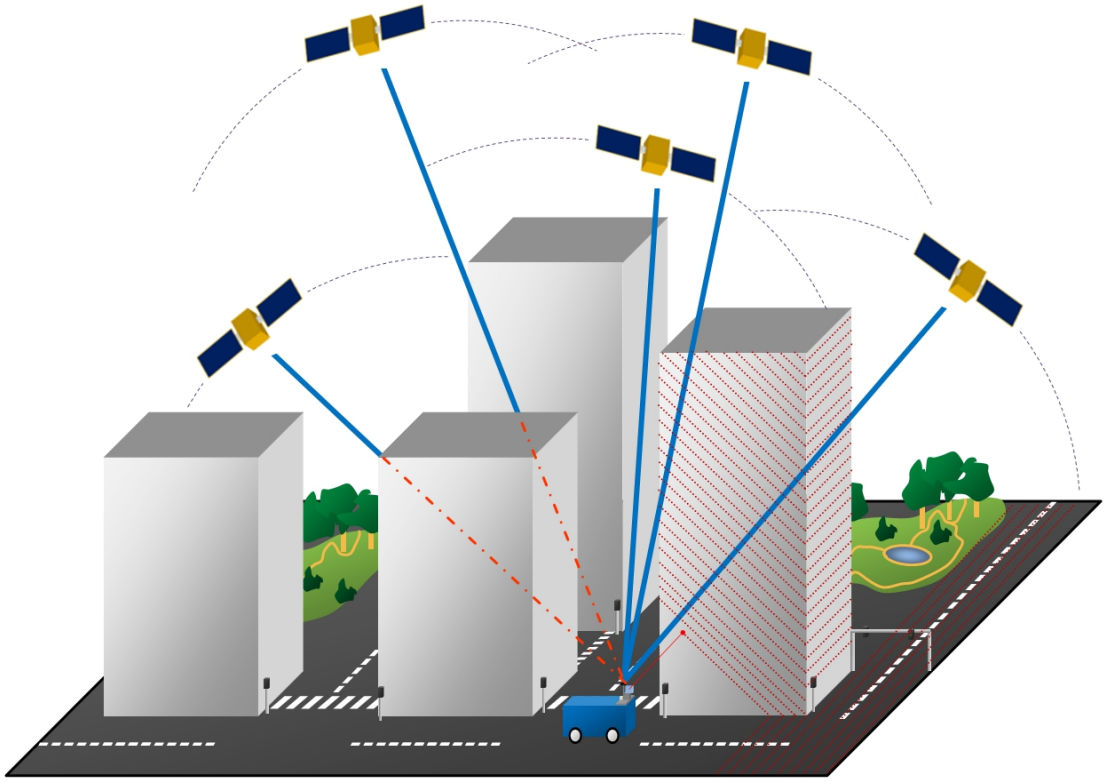

Figure 1. Mobile laser scanning utilizes GNSS-IMU positioning for direct geo-referencing of laser scanning data for three-dimensional mapping of objects (**IV**).

Mobile mapping is expected to provide ease of mobilization and lower costs when compared to ALS. These points are especially attractive for projects involving small areas and specific tasks. In addition, the sensor layout of an MMS and other surveying arrangement can be adjusted more freely in comparison to strictly regulated airborne platforms, in order to meet task-specific requirements. Furthermore, stationary data collection has some weaknesses: poor efficiency in data acquisition and difficulty of planning for viewpoints and directions in data acquisition when measuring large and complicated scenes (Zhao and Shibasaki, 2003a). One issue that is still being tackled is the complexity of a registration method capable of succeeding in automated registering of multi-modal range data from various sources, as shown by Biber, Fleck and Strasser (2004), Mitra et al. (2004) and Hansen (2006).

MMS and related technologies are a suitable method to collect data for road and urban mapping, planning and maintenance. Papers in the MMS field describing systems for different mobile mapping tasks prior and simultaneously to the ROAMER development include Karimi, Khattak and Hummer (2000), Habib, Morgan and Lee (2001), Tao (2001), Tao, Chapman and Chaplin (2001), Manandhar and Shibasaki (2001, 2002, 2003), Grejner-Brzezinska and Toth (2003), Zhang and Xiao (2003), Zhao and Shibasaki (2003a, 2003b, 2005) Clarke (2004), Talaya et al. (2004), Reulke and Wehr (2004), El-Sheimy (2005), Joo, Hwang and Choi (2005), and Hunter, Cox and Kremer (2006). Goulette et al. (2006) have proposed a system and method for automatically extracting the road surface, trees and vertical surfaces from the mobile laser data. Amoureus et al. (2007) have developed a method to integrate lidar and terrestrial mobile mapping technology for the creation of a comprehensive road cadaster using mobile mapping system.

More recent development is presented by Vock and Jungmichel (2011) for developing a low budget experimental MLS utilizing UHSPS (Z+F Imager 5006) scanner, but more interestingly replacing the usually utilized GPS-IMU with the electronic stabilization program (EPS) system of the vehicle. The sensor placement was similar than that used by Siteco in Road Scanner back in 2008 (Kukko, 2009). Puente et al., (2011) have carried out a short review of commercial MLS systems. More comprehensive overview of the commercial state-of-practice sensors suitable for mobile operations and integrated MLS systems is presented in Sections 2.5 and 2.6. The presentation there is limited to sensors providing ranging longer than 100 meters and FOV larger than 270 degrees.

Most of the mapping applications in various fields stand to benefit from the accuracy and efficiency of MLS technology. Compared to traditional mapping methods, which utilize digital aerial images and ALS, the precision of the data collected can be greatly improved. Furthermore, the time and cost of geodetic measurements with TotalStations and stationary terrestrial lasers can be reduced. Beyond that, numerous advantages arise when using MLS data to produce high-resolution 3D models. This is demonstrated by the application examples presented in Sections 4.5, and 5. Considering data acquisition, compared to stationary terrestrial laser scanning, MLS provides high efficiency and a precise way for generating dense point clouds. Furthermore, its mobility characteristics make it more suitable for surveying and modeling of large areas. 3D models processed from the data collected by MLS offer high-resolution visualization and surface analysis (see e.g., applications in Section 4.5), which cannot be achieved from ALS and/or aerial images, since they provide coarser renditions with considerably lower point density and precision.

For an MMS data to be qualified for surveying tasks, and further be useful for automated processing it is required that visible (i.e., visible to the sensor, e.g., sonar) objects be measured with surveying accuracy (typical requirement for large scale base mapping accuracy of 5-25 cm for buildings) at

normal road speeds (improves safety and efficiency), and desired objects should be collected at distances of several tens of meters from the sensor with precision of a couple of centimeters. Point density should be greater than 400 points per square meter (5 cm point spacing at right angled surface at 50 m, or 1 mrad angular resolution) to allow high level of detail in automated object reconstruction. When ROAMER development began, there were two benchmarking state-of-the-art MLS systems: GEOMOBIL (Talaya et al., 2004) and GeoMaster (Manandhar and Shibasaki, 2001). GEOMOBIL was a single scanner unit with narrow FOV covering only one side of the road at a time. GeoMaster provided wide FOV data from three scanners for low speed mapping at 20 Hz scan frequency.

High-resolution laser scanning in combination with the advancements and decrease in price of GNSS-IMU technology has revolutionized the field of mobile mapping in a dramatic way. After the commissioning of ROAMER, multiple LiDAR-based commercial MLS systems were introduced to the market, e.g., Optech Lynx derivatives, Mitsubishi MMS-X series, StreetMapper and Riegl VMX variants and Road-Scanner3, as well as numerous research platforms. Rapid development in data acquisition sensors (e.g., Riegl VQ-250, Velodyne HDL-64E, Faro Focus3D X330, Optech Lynx, Z+F Profiler 9012 and Dynascan S250) is expected to provide further improvement in automatic object detection and reconstruction with high levels of detail. Laser-based mobile mapping systems have ushered in a new era in kinematic mapping applications in terms of applicability, data rates, level of measured detail and accuracy of the obtained data.

2.2 Laser sensor technology

2.2.1 Laser beam deflection and beam propagation

A laser scanner is a device that measures its surroundings using LiDAR for range measurement and precisely determined beam deflection, deriving 3D points representing the surfaces of objects in the environment. Mainly two techniques are used for range measurement in current laser scanning systems: time-of-flight (ToF) and phase shift (PS) methods. ToF ranging utilizes precise timing for determining the range from the pulse time of flight and speed of light. Phase shift ranging instead makes use of continuous laser illumination and amplitude modulation of the beam to discern the range at high frequency.

Figure 2 illustrates the principle of a time of flight LiDAR observation; a laser pulse is transmitted towards the object and attenuates and spreads due to range and beam divergence. Thus, the beam foot-print size on the ground differs from that emitted from the scanner optics initially. Objects within the foot-print may have flat characteristics, resulting in a short pulse return back to the scanner, but more

often echoes may change its shape. This is due to inhomogeneity that may occur within the foot-print as a result of vegetation, ground slope and break lines, building edges, etc.

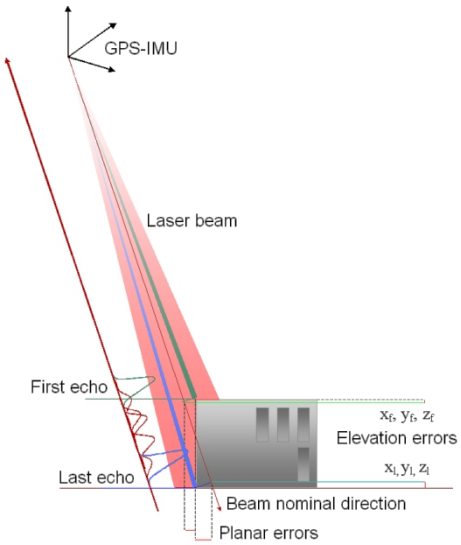

Figure 2. Principle of LiDAR observation. Beam divergence causes the spread of a beam over the footprint area, from which multiple echoes are collected. The nominal beam direction determines the final 3D position for the detected point (x_f, y_f, z_f and x_l, y_l, z_l). Multiple reflections from the object are schematically illustrated along the center line of the shifted beam. (A. Kukko, **II**)

Different techniques to beam deflection are illustrated in Figure 3, where the resulting scanning planes are indicated by the light red color. The extent of the beam field of view (FOV), which ranges from narrow angles to full 360 degrees, is defined by the particular deflection type in use (Wehr and Lohr, 1999). The main deflection techniques (and achieved scan FOV) are: oscillating (<90°, zig-zag), rotating polygon (<90°, line), rotating slant mirror (360°, line), and fiber optic line scan (<10°, line). A variation of the slant mirror technique is Palmer scanning, where a nutating mirror deflects the beam to form an elliptical pattern on the ground (Wehr and Lohr, 1999). In addition to these there are sensors, mainly terrestrial, utilizing fixed opening FOV producing multiple parallel profiles per scan (e.g., Velodyne HDL-64E and Ibeo LUX), or two axis scanners (Neptec Opal-360), which could provide up to 60° along-track FOV.

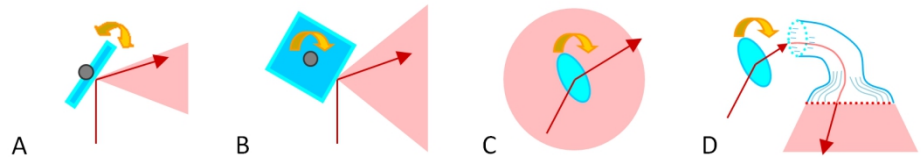

Figure 3. LiDAR beam deflectors; A: Oscillating, B: Polygon, C: Rotating, and D: Fiber optics.

Traditionally scanning LiDAR has been divided into two different classes: large- and small-footprint systems. Terrestrial scanning, however, utilizes beam sizes of 2–100 mm, which might be called very-small-footprint or terrestrial-footprint. Large-footprint systems typically have beam sizes between five and 25 m and full-waveform recording capability. Experimental studies using large-footprint systems include Anderson et al. (2006), Blair, Rabine, and Hofton (1999), Brenner et al. (2000), Carabajal and Harding (2001), Harding et al. (2001), Hyde et al. (2005), and Lefsky et al. (1999).

Widely used for DTM generation, city modeling, and forest inventory, small-footprint ALS systems use footprints of less than 1 m. Such systems mainly record the backscatter as discrete points (x, y, z, and intensity) for multiple echoes of the pulse, although more recently scanners to record the full waveform have emerged (Wagner et al., 2006; Mallet and Bretar, 2009).

Airborne LiDAR systems have been widely adopted for mapping purposes in the last fifteen years. Laser scanning is used in digital elevation model (DEM) production (e.g., Kraus and Pfeifer, 1998; Huising and Gomes-Pereira, 1998; Gomes-Pereira and Janssen, 1999; Petzold, Reiss and Stossel, 1999; Axelsson, 2000; Artuso, Bovet and Streilein, 2003; Reutebuch et al., 2003). Studies on building extraction using ALS data are reported e.g., by Haala et al., 1998; Maas and Vosselman, 1999; Vosselman and Dijkman, 2001; Vosselman and Süveg, 2001; Vosselman, 2002; Brenner, 2003; Brenner, 2005; Maas, 2001; Rottensteiner, 2003; Rottensteiner, Trinder and Clode, 2005; Kaartinen and Hyyppä, 2006; Dorninger and Pfeifer, 2008. Use of ALS for forest management has been dominantly a Scandinavian effort (e.g., Naesset, 1997; Hyyppä et al., 2001; Naesset, 2002; Persson, Holmgren and Söderman, 2002; Yu et al., 2004; Yu et al., 2006; Hollaus et al., 2007; Kaartinen and Hyyppä, 2008; Hyyppä et al., 2012). Matikainen, Hyyppä and Hyyppä (2003) have carried out studies on the development of automated map updating based on laser scanning data. In the references cited above, the algorithm development was focused on data obtained from small-footprint commercial LiDAR. In addition to airborne systems, there is also a burgeoning market for terrestrial scanners, and especially for mobile laser scanners mounted on vehicle platforms that provide 3D data on the road environment and in built-up areas (Talaya et al., 2004; Kremer and Hunter, 2007; Gräfe, 2007ab; Kukko, 2009; Kukko el al., 2009; **III**) and for the field of autonomous vehicle guidance systems (e.g., Montemerlo et al., 2006).

2.2.2 Incidence angle effect in laser scanning context

LiDAR systems have become a well-established tool for providing accurate 3D information of remotely sensed targets. There is abundant knowledge of system uncertainties and their effects on the topographic models, but there have been few studies on the role of the optical properties of the targets and the laser light interaction with the surface media. A number of studies on the light interaction with

surfaces and diffusive media are available (Ellis, Caillard and Dogariu, 2002; Ruiz-Cortés and Dainty, 2002) and the effect of the optical properties of different targets on their backscatter (van Albada and Lagendijk, 1985; Yoon, Roy and Straight, 1993; Wiersma et al., 1995; Kaasalainen et al., 2005ab). Simulations of the laser beam interaction with the target surface have provided some important information on the properties having the strongest effects on laser interaction and the interpretation of the backscattered pulse (Jutzi, Neulist and Stilla, 2005; **II**).

To fully exploit the full-waveform data there is a need for experimental data on the factors affecting the laser echo, such as the surface composition and structure, and especially the orientation of the target in relation to the observation direction. This is crucial for modeling and correcting the amplitude data for such effects prior use. Lin and Mills (2009) later investigated the effect of different factors on reflected echo and found surface roughness to be statistically the most significant. Also, when correcting echo waveform data, accurate echo amplitude normalization using local incidence angle is a critical aspect, which has been only partly addressed (Abed et al., 2012). Systematic experimental data on the effect of the incidence (i.e., scanning) angle on the intensity of typical laser scanner land targets provide an important reference for data interpretation and applications, e.g., simulations and calibration of full-waveform laser scanner data (Kukko and Hyyppä, 2007; Briese et al., 2008; Abed et al., 2012).

The observing geometry in all the current scanning LiDAR systems is basically the same. The returning pulse is recorded almost entirely at backscatter, i.e., the light paths of the source and detector coincide. This geometry is a source of some important scattering effects that are studied in many fields of optics and physics (van Albada and Lagendijk, 1985; Yoon et al. 1993; Wiersma et al., 1995; Ellis et al., 2002; Kaasalainen et al., 2005b). Since the observing geometry of the LiDAR remains the same in all scanning applications, the effects from changes in the geometry, i.e., differences in the transmitted and detected light paths, are mostly avoided.

The angle of incidence to the target plays an important role in both the 3D model and the backscattered intensity recorded by the LiDAR sensor. The effect of the incidence angle on backscatter has been addressed computationally and experimentally in numerous works in photonics and optics (e.g., Videen et al., 1992; Ellis et al., 2002; Ruiz-Cortés and Dainty, 2002; Jutzi, Eberle and Stilla, 2003; Landry et al., 2006). These studies have mostly concentrated on specific case studies, e.g., the polarized backscatter from diffusive media or fiber on a reflective surface, but the application of these results to remote sensing of natural surfaces is limited. No systematic experimental data on the effect of incidence angle on different materials, especially typical remote sensing targets, are available (Ellis et al., 2002). Such data would also be important for the investigation of a LiDAR-based reflectance measurement, which has become a topic of scientific interest (Kaasalainen et al., 2005b; Ahokas et al., 2006; Boyd and Hill, 2007; Kaasalainen et al 2007a; Kaasalainen et al., 2008ab; Pesci and Teza, 2008;). One of the

few attempts prior **I** to correct the incidence angle effect on LiDAR intensity is based on a simple cosine approach where a Lambertian surface is assumed (Coren and Sterzai, 2006; Höfle and Pfeifer, 2007).

Since the work published in **I**, Lin and Mills (2009) provided with an analysis of the factors affecting ALS pulse shape. Jutzi and Gross (2010) have presented an investigation finding the optimal surface reflection model to compensate for variables affecting echo amplitude signals including the angle of incidence. The echo amplitude variations caused by incidence angle and range effects were found to be able to be eliminated by using the Lambertian reflection model. As the radar equation commonly used for describing the laser scattering power includes all Earth surface feature properties, as well as atmospheric and system characteristics with the range effect, this approach was stated to be feasible for radiometric calibration of ALS data (Wagner et al., 2008). Lehner and Briese (2010) incorporated the incidence angle effect in the radiometric calibration workflow. Abed et al. (2012) have further developed methodology for local incidence angle derivation and amplitude normalization using full-waveform ALS data.

2.2.3 Laser ranging techniques

Phase shift ranging

In a phase shift ranging system a continuous multi-wavelength amplitude-modulated laser beam is transmitted to the target (e.g., Kikuta, Iwata, & Nagata, 1986; Paschotta, 2013). The phase shifts $d\varphi_i$, i=1…n of the modulated carrier and measurement waves between the transmitted and received signal are measured, the ambiguity N of the shortest wavelength is solved from the phase shifts in the modulated carrier waves, and finally the phase shift of the shortest measurement wavelength is converted into a range from the scanner origin to the object. The frequencies of the modulated amplitude waves must be known, since the shortest modulated wavelength λ_0 gives:

$$r = \left(N + \frac{d\varphi}{2\pi} \right) \lambda_0 , \tag{1}$$

where r is the range and N is the integer number of full wave cycles of the shortest modulated wave. With only a single wavelength modulation the maximum achievable measurement range is determined by λ_0, after that range the phase cycle begins to repeat itself (Wehr and Lohr, 1999; Paschotta, 2013). N could be solved using one or more longer modulation wavelengths λ_i (i=1…n). Multiple modulation frequencies are used for two reasons; longer ranges can be solved unambiguously, and with the shortest modulation wavelength being around a meter or so, the phase difference measurement can give

millimeter precision ranging capability, which is not achieved using only single long wavelength (e.g. λ>50 m) modulation.

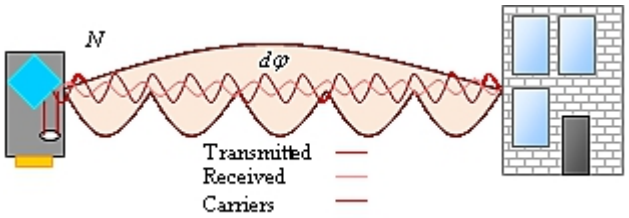

Figure 4. Principle of phase shift laser ranging.

Time of flight ranging

In a time of flight ranging system, a short (typically 5 to 10 nanoseconds) laser light pulse is transmitted towards the object. The time of flight *dt* of the transmitted pulse from the scanner to the object surface and back is recorded and converted to a range *r*, since the speed of electromagnetic radiation (light in case of LiDAR) *c* is known:

$$r = \frac{dt \cdot c}{2}. \qquad (2)$$

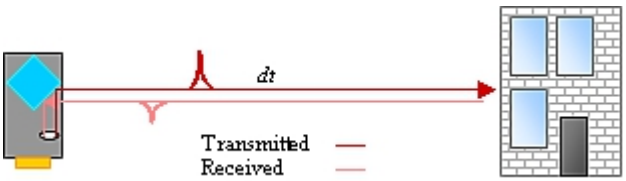

Figure 5. Principle of ToF laser ranging.

The pulse energy spreads around the beam center line on the way to the target due to beam divergence before it hits the target. Depending on the target geometry, the light pulse scatters back towards the scanner from the different target scatterers at different ranges within the beam footprint. This spreads the initially short peak pulse energy into an elongated waveform, which is then either turned into a discrete point with analogue detection or sampled and recorded digitally for object point extraction. With the full waveform technique, a practically unlimited number of echoes can be extracted, but this increases the data amount rapidly and not all echoes are easy to determine.

Thus, one of the most crucial factors for exact range determination from the returned echo is the target detection algorithm (Wagner et al., 2004). Since the length of the typical laser pulse (i.e. duration of the pulse times the speed of light) is longer than the accuracy needed (a few meters versus a few centimeters), a specific timing mechanism of the return pulse needs to be defined. In a non-waveform

ranging system, analogue detectors are used to derive discrete, time-stamped trigger pulses from the received signal in real-time during the acquisition process (Wagner et al., 2004). The timing event properties should not change when the level of signal varies, which is an important requirement in the design of analogue detection as discussed by Palojärvi (2003). For full-waveform digitizing scanner systems several algorithms can be used at the post-processing stage, e.g., leading edge discriminator/threshold, center of gravity, maximum, zero crossing of the second derivative, and constant fraction (Jutzi et al., 2003; Wagner et al., 2004; Wagner et al., 2006).

2.3 Positioning for mobile laser scanning

The purpose of a navigation system of an MLS is to provide the instantaneous location and attitude of the observer in a chosen coordinate system. To perform the task a primary coordinate frame and possible auxiliary coordinate systems are needed to be defined. Furthermore, as the Earth system is more or less in a constant movement, as is the observer, a proper time (epoch) frame is also needed. Finally, all data acquired from the environment are needed to be synchronized to the common time frame in order to be able to georeference them correctly. In this section the principle of GPS-IMU navigation is presented in general terms.

Mobile laser scanning systems typically rely on combination of global navigation satellite systems (GNSS) and inertial measurement unit (IMU) technology for direct georeferencing of the data (Grejner-Brzezinska, 1999). GNSS receivers, such as GPS or GLONASS, typically, but are not limited to, provide accurate positioning at low data frequency, typically 1-10 observations a second, when satellite visibility and constellation geometry is adequate. At a minimum, signals from four satellites must be visible to the receiver. If this criterion is met, RTK and differential GPS positioning can be accurate to within a few centimetres. If however, some or all of the satellite signals are blocked, the accuracy of the position reported by GPS could be degraded substantially, or may not be available at all. (Grimes, 2008; Poutanen, 1999; NovAtel, 2005.)

As GNSS-only positioning is prone to errors in conditions of poor satellite visibility, a condition that often realizes in urban environments and beneath high vegetation, and are the main obstacles within the MLS context. To overcome this and more importantly to provide attitude information for precise sensor orientation, IMU equipment is incorporated to the mapping systems. IMU devices produce location and attitude data at high rates, typically 100 Hz or more, by observing linear accelerations and rates of angle change along and around the three dimension axes, respectively (NovAtel, 2005).

Inertial navigation (i.e., using an IMU) provides accurate position over short periods of time, but the IMU solution becomes erroneous (i.e., drifts) due to accumulation of gyroscope and accelerometer

errors. These errors can be corrected using the GNSS positioning solution, but if the satellite signals become obscured for a long period of time, the errors will gradually become large (King, 1998). The rate of IMU drift depends on the type and quality of the IMU. By integrating the data from the two techniques into a common solution, typically computed using Kalman filtering, or linear quadratic estimation, theory originally proposed by Kalman (1960), the accuracy of the navigation solution can be maintained in varying conditions more reliably and with better coverage (King, 1998).

That being said, many modern integrated inertial navigation systems, such as IGI Iie, NovAtel SPAN variants and Applanix Pos LV, contain an embedded or integrated GNSS receiver module. GPS and inertial navigation are ideal synergistic partners, as their error dynamics are totally different and uncorrelated (King, 1998). The following lists the main advantages of GNSS-IMU integration (according to King, 1998):

- The integration with GNSS solves the problem of calibrating the instrument errors in a strapdown system.
- Similarly, GNSS provides a means of in-flight alignment, removing the need for the platform to be held stationary for up to 5 minutes while the inertial system initializes, prior to operation.
- Inertial navigation provides seamless coverage for GPS outages resulting from jamming, obscuration caused by maneuvering, etc.
- Inertial navigation provides a means of smoothing the noisy velocity outputs from the GPS, and a continuous high-rate measurement of position, velocity and attitude.

2.3.1 Global Positioning System – GPS

The GPS space segment consists of a constellation of satellites transmitting radio signals for positioning. The US Air Force manages the constellation to ensure the availability of at least 24 GPS satellites, 95% of the time. For the past several years, the US Air Force has been flying 31 operational GPS satellites, plus 3-4 decommissioned satellites ("residuals") that can be reactivated if needed. GPS satellites fly in medium Earth orbit (MEO) at an altitude of approximately 20,200 km. Each satellite circles the Earth twice a day. (GPS.gov, 2013; Grimes, 2008)

The GPS system includes a constellation of satellites and a remote receiver that uses range measurements to compute the position of the receiver using trilateration. Carrier phase differential GPS is an advanced method combining the carrier phase data from a remote and base receiver so as to eliminate errors from the observations, with the exception of the integer ambiguities in the number of full wave cycles between the two receivers' and each satellite observed (Mostafa, Hutton and Reid, 2001). From simultaneous observations of five or more satellites sufficient carrier phase data redundancy provides the information to resolve the satellite–receiver range ambiguities, thus solving the observations to precise ranges. Range data allows the computation of the baseline between the two

receivers involved, and hence the position of the remote receiver to decimeter or better accuracy (Poutanen, 1999). Most kinematic applications use low-noise dual frequency GPS receiver for obtaining the phase and range data for positioning (King, 1998).

Currently there are three other global positioning services similar to GPS either in operation, like GLONASS, or under construction (Compass and Galileo(Inside GNSS News, 2013)). With the improved satellite coverage obtained by combining two or more GNSS constellations, one can obtain more accurate positioning, especially in urban areas or other environments where there is significant signal attenuation.

2.3.2 Inertial navigation

Inertial navigation equipment is essential for any survey or mapping system not relying on indirect observations of control points but rather direct georeferencing of data (Grejner-Brzezinska, 1999). An inertial navigation system (INS) is a navigation device that, once initialized, uses a computer, motion sensors (accelerometers) and rotation sensors (gyroscopes) to continuously calculate the position, orientation, and velocity of a moving object without the need for external references (King, 1998).

Inertial navigation is typically put into realization with a so-called strapdown inertial measurement unit (IMU). These are cheaper and simpler to build than a gimballed system (null-seeker trying to maintain the gyroscope orientation), which is a benefit for commercial applications, but on the other hand, they are inferior in accuracy (King, 1998; Napolitano, 2010). The Gyroscopes' role in an IMU is to measure the rotation of a device in free space. Typically, Ring Laser Gyroscopes (RLG) and Fiber Optic Gyroscopes (FOG) are implemented in commercial IMUs. Both technologies use phase interferometry to achieve the rotational measurements. The RLGs or the FOGs are arranged in a group of three and complimented with three matched accelerometers, in order to form a 6 degree of freedom (DOF) inertial measurement unit. Currently the FOG technology outperforms the RLG in terms of scalability, reliability, lifetime and level of random noise (Napolitano, 2010).

Strap down IMU

In a strapdown realization, the mechanical gimbals (gimbal can be any support that can pivot around an axis, most gimbal systems look like a series of concentric rings) of a gyroscope system are eliminated altogether by strapping down the gyros and accelerometers onto the mounting frame. The principle is to not use the gyros as null-seekers, but as a means of measuring rotations in space so that the system always knows in which direction the accelerometer axis set is pointing. In effect, the mechanical gimbals are replaced with a mathematical gimbal set. (King, 1998.)

In a gimballed system, gyros need to measure down to a few thousandths of a degree per hour. However, they only have to measure rotations up to a few tens of degrees per hour – a dynamic range of about 10^5 (King, 1998). In a strapdown system, the same drift accuracy is needed, but it is also necessary to measure rotations within the full maneuver envelope of the platform – up to several hundreds of degrees per second. Furthermore, the gyro scale factor has to be extremely accurate and linear. As rotations in three axes are not commutative, tiny errors in scale factor accuracy can lead to large attitude errors, and thus the scale factor accuracy needs to be a few parts per million at the most (King, 1998).

The initial enabler for strapdown IMUs was the development of RLG. This had been under development since the mid-60s, originally with the motivation of achieving better reliability than that of the then state-of-the-art. An RLG has virtually no moving parts, and it had been turned out that the RLG inherently has extremely good scale factor accuracy, typically about 5 ppm, and furthermore it dissipates the same power, regardless the rotation rate. (King, 1998.)

RLG

Since the demonstration of the laser gyroscope by Macek and Davis (1963), the optical gyros have become a standard in inertial navigation, especially for strapdown mechanization (Dorobantu and Gerlach, 2004; King, 1998). They provide high dynamics with better insensitivity to mechanical accelerations, smaller biases, drifts and random walk, very good scale factor stability and negligible gyro scale factor asymmetry and gyro misalignments (Krempasky, 1999; King 1998; Dorobantu and Gerlach, 2004). RLG is extremely reliable, and compared to the mechanical gyroscopic sensors, RLGs are practically insensitive to temperature variations. RLG also has a quasi-instantaneous initialization time-period (Dorobantu and Gerlach, 2004; King, 1998).

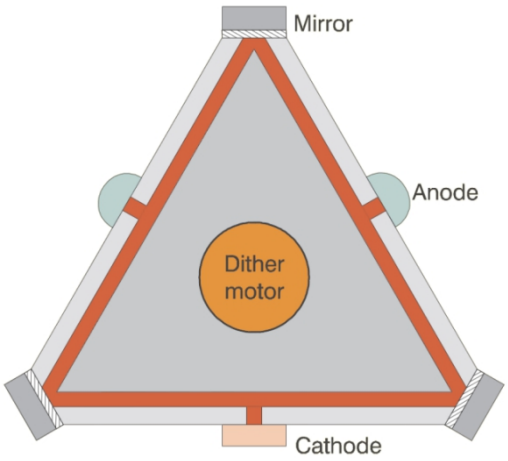

Figure 6. Ring laser gyroscope – schematic (from King, 1998).

The construct of an RLG body is a solid glass block, with three narrow tubes drilled in it (King, 1998; Dorobantu and Gerlach, 2004). A mirror is placed at each corner, forming a triangular optical resonator path. The tubes are filled with a helium-neon gas mixture at low pressure. A high voltage (around 1kV) is applied between the cathode and the two anodes, causing a discharge. The discharge provides enough energy to cause regenerative lasing action in the gas, with light beams circulating around the triangular resonator path (King, 1998). The principle of the optical RLG is based on the pure relativistic Sagnac effect (1913): the phase difference between two opposite electromagnetic coherent light-waves propagating in a rotating closed optical path is proportional to the rotation rate (Dorobantu and Gerlach, 2004). Thus, there appear to be two lasers within the same cavity – one with a clockwise (CW) beam, the other counterclockwise (CCW) (King, 1998). When the gyro is at rest, the two beams have the same frequency. The block rotating in a CW direction causes a photon in the CW beam, starting at the bottom left-hand mirror to find, after one traverse of the cavity, that the mirror has moved slightly further away. So that results it to see a slightly increased path length.

Similarly, a photon in the CCW beam finds a shorter path length. The difference in path lengths causes a small difference in frequency. By making one of the mirrors partially-transmitting, samples of both beams can be extracted and the frequency difference measured. This is precisely proportional to the applied rotation rate. However, very low rotation rates causes complications. The mirrors are not perfect and thus produce miniscule between the two beams. This coupling of energy between two very high-quality oscillators can cause the frequencies to lock together. To overcome this, the dither motor shown in Figure 6 applies a very small oscillatory rotation to the entire block. (King, 1998; Dorobantu and Gerlach, 2004.)

2.3.3 Direct georeferencing

The motion of a vehicle-based terrestrial mapping system is described in a local coordinate frame, the so-called navigation frame. The determination of the position and attitude of the vehicle, or platform, is based on measurements from various sensors attached to the sensor platform on the vehicle, typically a GPS-IMU system, and possibly aided with an odometer wheel. These sensors deliver physical quantities, i.e., accelerations and position, measured within independent frames, each defined according to the instrument's characteristics.

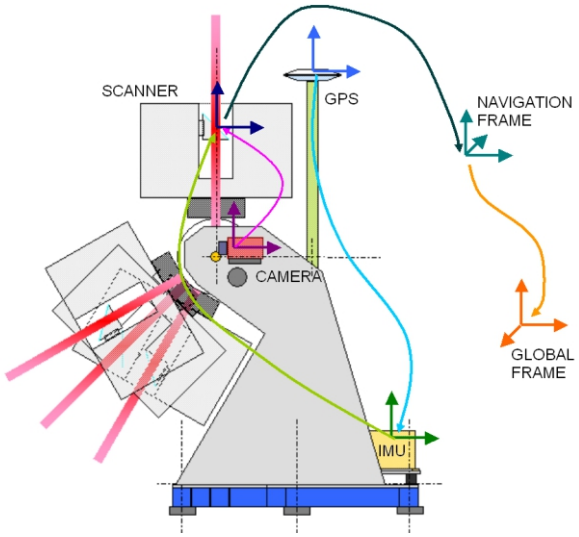

Figure 7. Coordinate frames associated with the ROAMER system (Kukko, 2009).

Mapping sensors operate in the coordinate frames of their own independently. Each of the observations is defined within the sensor frame and is not directly tied to the world coordinates. Platform frame is the co-ordinate frame to which all of the mapping sensor observations are tied with, and which is defined by the IMU attached. More generally speaking, navigation, body and sensor frames are local frames defining the reference frames describing the primary observables measured from the moving vehicle (Figure 7). Coordinate frames and their mutual transformations are needed to deliver all acquired object data, e.g., images and lidar points, in a specified map coordinate system (through ECEF) for modeling, measurement and analysis purposes. Excluding the sensor frame, these are illustrated in Figure 8.

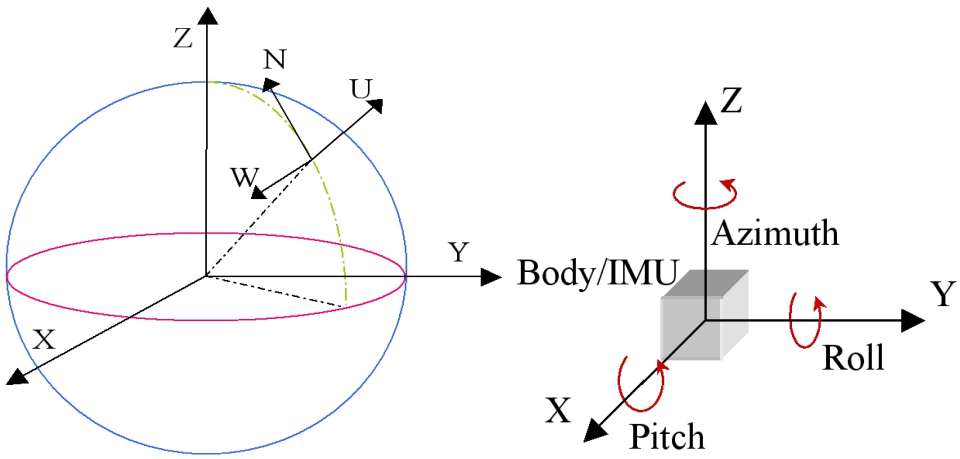

Figure 8. Coordinate frames for the GNSS-IMU navigation. Left: EFEF (XYZ) and navigation (NWU) frames. Right: IMU body frame. Kukko (2009).

To further understand the role of different frames to the operation of a mobile mapping system, all the relevant global and local co-ordinate frames are briefly described. Global frames are the Earth centered inertial and the Earth centered Earth fixed frames that define the position of the MMS on the Earth surface. Navigation and body frames are local frames that are needed to maintain the attitude information. TLS and image frames are local sensor coordinate systems, and time frame couples the navigation and sensor data streams.

Earth Centered Inertial – ECI frame

In real time positioning, the user is fixed in inertial space. Positions are expressed in the Earth Centered Inertial (ECI) system and True Time. ECI is a non-rotating system with the X-axis aligned with a vector from the Sun's center to the Earths position at the Vernal Equinox, Z-axis is determined to coincide with the mean rotation axis, and the origin of the system is located at the center of mass (CoM) of the Earth (Parkinson and Spilker, 1996; Walchko, 2002). Alternatively, the X-axis could be aligned with the fixed stars (Walchko, 2002).

Earth centered Earth fixed – ECEF frame

Earth Centered Earth Fixed (ECEF) is similarly to the inertial system a three dimensional Cartesian coordinate system, except the axes rotate with the Earth. The XZ-plane contains the meridian of zero-longitude – the Greenwich meridian, the XY-plane of the system is coincident with the equatorial plane, and the Z-axis is coincident with the minor axis of the reference ellipsoid (Hooijberg, 1997). This helps in establishing and transforming data to a specified map coordinate system (Walchko, 2002). Figure 8 illustrates the ECEF XYZ-system.

For practical applications the ECEF system needs to be realized. One of such realization, especially for GPS use, is the World Geodetic System 1984 (WGS 84). It is a global terrestrial reference frame (TRF), or datum, with its origin located at the center of the Earth, and defines a reference ellipse. The reference ellipse is itself defined by the major and minor axes of the Earth. (DMA, 1987; Hooijberg, 1997)

The original WGS 84 reference frame established in 1987 was realized through a set of Navy Navigation Satellite System (NNSS) or TRANSIT (Doppler) station coordinates. Moreover, this original WGS 84 TRF was developed by exploiting results from the best available comparisons of the Department of Defense reference frame in existence during the early 1980s, known as NSWC 9Z-2, and the BIH (Bureau International de l'Heure) Terrestrial System (BTS). (DMA, 1987; NIMA, 2000.)

Navigation frame

A local coordinate frame can be defined variously. In classical geodetic applications a typical definition of a local coordinate frame would set the 3rd axis of the local system coinciding with the direction of the ellipsoidal normal and pointing outwards the ellipsoid. The 2nd axis would point in the north direction residing in the respective meridian plane, while the 1st axis would point in the eastward completing the orthogonal axes triad. For INS applications on the other hand most popular is the choice of a different axes orientation. Thus, a typical body or vehicle frame is a so-called local north-east-down coordinate frame, with the third axis (z) pointing downwards towards the ellipsoid (on the direction of ellipsoidal normal h), the 1st axis (x) defining the north-direction (a direction parallel to the tangent to the respective meridian) and the 2nd axis (y) pointing to the eastern direction. (Tsoulis, 2006).

On the left in Figure 8 a local left-handed definition for a navigation frame (NWU) is described, where the axes are pointing north (N), west (W), and up (U). The origin of the system coincides the observer location, for example the GPS-IMU CoM, and is uniquely defined by the latitude, longitude and ellipsoidal height in the ECEF system. Local anomalies in the Earth gravity field cause variation in the plump line direction, as the normal to geoid is not parallel to the ellipsoidal normal. Such variation is fortunately small enough (< 7 arcsec in Finland) to be neglected when regarding mobile mapping, but must be taken into account for accurate long-range geodetic applications.

Body frame

Body reference frame, as seen in Figure 8, is the coordinate system associated with the vehicle, or with the IMU attached to the system. Typically, but not always, the y-axis points out of the front of the vehicle, the x-axis is pointed out the right side, and the z-axis is pointed upward. All navigation measurements will be taken in this coordinate system. Furthermore, the body frame is the basis of the platform frame on which all of the mapping sensor data is tied with.

Mathematical relations of direct georeferencing

The MLS utilizes direct georeferencing (e.g., in Schwarz et al., 1993; Grejner-Brzezinska, 1999; Cramer, Stallmann and Haala, 2000) to establish coordinate transformations from the sensor level to the object space. The term georeferencing is used here to describe the procedure to resolve the orientation of a data sensor mounted on a moving vehicle for mapping applications. Direct georeferencing is defined mathematically by a transformation between the rectangular sensor coordinates specified in the sensor (TLS or camera) frame and the geodetic (mapping) reference frame:

$$\vec{X}^{e} = \vec{X}^{e}_{GPS-IMU} + R^{e}_{b} R^{b}_{s} \left[\lambda \vec{x}^{s} + \Delta \vec{X}^{s}_{GPS-IMU} \right], \tag{3}$$

where:

Equation term	*Description*
$\vec{x}^s = (x\, y\, z)^T$	Object coordinates in sensor frame
$\vec{X}^e = (X^e\, Y^e\, Z^e)^T$	Object coordinates in ECEF frame
$\vec{X}^e_{GPS-IMU} = (X^e_o\, Y^e_o\, Z^e_o)^T_{GPS-IMU}$	$CoM_{GPS\text{-}IMU}$ in ECEF mapping frame
$\Delta\vec{X}^s_{GPS-IMU} = (\Delta X\, \Delta Y\, \Delta Z)^T_{GPS-IMU}$	Lever Arm vector between $CoM_{GPS\text{-}IMU}$ and sensor origins.
R^e_b	Rotation from body frame to ECEF frame
R^b_s	Rotation from sensor frame to body frame (boresight misalignment)
$R^e_s = R^e_b\, R^b_s$	Rotation from sensor frame to ECEF frame
λ	Scaling factor

Two rotation matrices are needed to transition between these different reference frames. The rotation R^b_s from the sensor frame to the body frame is determined in the system boresight calibration. The rotation in Equation 4 takes the measurements in the body frame and transforms them into the navigation frame:

$$R^n_b = \begin{bmatrix} \cos\theta\cos\psi & \sin\varphi\sin\theta\cos\psi - \cos\varphi\sin\psi & \sin\varphi\sin\psi + \cos\varphi\sin\theta\cos\psi \\ \cos\theta\sin\psi & \cos\varphi\cos\psi + \sin\varphi\sin\theta\sin\psi & \cos\varphi\sin\theta\sin\psi - \sin\varphi\cos\psi \\ -\sin\theta & \sin\varphi\cos\theta & \cos\varphi\cos\theta \end{bmatrix}, \tag{4}$$

where φ is roll around the y-axis, θ is pitch around the x- axis, and ψ is yaw around the z-axis of the local navigation frame.

The following matrix in Equation 5 would rotate points from the ECEF frame to the navigation frame:

$$R^n_e = \begin{bmatrix} -\sin\varphi\cos\lambda & -\sin\varphi\sin\lambda & \cos\varphi \\ -\sin\lambda & \cos\lambda & 0 \\ -\cos\varphi\cos\lambda & -\cos\varphi\sin\lambda & -\sin\varphi \end{bmatrix}, \tag{5}$$

where φ is latitude and λ is longitude of the observer. With these two orthogonal rotations the measurements in the body frame are eventually mapped to the ECEF mapping frame, namely:

$$R^e_b = R^e_n R^n_b, \tag{6a}$$

where

$$R^e_n = R^{n^T}_e. \tag{6b}$$

The rotation R_s^b and translations $\Delta\vec{X}_{GPS-IMU}^s$ between the sensor and GPS-IMU body frames are determined either from the design of the particular system or from calibration. Typically the translations are determined reliably enough from the design, and are to be considered constant, but rotations are more critical as they possess the range dependent factor for the uncertainty in object location determination. The calibration procedure for determining R_s^b is introduced in Section 3.2.6, and the results for MLS data are discussed in Sections 4.3.3 and 4.4.2.

2.4 MLS Simulation

A laser scanning simulator is aimed at emulating the LiDAR data capture process with the use of mathematical models under a computational environment. Data generated by a simulator should exhibit all characteristics of data acquired by actual LiDAR sensor (Lohani and Mishra, 2007), yet incorporate the object characteristics as well for valid results (Kukko and Hyyppä, 2007). Literature reveals that only a few attempts have been made by researchers to develop simulator for laser scanner instrument. It is expected that simulation of this kind would provide an important adjunct to the analytical error modeling and estimation that has taken place (e.g., Baltsavias, 1999; Schenk, 2001; Wagner et al., 2006; Balsa-Barreiro, Avariento and Lerma, 2012).

Significant simulation and modeling work had been done prior to **II** for large-footprint LiDAR systems (e.g., Sun and Ranson, 2000; Ni-Meister, Jupp and Dubayah, 2001; Koetz et al., 2006). Simulation and modeling for small-footprint systems was rarer, even though the same large-footprint system knowledge can be applied. Earlier attempts at three-dimensional simulations of forests using small-footprint airborne laser scanner include modeling of the scanning angle effect in the measurement of tree height and canopy closure (Holmgren, Nilsson and Olsson, 2003) and the establishment of optimal LiDAR acquisition parameters for forest height retrieval (Lovell et al., 2005). In these cases, two assumptions were made: the simulated laser pulse was assumed to be a single ray without any divergence, and the coarse objects simulated were assumed to be solid. In general, such simulation methods were useful, but the implementation was relatively simple. It is thus unsurprising that the results obtained with the simulation method in Holmgren et al. (2003) systematically overestimated the laser height percentiles by 2.25 m. Beam interaction, waveform, and threshold detection were not simulated in this particular study.

Even though the modeling in Goodwin, Coops and Culvenor (2007), called LiDAR Interception and Tree Environment (LITE), was improved, when the simulations were compared to coinciding airborne LiDAR data, the estimates differed around 2.4 m in maximum tree height and about 2.3 m in mean heights of the first return data. Thus, the geometry of the modeling and the interaction between the

LiDAR pulses and forest canopies should be further improved. Lohani and Mishra (2007) presented an educational tool for generating simulated ALS data. This simulator provided an easy way to generate model data and for altering scan parameters for simulated data, but no validation of the generated data was presented. Beinat and Crosilla (2001) have studied the ALS data registration adjustment methodology using stochastically generated artificial LiDAR data. This approach, however, does not incorporate any of the actual laser scanner geometrical characteristics.

There are possible applications in which simulation, together with good simulation models for the sensors, target, and beam interaction could provide further insights and answers. Optimization of the laser acquisition parameters is one feasible application area; an example is tree height estimation, in which it is not precisely known why a bias in tree height is found to be 1.3 m in one study and 0.5 m in another (see e.g., Rönnholm et al., 2004). Furthermore, it is unknown how much the repeatability of laser surveys affects object extraction (building or tree extraction) and detection of certain small targets. Opportunities for the use of small-footprint waveform data are long delayed due to the lack of experimental data. Even the capabilities of future laser instruments can be estimated with simulation and appropriate target models.

In the mid-2000's, MLS was still a special group of applications for LiDAR attached to ground-based mobile platforms, and commercial MLS had not yet been launched. Some experiments had been done, of which Talaya et al. (2004) presented the most advanced approach at the time. The MMS development at the FGI was in its early stages, and relevant information of possible system characteristics was needed. In this area of interest, optimal constructs and arrangements were investigated by applying simulation. Performance analysis and comparison between desired layouts and scanner properties was also carried out.

The simulation approach developed and reported in Kukko and Hyyppä (2007) and later validated for ALS and MLS study cases in **II,** was based on research conducted for sampling of directional reflectance data from multi-angular digital aerial sensor HRSC-A (High Resolution Stereo Camera-Airborne) imagery (Kukko, Hyyppä and Kuittinen, 2005). The developed simulator was the first to combine the accurate modeling of the scanner and beam propagation geometries and artificial waveform generation. Publication **II** discussed the potential and results for ALS simulations. For analyzing MLS system performance and data characteristics for ROAMER development in 2005–2006 there were little published literature to rely on. The simulators especially for MLS use appeared after **II**, are compared in the discussion section of this thesis.

2.5 Laser sensors for MLS

For current MLS applications, 2D scanners are the most common approach. The third dimension of the data is obtained from tracking the vehicle movement. 2D scanners with 360° field of view are ideal for mobile laser scanning, as they give full data coverage and are cheaper to manufacture than sensors with two rotating axes. Such sensors are widely deployed for kinematic mapping, and different multi-sensor layouts are put to use in research platforms as well as in commercial systems. The latest trend in MLS sensor development incorporates multi-line scanning with fixed angles (e.g., Velodyne HDL-64E, Ibeo LUX) or oscillating beam axis (Neptec Opal-360) for gaining an along-track FOV, thus producing multiple profiles per one scan revolution. This improves the spatial coverage of data and helps to overcome some of the shadowing effects, thus reducing the time spent in the field.

The laser sensors currently used in the most prominent operative mobile mapping platforms can be divided into two main categories according to the applied ranging technique: ToF and PS. The fundamental differences between the two approaches are precision of the ranging and the rate of point measurements, although the gap is narrowing. The maximum range for ToF sensors is typically longer than that of PS ranging sensors. Considering point distribution and density obtained with typical angular resolutions used in MLS and object shadowing/occlusions, however, ranging capability greater than 150–200 m is of limited use. One of the most critical geometric parameters of an MLS sensor is the scan frequency, as it determines the along-track line distribution. This characteristic is related to the deflection optics, not the ranging technique. Table 1 summarizes sensors used currently on commercial MLS systems. Sensors with ranging capability (less than 50 m) are not listed, as they provide data only for limited applications and usually provide low PRF and angular resolution with large beam sizes (e.g., SICK LMS-291).

Table 1. Laser scanning sensors employed in commercial MLS (October 2013).

Sensor	**Ranging**	**Range (m)** @ >80 %	**Scan freq.** Hz	**Point rate** kHz	**Angle resolution** deg	**Range resolution** mm	**Range accuracy** (one sigma) 80 %	**Range repeatability**	**Beam divergence** (mm × mrad)	**Spot size** @ 50 m	**Field of view**	**Wave length** nm	**Specific**
Dynascan SLM 150/500	ToF	150/500	10	36	0.01	10	N/A	50 mm	2.5 × 0.2	10 mm	360	905	IP66
Dynascan S250	ToF	250	20	36	0.01	10	10 mm	50 mm	2.5 × 0.2	10 mm	360	905	IP65, 160° cone
Optech V200 (iFlex)	ToF	200	80-200	75-200	0.144	N/A	±50 mm[1]	8	0.5	N/A	360	1064	4 Echoes
Optech M1 (iFlex)	ToF	200	80-200	75-500	0.058	N/A	±50 mm[1]	8	0.5	N/A	360	1064	4 Echoes
Riegl VQ-250	ToF	500	-100	300	0.001<0.72	N/A	10 mm	5 mm	7.0 × 0.35	18 mm	360	1550	Full waveform
Riegl VQ-450	ToF	800	-200	550	0.001<0.48	N/A	8 mm	5 mm	7.0 × 0.3	15 mm	360	1550	Full waveform
Velodyne HDL-64ES2.1	ToF	120	5-20	>1300	0.09 × 0.5[2]	N/A	20 mm	N/A	2.0	~10 mm	360 × 31.5	905	Multi-line
Velodyne HDL-32E	ToF	70	10	700	0.16 × 1.33[2]	N/A	20 mm	N/A	2.79	14 mm	360 × 40	905	Multi-line
FARO Photon 120	PS	153	61	976	0.009	0.07	2 mm	2.7 mm @ 25 m	3.3 × 0.16	8 mm	320	785	TLS
FARO Focus 3D	PS	153	97	976	0.009	0.07	2 mm	2.2 mm @ 25 m	3.0 × 0.16	8 mm	305	905	TLS
Faro Focus 3D X330	PS	330	97	976	0.009	0.07	2 mm	0.5 mm @ 25 m	2.25×0.19	10 mm	300	1550	TLS
Z+F Imager 5010C	PS	187	50	1016	0.0004	0.1	2 mm	2 mm @ 100 m	3.5 × 0.3	15 mm	320	1500	TLS
Z+F Profiler 9012	PS	119	50-200	1016	0.009	0.1	0.9 mm	0.9 mm @ 50 m	1.9 × 0.5	25 mm	360	1500	Only 360° PS scanner

For further technical details, please refer to manufacturer data sheets: www.mdl-laser.com, wwww.optech.com, www.riegl.com, www.velodynelidar.com, www.faro.com, www.zf-laser.com

[1] Absolute accuracy, range accuracy about 10 mm.

[2] Multilayer scanner: Horizontal × Vertical

2.6 Integrated MLS systems

Mobile laser scanning technologies and applications are currently under rapid development. This means that new systems with increasingly varying component combinations are being introduced at increasing rates at the moment. In this section, the most prominent and widely spread mobile laser scanning systems up to 2013 are presented. The presentation lists systems –all introduced after ROAMER– capable of producing point measurements at high rates and utilizing state-of-the-art GNSS-IMU positioning for high quality data.

The state-of-practice MLS systems were divided into three categories based on the ranging method and speed of point measurement (Table 2): High-speed ToF (HSToF), Ultra-High-speed PS (UHSPS), and Low-speed ToF (LSToF) systems. The HS ToF category includes systems utilizing ToF ranging laser scanner units capable of greater than 200 kHz PRF with high scan frequencies (> 100 Hz). These typically have ranging capability over 200 meters and usually provide multiple echoes or full waveform recording. The UHSPS category comprises systems with PS ranging scanners up to 1 MHz PRF and higher. With these systems, the maximum range is slightly less than that of HSToF systems, typically below 150 meters, but is improving (e.g., FARO Focus X330), and they operate at medium scan frequencies (50–100 Hz). LSToF systems instead have typically PRF of 1–20 kHz; maximum ranges are similar to HSToF, but many operate only in close range region (<50 m).

Table 2. The state-of-practice of MLS systems by category (October 2013).

HSToF	UHSPS	LSToF
StreetMapper	IGI SAM	MDL Dynascan S250X
Optech Lynx	MDL	MDL Dynascan M500
Riegl VMX-250	ROAMER	Mitsubishi MMS-X
Trimble MX-8	Scanlook	Sensei
NAVTEQ True	Road-Scanner3	
Nokia HERE 3D		
Topcon IP-S2 HD		

StreetMapper was the first commercially available multi-scanner mobile mapping system of its type. It was initially aimed at highway asset inventory but has been developed also for other applications since its first appearance (Hunter et al., 2006; Kremer and Hunter, 2007). The StreetMapper system has been implemented with Riegl VQ-250 scanner units for high speed data collection with a similar functional construct to the Optech Lynx, launched in 2007, and later inherited by the Trimble MX-8 system. On PS ranging instruments, FARO-originated scanners (Photon 120 and Focus3D) seem to be dominant (helical scanning can be claimed to have been FGI initiative in 2005) and are used in systems such as Road-Scanner3, IGI SAM and Scanlook. It is expected that PS sensors with full 360° FOV, e.g., Z+F profiler 9012, will emerge into the vehicle MLS systems probably sooner than later. Moreover, there

are some mobile systems especially dedicated to rail and tunnel measurements that utilize Leica or Z+F branded PS scanners, such as GRP 5000 from Amberg Technologies. These systems typically rely on other than GNSS-IMU positioning, e.g., precision TotalStation and wheel sensor measurements for relative positioning to the rails.

Mobile laser scanning techniques are ever increasingly brought into the mapping industry as vehicle mounted systems to derive geometric information about the environment to be mapped. This seems to be mainly due to the precision the laser scanning systems can provide and level of detail in terms of spatial resolution, which cannot be achieved by imaging technology without remarkable post-processing and time. Common to all of the presented systems is that the instrumentation is mounted on a compact platform that can be easily removed and replaced. The compact structure helps in maintaining the relative calibration of different sensors involved, and system modularity is emphasized. Two antenna systems are preferred due to faster heading acquisition times. The trend shows also an increase in the number of scanners mounted on single units to overcome object shadowing. The other trend is to have more than one laser layer, or line, per revolution, which provides mutual overlap between the "scan lines". Low-cost line systems are also entering the market, providing moderate performance with affordable pricing.

2.7 Summary

In this chapter different technologies applied to mobile laser scanning were presented. Section 2.1 discussed the general principles and historical background of the MLS. In Section 2.2 techniques and issues related to scanning lidar were briefly addressed. Direct georeferencing and technologies applied for the determination of MLS trajectory were introduced and formulated in Section 2.3, while Section 2.4 summarizes the LS simulators developed and used prior the one presented in **II**. A comprehensive collection of LS sensors suitable for high-performance MLS operations were reviewed, and presented in Section 2.5, and complemented with an overview on the current state-of-practice in commercial MLS operations in Section 2.6.

3 CONDUCT OF THE STUDY

This chapter describes the data sets produced and used in the studies of this thesis. These data sets include laboratory, ALS, TLS and MLS laser data, but also geodetic reference data obtained with Real-Time Kinematic GPS (RTK-GPS), Virtual Reference Station GPS (VRS-GPS) and robot tacheometers (referred hereafter as TotalStations). Each data set is either the input or outcome of the particular study indicated in the text. Studies have been conducted in several different areas, which are briefly described and located. Section 3.2 and onwards describe the methods, samples, and auxiliary data generated and used in the studies for performance analysis.

3.1 Data and study sites

Table 3 summarizes the MLS datasets produced and used in the studies described in the publications **I–VII** constituting this thesis. The data collected and used as reference for MLS validation analysis are described in Table 4. The sources for the data used in this thesis are ALS, TLS and MLS, laser laboratory, GPS-IMU, and geodetic surveys. For the simulations conducted for publication **II,** some artificial forest model data were created.

Table 3. Summary of the MLS datasets (PRF=Point Repetition Frequency).

Paper	Data	Original data source	PRF kHz	Scan frequency Hz	Scan Angle Degrees	Purpose of use
IV	MLS June 2011	AKHKA	244	49	-40	To produce 3D geometry of the palsas, calibration validation
IV	MLS September 2011	AKHKA	244	49	-40	To produce 3D geometry of the palsas, calibration validation
IV	MLS March 2010	ROAMER Photon 120	244	49	+90	Snow surface characterization
IV	MLS May 2010	ROAMER Photon 120	244	49	+90	City modeling for interactive virtual reality and 3D pedestrian navigation for Shanghai WorldEXPO
IV, V	MLS June 2009	ROAMER Photon 80	122	49	-45	Validation of ROAMER MLS data on a test field
VI, VII	MLS August 2008	ROAMER 880HE80	122	15	+90	Topographic modeling of the river banks
VII	MLS September 2009	ROAMER Photon 80	122	30	+90	Topographic modeling of the river banks, change detection and geomorphology

Table 4. Summary of reference datasets.

Paper	Data used in the study	Original data source	Purpose of use
I	Laboratory Nd:YAG and super-K data	Nd:YAG, Koheras Super-K	Study the incidence angle effect on different target types, simulation
I	Laboratory TLS data	FARO LS 880HE80	Study the incidence angle effect on different target types
I, II	ALS point cloud May 2003	TopoSys II	Incidence angle analysis, environment modeling for simulations, simulator verification, MLS simulations
II	LAB	I, Nd:YAG, Koheras Super-K	Simulated waveform generation
II	Virtual forest		Simulator verification
III	GPS-IMU 2007	NovAtel SPAN	Analysis of the navigation performance
IV	TLS September 2011	Leica HDS6100	To produce 3D geometry of the palsas, Calibration, validation of AKHKA data
IV	Geodetic	RTK-GPS	Geometric validation of AKHKA data
V	TLS, Stop-and-Go June 2009	ROAMER Photon 80	Geometry of the permanent MLS test field, validation of MLS systems
V	Geodetic May 2009	VRS-GPS, RTK-GPS, TotalStation	Geodetic network over the test site for TLS data georeferencing
VI, VII	TLS August 2008	Leica HDS6000	Completion of topographic models, validation of MLS
VI, VII	Geodetic August 2008	RTK-GPS, VRS-GPS	Georeferencing for the TLS data, accuracy assessment of the MLS data
VII	TLS September 2009	Leica HDS6000	Topographic modeling of the river banks, change detection and geomorphology, accuracy assessment of the MLS data
VII	Geodetic September 2009	RTK-GPS, VRS-GPS	Georeferencing for the TLS data, accuracy assessment of the MLS data

The study areas related to the thesis are quite widespread, extending spatially from the south to the northernmost tip of Finland. Table 5 gives a brief description of the main study sites related to the publications of this thesis.

Table 5. Summary of the study areas.

Paper	Location of the study area	Description of the study area
II	Espoonlahti	Suburban area with industrial, high- and low-rise residential areas Varying topography with low hills Plenty of coniferous and deciduous vegetation
III	Espoo	18 km road stretch with varying satellite visibility
IV,V	Espoonlahti test field	Suburban area with industrial, high-rise residential and low-rise residential areas, public buildings, and streets Varying topography with low hills Plenty of coniferous and deciduous vegetation
IV	Tapiola	Urban scene with residential and commercial buildings, pedestrians only
IV, VI, VII	Pulmankijoki	Fluvial study site with a meandering river, open sand point bars and steep sandy banks
IV	Vaisjeaggi	Plain marshland with palsa formations Heathers and hay Low fell shrubs
IV	Toholampi	Agricultural farmland of 16 plots, crops at shoot phase, and grass
IV	Sodankylä	Open marshes and pine dominant forested areas with old and fresh snow cover

3.2 Methodology

3.2.1 Laboratory experiments for incidence angle effects

For investigating incidence angle effects on lidar backscattering, a laboratory laser instrument was constructed to operate under similar illumination/observation geometry as in laser scanning (i.e., exact backscatter where the source and detector light paths coincide). The instrument (depicted in Figure 9) comprised a 1064nm Nd:YAG laser (wavelength similar to most airborne scanners) and a 16 bit monochrome CCD camera (Sbig ST-7), which is a commonly used detector in laboratory (laser) measurements in, e.g., optical physics (Yoon et al., 1993). Altogether five three-second exposure images were taken and averaged for each sample. To illuminate an area of the sample larger than the 3 mm laser spot (and hence reduce the deviation in data), the samples were placed on a rotator, allowing the laser spot to move around the sample surface during the image exposures. The backscattered laser intensities were measured from the CCD images by means of standard photometric techniques. More details on the experiment are found in (Kaasalainen et al, 2007a; Kaasalainen et al., 2008b). The

incidence angles were changed using a precision goniometer to tilt the sample from normal (0°) incidence.

To demonstrate the dependence of incidence angle effects on wavelength, also a hyperspectral measurement for some of the samples was carried out. The measurement was made similarly to the 1064nm experiment (i.e., at the exact backscatter angle) by replacing the Nd:YAG with a supercontinuum (KOHERAS SuperK RED) laser and installing a spectrograph (Specim ImSpector) in front of the CCD camera. The spectra were measured at the wavelength range of 600–900 nm. The instrument was similar to that presented in (Kaasalainen, Lindroos and Hyyppä, 2007b) with a better alignment and thus improved accuracy.

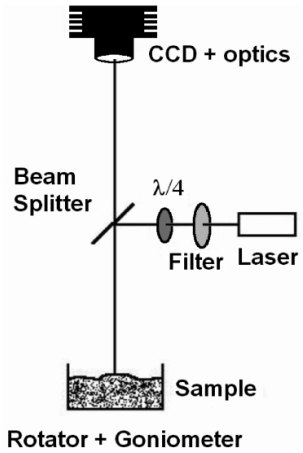

Figure 9. Laboratory laser (Nd:YAG) measurement arrangement. The sample surface was tilted using a goniometer to change the incidence angle (**I**).

The validation of the results of the laboratory laser measurements was carried out with the FARO LS 880HE80 (FARO LS) TLS operating at 785 nm. The scanner uses the PS technique for the distance measurement with an accuracy of 3–5 mm and a 360° × 320° field of view. The detector of the FARO LS is not optimized for intensity measurement. There are modifications in the detector that affect the intensity, e.g., a brightness reducer for near distances (< 10 m) and a logarithmic amplifier for small reflectances. These all required extensive and systematic distance and reflectance calibrations, which were carried out in the laboratory using a calibrated gray scale reference and a calibrated four-step Spectralon reflectance panel (Kaasalainen et al, 2007a; Kaasalainen et al., 2008b). The incidence angle measurements were carried out at a 1 m target distance with the samples placed on the goniometer for the incidence angle variation.

Three of the brightness scale targets with 10 %, 20 %, and 50 % nominal reflectances were also measured during the Espoonlahti ALS campaign, conducted 31 August 2006 using the TopEye Mk II

1064 nm laser scanner. The flight altitude was 300 m, and the test area consisted of the Espoonlahti boat harbor and beach. From each sample, 20–100 hits (i.e., returned pulses) were recorded.

A set of targets used in ALS intensity calibration and a set of natural and artificial (such as brick material) samples representing typical ALS land targets (see also Kaasalainen et al., 2009b for results in this context) were investigated. The brightness calibration targets (tarpaulins, referred as 'tarps' from here on) measured in this study have been used in radiometric calibration of aerial cameras and ALSs. The tarps were made of polyester fiber with a polyvinyl chloride (PVC) coating and span a brightness gray scale from 5 % to 70 % reflectance (Ahokas et al., 2006). A set of four targets were measured with calibrated reflectances of 8 %, 26 %, 50 %, and 70 %. All the measurements were relative to the Spectralon 99 % reference target at 0° incidence. The incidence angle effect of the Spectralon target was also measured.

The sand and gravel chosen for this study were commonly used in sandblasting and construction. The sandblasting sand of two grain sizes were measured, as well as black gabro gravel, crushed redbrick, and light expanded clay aggregate (LECA), which consisted of small, lightweight, bloated particles of burnt clay. These gravel types were also chosen because of their easy availability in standard hardware stores, which makes them practical for the calibration of airborne laser data taken at different campaigns in varying locations. The preliminary test measurements for a large set of gravel types showed that it is difficult to find a gravel of high reflectance suitable for calibration. Therefore, to extend the brightness scale toward higher reflectances, a sample of polystyrene was included into the investigation. (**I**).

3.2.2 Laser scanning simulator

Technical design of a laser scanner affects the characteristics of the resulting point cloud. To study and analyze the effect of different optical and geometrical properties of laser scanners on the data, simulation software was implemented for the use in the Matlab environment. The methodology includes implementation of the geometric properties of the scanner system, beam propagation, laser radiation and scattering on the target surface, and the signal waveform processing. A complete LiDAR simulator could cover platform and beam orientation, pulse transmission, beam interaction with the target surface, computation of waveform prototype, and eventually digitization of the waveform.

Airborne laser scanners typically have three basic scanning geometries or modes: line, oscillating, and conic, all of which were implemented into the simulation system. The other relevant system-specific parameters affecting the achieved scanning pattern (and thus the data coverage on the ground surface) that were implemented are pulse frequency, scanning frequency, scanning angle, and the along-track

velocity of the platform. The parameters determining the sensor trajectory are speed and drift of the aircraft, altitude, and the direction of the flight strip. Since the sensor was assumed to follow a flawless trajectory, navigation errors could be introduced for each computed pulse firing time. Platform accelerations were not introduced in to the simulator.

The transmitted pulse energy was modeled as a function of time with known time-interval sampling. For simulation purposes, 100 ps sampling was chosen to obtain the inside-simulator prototype echo waveform. This provided a sampling frequency 5 to 10 times higher than that provided by the operational scanners. Each single laser beam shot was modeled using multiple rays with uniform angular distribution around the centerline of sight of a single laser pulse.

The waveform data generated by the simulator was based on that spatial discretization of the laser beam to a bundle of rays, Gaussian pulse power approximation and TEM00 intensity pattern model, computation of object intersections for each sub-beam, and the interaction of the sub-beams with the target surface scatterers. The angular difference between adjacent rays, or sub-beams, was chosen according to the flight altitude and surface model grid spacing used. This beam subdivision was implemented since it corresponds to the illumination integral, and it makes it possible to detect small and narrow objects like branches and power cables within the beam, thus allowing the addition of such objects into the artificial models.

The basic assumption of the FGI LiDAR simulator was that there already exists a high-resolution environmental model of the target (e.g., a raster surface), either obtained from ground truth measurements, created artificially, or generated from a previous laser survey. Environmental models employed in this study were created using multiple overlapping laser scanning strips, or they were artificially created for small areas. Environment models based on laser surveys were typically hundreds of meters in size and were generated in the following way: First, the area of interest was delineated from the data, and an appropriate grid cell size was chosen. Next, the grid cells (i.e., pixels) were populated using the elevation of the highest data point within the cell. The elevation values were stored at one-centimeter resolution in 16-bit signed integer data format, so in the simulation computations, the metric values were obtained by multiplying the grid cell value by a factor of 0.01.

Validation of the study cases was carried out using the environment model built usingreal laser scanning data, and in the first case, independent reference laser scanning data, acquired with the TopoSys II laser scanner, was used.

The developed simulation method was validated for the simulation of three different existing laser systems: TopoSys II, TopEye Mk II, and Optech ALTM 3100. In this test, the reference environmental model of the Espoonlahti test area was used. The environment model was computed from the first echo

point data of 18 overlapping scanning strips, acquired with TopoSys Mk II in May 2003 at an altitude of 400 m. This was partly the same area featured in the EUROSDR/ISPRS project "Tree Extraction," coordinated by the Finnish Geodetic Institute (Kaartinen and Hyyppä, 2008; Kaartinen et al., 2012). The same model was also used in the simulation case for mobile laser scanner presented in the study.

3.2.3 Development of MLS systems

The initial goal during the development of the mobile laser scanning system was to create a system that would maximize the automation of feature extraction at the post processing phase (**III)**. To accomplish a high level of automation in data processing, a laser scanner capable of providing dense point clouds was required with an assumption, that dense data would allow more reliable recognition of a variety of objects. Additionally, the system was required a great deal of flexibility, in order to provide a moving laboratory that could be mobilized and modified for various applications. Finally, imaging capability was desired for complementing the mapping data capture and object modeling.

The evolution of the sensor integration platform started from a multi GPS-antenna array system (Figure 10) in order to provide the sensor orientation on the basis of computations derived from the data from multiple GPS receivers/antennas. This was mainly due to early demands to build a low cost system. However, it was quickly determined that the requirements for the data quality and accuracy were too high to be achieved with such an arrangement. The size of the platform (2 m × 3 m) was also impractical for everyday use with a vehicle frequently used for other purposes.

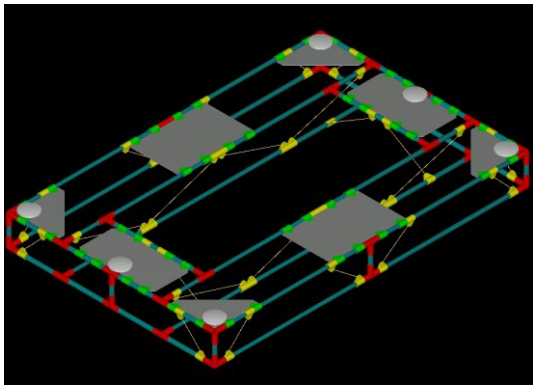

Figure 10. Design of a multi-antenna array platform for mobile mapping.

It soon became obvious that GPS-IMU based navigation could provide the required accuracy level, and at the same time the pricing was decreasing to an affordable level. A NovAtel DL-4plus GPS receiver with GPS-702 antenna and Honeywell HG1700 AG11 tactical-grade RLG IMU navigation system was acquired by the institute, and the integration platform was redesigned. With GPS-IMU navigation, the platform size could be reduced significantly. The first idea was to simply put the scanner upright on a

sturdy plate, tightly coupled with the GPS antenna and IMU enclosure. The first tests were conducted with such an arrangement, but as expected, a more complicated design later evolved.

The third version of the platform was the first to carry the name ROAMER, and the backbone of the design was to build a versatile, multipurpose platform for research purposes, not limited only to city and road mapping. In the end, the main hardware sub-systems integrated in ROAMER included: 1) laser scanner, 2) GPS-INS navigation equipment, 3) camera system, 4) synchronization electronics and 5) mechanical support structure. The first three sub-systems were state-of-the art in their respective categories of performance, and were purchased from third-party vendors. The synchronization electronics was specified and designed by FGI according to the scanner and GPS-IMU I/O specifications, as well as to support synchronization of image data. It evolved concurrently with the system development.

The development of the ROAMER system comprised the hardware integration, data acquisition practices with appropriate calibration development, implementation of the georeferencing processes, as well as system and data evaluations. The research and development resulted in the creation of two distinct MLSs: ROAMER and AKHKA. The ROAMER system is a robust, but adjustable, vehicle-mounted multi-modal system, backed up with camera equipment, whereas AKHKA is a compact personal surveying system. Both systems use the same instrumentation, but the integration platforms differ from one another. The direct georeferencing of ROAMER point clouds was computed using the Waypoint Inertial Explorer™ GPS-IMU post-processing software for trajectory solution, combined with a Matlab software developed in-house, used to produce point clouds from the raw laser points with direct georeferencing. The performance results of these systems are described in more detail in Sections 4.3, and 4.4; results of tests of the usability in different application scenarios are presented in Section 4.5.

3.2.4 FGI MLS test field

The ROAMER and AKHKA systems have been used in numerous studies with a good success rate. To validate the geometric data quality, the performance of the systems has been investigated thoroughly. The geometric accuracy of the different data sets acquired within the scope of various projects has been studied and reported case-by-case. However, it was clear during these projects that MLS data quality was an important issue that needed to be extensively investigated in a well-referenced environment. This need led to the establishment of a permanent urban test field for MLS performance testing. This work has been reported in **V**.

To summarize these efforts, the ROAMER system was deployed in May 2009 to collect the reference laser scanning data, in order to build up a test via stop-and-go scanning capabilities, i.e., performing stationary GPS-IMU aided TLS scans from a vehicle platform at various locations. Altogether 58 scan stations were obtained, where the position of each station was determined by ROAMER's GPS-IMU and further validated against a network of about 150 control points surveyed with VRS-GPS, RTK-GPS and TotalStation, applying corrections as needed. The absolute horizontal accuracy of the reference scan data of the test field was estimated to be around 2 cm, whereas the accuracy of elevation measurements was 3 cm, corresponding to the standard deviation of the collected GCP network (**V**). Figure 11 shows the test field area as generated by the stop-and-go scans.

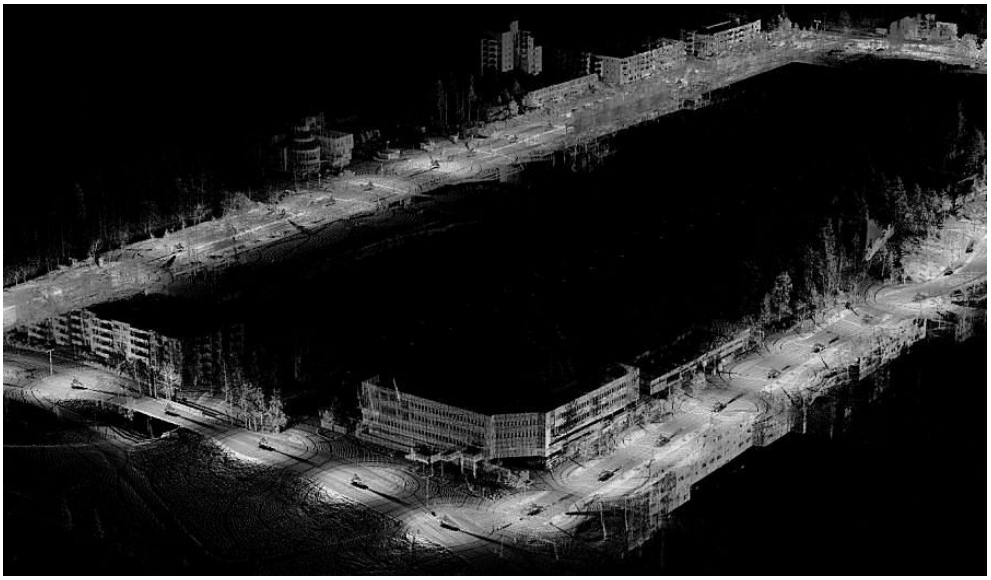

Figure 11. Stop-and-go scans of Espoonlahti urban MLS test field. Image: H. Kaartinen, 2009.

3.2.5 MLS Benchmarking in the test field

For performance testing of ROAMER two versions of the point cloud were analyzed. In the first one, the georeferencing was computed using the calibration values between the instruments determined only in laboratory calibration. The laboratory calibration was based on measuring the physical offsets and rotations between the scanner, IMU and the GPS antenna (see Kukko (2009) for the principles). For the second attempt, the laboratory calibration was fine-tuned using field data, i.e., by utilizing the MLS data acquired by driving the same location in two directions and using some control targets. These fine-tuned calibration values (rotations $\varepsilon_{\text{Roll}}$, $\varepsilon_{\text{Pitch}}$ and $\varepsilon_{\text{Heading}}$ around the IMU axes, R_s^b) were then applied in re-computing the data to produce the second set of point clouds for analysis. (**V**).

The GPS reference station data were acquired from the Finnish VRS network (www.gpsnet.fi). After georeferencing, "dark points" were deleted (to reduce noise and erroneous points) by filtering out points with an intensity value of less than 800 (whole data set ranged from 0–2047, 11 bit). Isolated points (to reduce random stray noise) were deleted by filtering out points that had less than 50 points within a 2 m radius around them. (**V**).

3.2.6 Field target method for MLS calibration

Idea

The procedure of field target method for MLS calibration for ROAMER was described in its basics first time in Kukko (2009). In the procedure, the initial estimates for the boresight angles between the IMU and the scanner axes were determined by direct measurements in laboratory. It should be noted, that even 1 mm uncertainty in the axis end orientation, given that the size of the IMU enclosure of c. 200 mm, leads to a misalignment uncertainty in the order of 0.3°. This translates to about 25 cm error in the point cloud data at 50 meters from the scanner. Therefore, either the laboratory setting must be extremely accurate, which in most cases is impractical, or the calibration must be performed based on the actual field data from the instruments. This would provide a wider span of the targets, but more importantly, would eliminate the need to physically measure the sensor axes at high precision. Thus, the estimation of the angular misalignments was to be obtained from the systematic discrepancies in the observations of spherical targets from the point cloud and field reference data. Errors due to positioning were to be eliminated by observing targets from different sides of the scanner FOV nearly simultaneously and subtracting systematic shifts before solving the angles, i.e., using direction vectors connecting observed target centers. When the positions of the targets and the scanner are known, the misalignments can be determined e.g., iteratively by least squares estimation.

The field target method is based on the following principles (refined from Kukko (2009)):

- A set of spherical targets are set up as gates of two targets, and their positions are determined;
- MLS data is obtained so that the trajectory goes through several of the gates in different directions;
- Targets are detected from the MLS data, fitted with model spheres, and geometric errors are linked to the trajectory based on data timing;
- Calibration corrections for the three rotational misalignments are computed.

As a result, the rotational offsets R_s^b between the IMU and scanner around axes are determined, and the data can be recomputed to obtain an accurate georeferenced point cloud.

Figure 12 shows the typical effects of the angular errors on the target gate representation. The light grey spheres show the correct location of the targets and light blue and red spheres indicate the targets observed by the MLS from two passes through the target gate from opposing directions that are expressed by arrows of corresponding color. In case (a) the heading angle error is to be determined from the horizontal displacement of the targets. However, if the passes differ in direction, but are along exactly the same path the targets are displaced with no distinction (here the red targets are displaced downward for the illustration purpose only). If the target locations were not known the heading angle error could not be determined due to the singularity in geometry. If different paths are used the target displacement becomes different in magnitude, and the heading angle error becomes detectable.

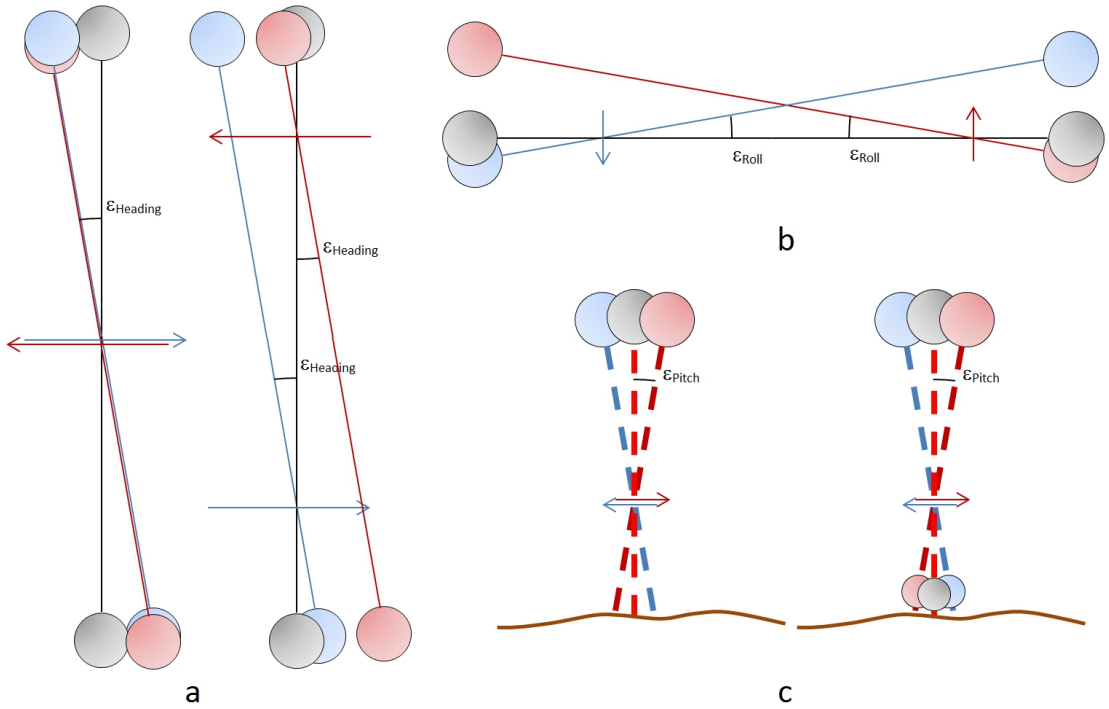

Figure 12. Effect of angular errors in the target gate reconstruction. In (a) the target gate is viewed from top, and where the heading angle error is determined from the horizontal displacement of the targets. In (b) the roll angle error is determined from the tilt in the vectors connecting the target images (view through the gate). In (c left) the pitch angle error could be determined from the along-track component of target error and the stake (tripod etc.) orientation. To help automated computation additional target spheres could be used at close to ground or higher above (c right).

Case (b) shows the principle for roll angle error determination. Roll angle error yields to a vertical displacement of the target spheres, and the amount of the displacement is a function of distance from

the target. This error could also be measured from the tilt of the ground in transects over the point cloud data, where the span of the observation can improve the accuracy, but does not allow automated determination so easily.

Case (c) illustrates the pitch angle error effect, where vertical object gets tilted in the along-track direction of the MLS. The "cross-hairs" formed by the two reconstructions appear at the exact altitude of the sensor suggesting the target placement to be below and above that. Here again, extending vertical span of the gate improves the angular accuracy. A good alternative in urban scene for the target gate would be pair of lamp posts, as they could provide precise localization and spatial extent (width and height) for accuracy, and moreover are automatically detectable from point clouds (Lehtomäki et al, 2011). They may also provide with a control and adjustment scheme for MLS data in general as poles are a typical road asset present almost everywhere. Such approach is yet a subject for a future study.

Experimental setting

GPS-IMU positioning has an upper-limit accuracy of 10–20 mm, so the selection of the gate locations is critical for reliable results. The wider the target gate, the more accurate the angle determination should be, provided that the point resolution is sufficient for detecting the targets with the given setting. Because the translation-offset parameters $\Delta\vec{X}^{s}_{GPS-IMU}$ are considered known from the design of the platform with an estimated accuracy of 2 mm, the three angular parameters can be solved even from erroneous positioning data. However, the performance of the IMU in use has an influence on the achievable accuracy and solution stability in the field.

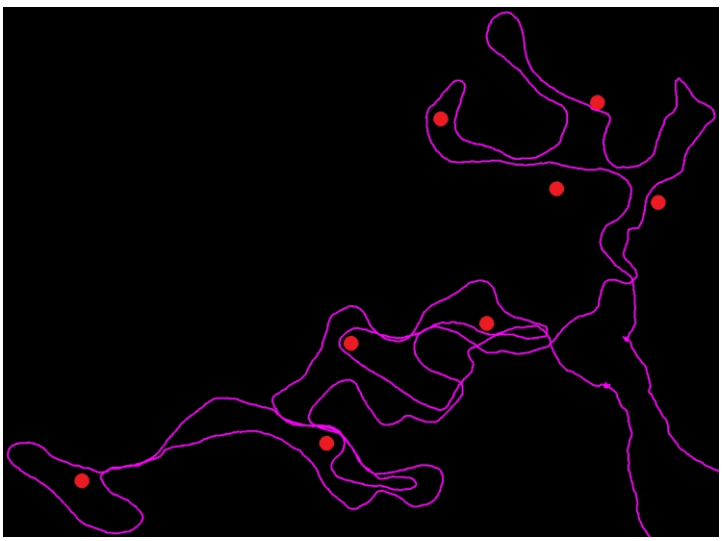

Figure 13. Field target calibration setup for the AKHKA on September 2011. Targets are shown as red points, system trajectory as purple line.

For calibration of the AKHKA system, a bundle of eight spherical reference targets (ATS Scan Reference System), 198.8 mm in diameter, were erected around the study area in Vaisjeaggi bog in connection with the September 2011 data acquisition, in order to assess the quality of AKHKA data in the field. The location of each sphere center was measured using RTK-GPS, which operated with an around 600 m baseline from the GPS base station. According to Bilker and Kaartinen (2001), RTK-GPS can be expected to provide 10 mm + 1–2 ppm (parts per million, scale dependent component) horizontal accuracy and 15–20 mm + 2 ppm elevation accuracy for the target locations. The spheres were also scanned with a Leica HDS6100 terrestrial scanner with a resolution of 0.036° (0.6 mrad, 'High' setting) from three locations to provide internal dimension reference for the target field and also to produce reference data about the ground surface. The TLS scans were georeferenced using least squares estimation, according to the sphere coordinates from the RTK-GPS positioning. The target field setting is shown as red points in **Figure 13** for the September 2011 data campaign.

3.2.7 Statistics for performance analysis

The accuracy of the benchmarked method or system is presented using descriptive statistics of the differences between the reference and the measured values. Root mean squared error (RMSE) expressed in Equation 7 was calculated for MLS planimetric and 3D accuracy in Publications **IV** and **V**.

$$RMSE = \sqrt{\frac{\sum_{i=1}^{n}(e_{1i} - e_{2i})^2}{n}} \tag{7}$$

where e_{1i} is the result obtained with the method or system, e_{2i} is the corresponding measured reference value, and n is the number of samples. Additionally, minimum, maximum, medium, mean, and standard deviation values were calculated. If the observed value differed from the reference value by more than 3×std from the mean value, it was considered as a gross error, i.e. outlier, and removed.

Additionally, the coefficient of determination R^2 was used in **VII** for estimating the reliability of the change detection. This variable is defined by:

$$R^2 = \frac{SS_{err}}{SS_{tot}}, \tag{8a}$$

where

$$SS_{tot} = \sum_i (y_i - \bar{y})^2 \tag{8b}$$

is the total sum of squares, y_i are the values of the data, and $\bar{y}$ the mean of the observed data. The sum of squares of residuals is formulated as:

$$SS_{err} = \sum_i (y_i - f_i)^2, \tag{8c}$$

where f_i is the reference model data.

For MLS system analysis (Publications **IV** and **V**) the analyzed point clouds were first checked by comparing them with the reference data to detect any gross errors either in elevation or plan. If there was a systematic shift larger than of a few centimeters, caused for example by the differences in GNSS base station coordinates, this was compensated for, in order to ensure validity in the comparison. In particular, a large systematic shift in plan can lead to distorted elevation results, and it is common practice to use some ground control points in laser scanning surveys to eliminate this bias. The check points deviating the most from the reference data were checked visually against the ground truth and removed from the analysis if there was any suspicion that the error was due to the target, not due to the system. These errors were mainly detected in the analysis of elevation accuracy, and they could be explained by parked cars or changes in vegetation. Following this 'gross error filtering', systematic errors were removed, separately for easting and northing, and the accuracy values were computed.

3.2.8 Formulation for sensor parameter analysis

The laser sensor arrangement, scan frequency and angular resolution affect the data characteristics greatly, in addition to the obvious surface topographic effects. The scan frequency, i.e., the frequency scan line is repeated with, determines the MLS data coverage and distribution, especially at high platform velocities. The higher the frequency, the faster one can conduct the survey with adequate point density. This, however, requires that the point repetition frequency (PRF) increases with the scan frequency so that the angular resolution within the scan line can be maintained. The platform velocity v effect on the scan line separation D_{sl} was analyzed for selected scan frequencies available on state-of-the-art scanners, which follows a straightforward relation:

$$D_{sl} = \frac{v}{Scan\ frequency} \tag{9}$$

Further, the effects of PRF and scan frequency in providing the particular angular resolution for the scanning system was studied, which is related by the following equation:

$$Angular\ resolution = 2\pi\left(\frac{Scan\ frequency}{PRF}\right) \tag{10}$$

The relation of angular resolution to the ground distance for a given sensor elevation was formulated as follows: The horizontal step increment D_p of subsequent points in a profile on the ground surface, caused by the angular resolution size of increment, depends on the beam direction:

$$D_p = h\,(\tan(\alpha_i + \gamma) - \tan\alpha_i), \tag{11}$$

where α_i is the beam incidence angle (i.e., the angle between the laser beam and surface normal) to the horizontal ground, γ is the angular resolution increment, and h is the sensor elevation from the ground. The incidence angle α_i is a function of horizontal distance from the scanner D and the sensor elevation h:

$$\alpha_i = \operatorname{atan}\frac{D}{h} \tag{12}$$

The effect on point distribution due to turning of the vehicle is prominent for vertical scanning. Turning increases the profile spacing, especially on the outer side of bends, thus reducing the ability to detect vertical objects, such as tree trunks and poles. This, however, depends largely on the scan frequency provided by the scanner and also the rate of turning (deg/s) and the range from scanner:

$$D_{sl} = R * \tan(\frac{Turn\ rate}{Scan\ frequency}). \tag{13}$$

3.3 Summary

This chapter introduced the data and study sites used in the separate studies of this work. The data and sites are diverse and resulted from a variety of applications of the proposed MLSs. The applied methods and experimental setups were also described in brief. The laboratory experiment for the incidence angle study was explained in detail, and an overview on the LS simulator was presented. The development of the proposed MLS systems was summarized discussing the background and evolution of the ROAMER and AKHKA systems. The conduct of establishing a permanent performance test field for MLS use was expressed, and the following benchmarking study and methodology was presented. Further, the principle for the field target method for MLS system calibration was explained. The performance statistics presented were used for MLS data quality analysis in publications **IV**, **V** and **VII**, and are summarized and discussed in Chapter 4 representing results of the calibration and performance studies gained in the separate publications, and introducing further application scenarios. Sensor parameter analysis based on the formulations presented in Section 3.2.8 is conducted in Chapter 5.

4 RESULTS

This chapter summarizes the highlights obtained from the studies in the separate papers of this thesis. Section 4.1 presents the findings in the incidence angle effects on a set of laboratory samples (**I**). Section 4.2 discusses the validation of the LiDAR simulator and its use for MLS system analysis (**II**). Chapter 4.3 describes the current ROAMER system (**III**, **IV**) and summarizes the results from performance testing of the GPS-IMU navigation component (**III**) and performance testing of the complete system and comparison with the state-of-the-art MLS systems on a permanent MLS test field (**IV**, **V**). Section 4.3 also disseminates the results for applications of ROAMER on geomorphological studies on boat and cart platforms (**VI**, **VII**). Section 4.4 presents the AKHKA backpack MLS system and the performance analysis results based on a realization of the proposed field calibration method (**IV**). Section 4.5 discusses the influence of certain sensor parameters on the MLS data characteristics and practical implications. Finally, Section 4.6 presents different applications where ROAMER and AKHKA systems have been utilized and discusses the implications.

4.1 Incidence angle effect experiment

The incidence angle and brightness functions for the brightness tarps and gravel, measured with the Nd:YAG laboratory laser and the FARO LS 880HE80, are presented in Figure 14 and Figure 15. The dependence of brightness on incidence angle is practically negligible for most of the targets at incidence angles up to 20° (and even up to 30° for targets with reflectance < 50 %). For the brightest targets (Spectralon 99 % and the polystyrene target) the decrease in brightness is significant even at small angles of incidence. The incidence angle effect seems to be stronger for the targets of high reflectance, but the effect of other parameters, such as the surface roughness compared to the laser spot size, should be further investigated for quantitative results.

Table 6. Comparison of ALS (TopEye Mk II, 1064nm) and TLS (FARO, 785 nm) Relative Reflectances for 50 %, 20 %, and 10 % Test Targets.[a] (**I**)

Tarp	TopEye 12°	TopEye 18°	TopEye 20°	FARO 12°	FARO 18°	FARO 20°
50 %	0.68	0.68	0.72	0.79	0.79	0.78
20 %	0.36	0.37	0.38	0.24	0.24	0.23
10 %	0.12	0.12	-	0.12	0.12	0.12

[a] The results are relative to the 70 % test target. For the ALS data the incidence angles were 12°, 18°, and 20°, and the TLS data were chosen accordingly.

The effect of surface roughness on brightness variation can be reviewed qualitatively in the 3D structure plots in Figure 14. It seems that features other than surface roughness play a stronger role in the incidence angle effect. For example, the crushed redbrick sample shows strong variation in overall intensity, which is partly due to the large grain size (1–2 cm) compared to the laser spot size (5 and 3

mm for Nd:YAG and FARO, respectively), but the decrease in intensity due to incidence angle is not stronger than that of other gravel with smaller grain size (see Figure 14).

The comparison of the TopEye ALS and FARO TLS data are presented in Table 6. The reflectances are expressed in relation to the 70 % brightness target with the same angle of incidence as the samples. These results are reproduced fairly well at small (up to 20°) angles of incidence.

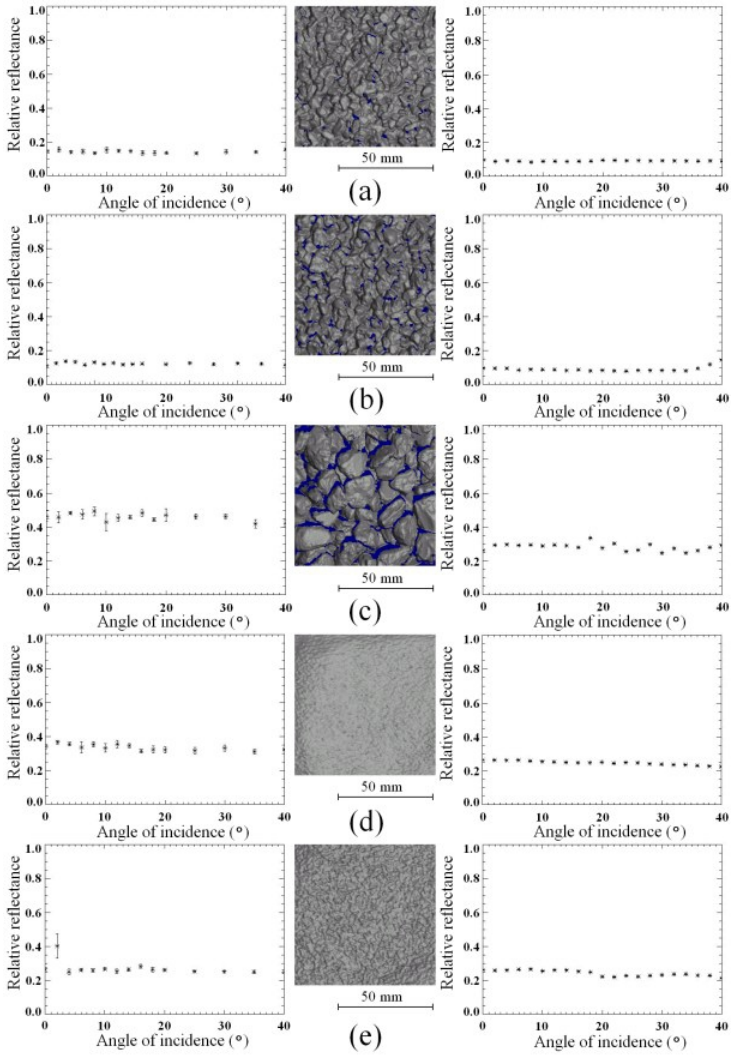

Figure 14. Relative reflectances plotted as a function of incidence angle for the (a) gabro gravel, (b) LECA gravel, and (c) crushed redbrick. Samples in (d) and (e) are from sandblasting sand of two different grain sizes (0:1–0:6 mm and 0:5–1:2 mm, respectively). The left panels were measured with the 1064 nm Nd:YAG instrument and the right panels with the FARO TLS. In the middle panels, the 3D structures of the samples were measured with a Konica–Minolta VI-9i laser digitizer. The sample images are presented at the same scale. (**I**)

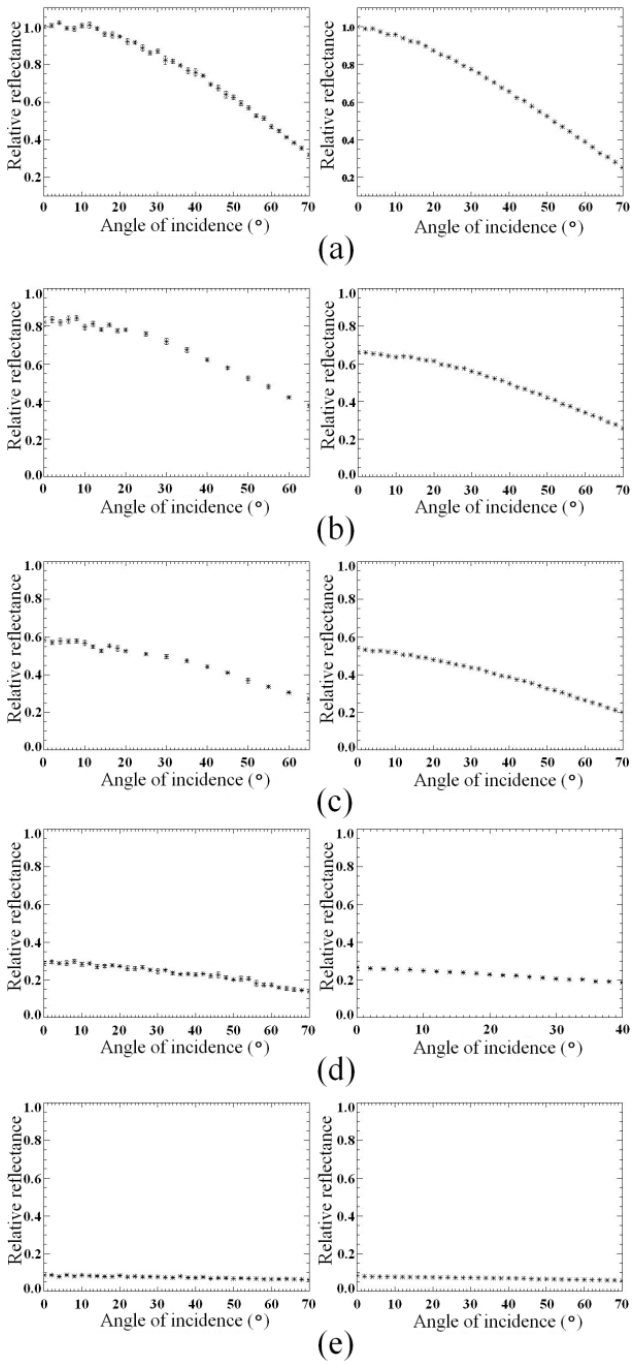

Figure 15. (a) Relative reflectances plotted as a function of the incidence angle for the 99 % Spectralon reflectance target. (b)-(e) PVC brightness calibration tarps with brightness values of 70 %, 50 %, 26 %, and 8 %, respectively. The left panels were measured with the 1064 nm laboratory instrument and the right panels with the FARO TLS. (**I**)

4.2 Simulation performance

4.2.1 Scan pattern analysis for ALS sensors

The simulated laser scanning point clouds were acquired using typical system characteristic parameter values of the three scanners, determining the spatial distribution of the laser beams, pulse transmission, and waveform detection. These parameters are listed in Table 7. The simulated trajectory was produced for an altitude of 400 m and 80 m/s groundspeed, which was kept constant for each simulation. Images captured from the simulated point clouds for the three discussed scanners are presented in Figure 16. Points were colored by elevation, and each image is of the same modeled location. The data characteristics for each scanner type are clearly observable in the images, and the capability of each system to capture objects in along- and cross-track directions is illustrated. The level of detail in the original TopoSys II first pulse data and the environment model was reproduced by the simulation. Some erroneous points can be detected on the walls, as the environment model computation from the laser survey data could lead to false artifacts, the effect of which depends on the grid cell size that has been used.

Table 7. Simulation parameters for the scanning geometry simulation (f_p=Pulse repetition frequency, f_s=Scan frequency, θ_{max}=Maximum Scan angle, D_p=Pulse duration, N_{wf}=Number of wave samples, f_{wf}=Sampling frequency).

Parameter	ALTM3100	TopoSys II	TopEye Mk II
f_p	50,000 Hz	83,500 Hz	50,000 Hz
f_s	70 Hz	653 Hz	35 Hz
θ_{max}	14.3°	14.3°	14.3°
D_p	8.0 ns	5.0 ns	4.0 ns
N_{wf}	128	128	128
f_{wf}	1 GHz	1 GHz	2 GHz

Data validation was carried out by comparing the simulated first echo data to the environment model. Each simulated point cloud was converted into a 20-cm resolution grid, and the elevation value was taken to be the highest point elevation value within each cell. Cells that contained no data points were disregarded, but for all not empty cells, the elevation values were subtracted from the corresponding model elevation values, in order to evaluate the accuracy of the simulated elevation measurements. In addition, this procedure was repeated using first echo data from an independent TopoSys II flight strip (later referred to as reference point cloud) that was not used for the environment model computation, in order to compare the simulated results to results from real field data. The mean values and standard deviations for the elevation differences are presented in Table 8.

Table 8. Elevation differences between the environment model E_{mdl} and simulated and reference point clouds.

	E_{mdl}-ALTM3100	E_{mdl}- TopoSys II	E_{mdl}- Mk II	E_{mdl}-Reference
MEAN	-0.056 m	-0.032 m	-0.377 m	0.160 m
STD	0.537 m	0.776 m	7.38 m	1.85 m

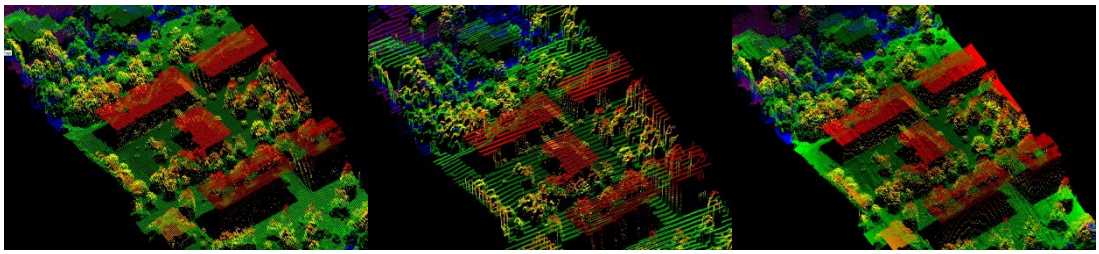

Figure 16. Simulated point clouds for the three scanner types. From left to right: TopoSys II, Optech ALTM 3100 and TopEye Mk II (**II**).

The mean differences reveal that the simulator slightly overestimates the object elevations. For the TopEye Mk II scanner, the overestimation is 5–10 times larger in comparison to the two other simulations for TopoSys and Optech scanners. This could be explained by the differences in scanning operation and especially by the scanning angle, as the data contains much more echoes reflected from vertical objects, such as walls, than the corresponding TopoSys Mk II and Optech ALTM 3100 data. When the wall hits were neglected, the mean elevation difference decreased from 0.337 to 0.066 m with a 0.441 m standard deviation. The results were then comparable to the results from the two other simulated data sets. The elevation differences between the environment model and the TopoSys II reference point cloud show 0.16 m drop for the point elevations in the reference data. Deviation between the real TopoSys point cloud and the environmental model was 2 to 3 times larger than for the simulated Optech and TopoSys data sets. The systematic discrepancy in mean elevation differences for the simulated and reference data sets were due to navigation errors in the reference data.

In Table 9, the results for cross-comparisons between the simulated and the reference 3D point data (TopoSys II) are given. Two regular grids of 20 cm resolution were computed each of the point data, the first to contain the highest point elevation data, and the second the lowest point elevation data, and pairwise elevation comparisons between the corresponding reference and simulated data grids were performed.

The comparisons show that the simulations yield an approximately 0.20 m systematic overestimation in point elevations for both the highest and the lowest point comparison, as the simulated points were found to be a bit higher than the corresponding points in the reference data. When grid cells with a deviation larger than 0.5 m in point elevations (e.g., wall points) were neglected from the computation, the mean elevation difference, e.g., for the simulated TopEye Mk II data was reduced to 0.08 m with 0.10 m standard deviation in comparison to the reference point cloud.

It is also noted that the reference data strip was found to be systematically 0.16 m below the environment model (see Table 3 in **II**), which explains the larger elevation differences between the simulated and reference point data. By eliminating this systematic bias, the mean elevation differences in the point data comparisons closely corresponded to the 0.08 m mean difference of the wall elimination case (see also Table 9). The point spacing and elevation information were comparable to the reference TopoSys II data, noting the observed elevation difference between the reference point data and the environment model used in the simulation.

Table 9. Elevation differences between the reference and simulated data for three simulation cases. Differences were computed for highest and lowest hit grid pairs (High, Low).

	Reference-ALTM3100		Reference-TopoSys II		Reference-Mk II	
	High	Low	High	Low	High	Low
MEAN	-0.24 m	-0.24 m	-0.21 m	-0.29 m	-0.23 m	-0.23 m
STD	1.41 m	1.58 m	1.60 m	1.78 m	1.47 m	1.55 m

In addition to ALS sensor modeling, the simulator was complemented with MLS sensor model that could be used for deriving datasets for analyzing MLS configurations from mobile terrestrial perspective. This case is summarized in the next section.

4.2.2 Mobile mapping system analysis

Figure 17 shows a cloud of points simulated for a SICK LSM 221-30206 2D scanner in mobile use (**II**). The scanner was simulated for a scenario where it is approximately 2 m above the ground and moving with a groundspeed of 11 m/s. The scanning plane was 30 degrees off-nadir, and the maximum range was assumed to be 30 meters. The angular resolution of the sensor was set at 0.5°. A surface model with 20 cm ground resolution was used in the simulation. The mean elevation difference for the highest hit grid was 0.02 m, and 0.05 m for the lowest hit grid, in comparison to the environment model used in the simulation. Standard deviation in both cases was 0.39 m, which can be to a large extent explained by the obvious vertical structures captured by the simulated scanner (**II**).

From the simulation data illustrated in Figure 17, it can be seen how the spatial data distribution changes over the measurement angle: at close range, the number of ground hits is far greater than at distances further from the scanner, where the measurement angle is more than 50 degrees off-nadir cross-track. This effect and it implications for practical mapping is analyzed in more detail in Section 5.3. According to these simulations, the 0.5° angular resolution provided by the SICK LSM 221-30206 scanner was determined to be too coarse for applications requiring detailed models of objects from a distance, such as is typically needed in forest management, terrain analysis, and façade modeling of tall buildings. What can be seen from the simulated data Figure 17 is that details, such as cars on a parking lot and the trees around it, are clearly visible. Shadowing of different obstacles in the scene can be

detected, and such information is valuable when determining the effect of sensor elevation and measurement geometry on the data acquisition and coverage, especially for street mapping purposes.

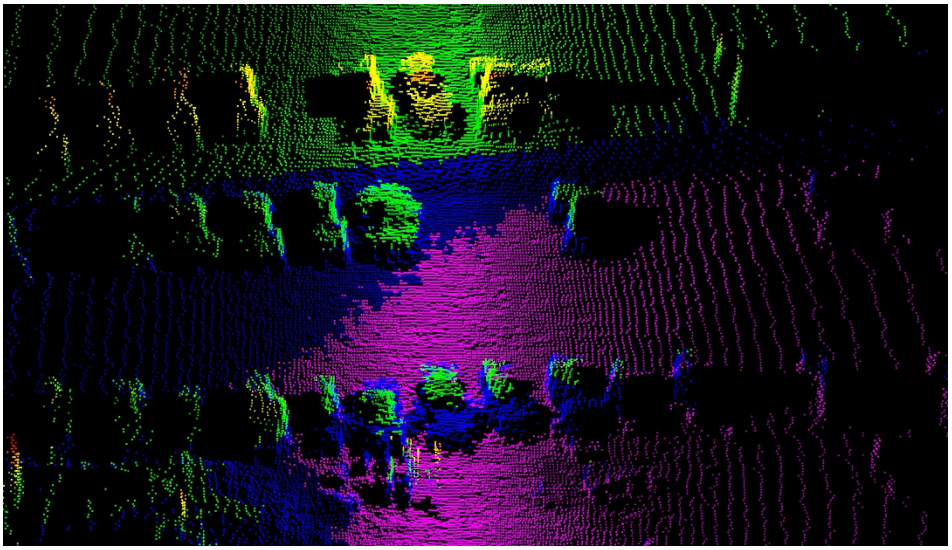

Figure 17. An example of simulated data for SICK LSM 221-30206 2D laser scanner for analyzing the feasibility for mobile mapping (edited from **II**).

Further simulations performed for the MLS platform design indicated a need for vertical and tilted scan lines because the objects to be mapped differ in orientation. The extent of shadows caused by different objects was shown to be largely dependent on the sensor arrangement and especially the sensor altitude. In urban scenes there are two types of objects that caused the majority of shadowing problems: cars and trees. Cars often cause gaps in the ground data, whereas trees often inhibit façade visibility. Thus, the higher the sensor, the less shadowing is to be expected, bearing in mind regulations for the maximum vehicle height. Simulations also indicated the need for high scan frequency, as it can improve the output of an MLS by allowing higher surveying speeds.

4.3 ROAMER

4.3.1 System integration

The FGI‘s ROAMER mobile laser scanning system, seen on top of a vehicle in its latest (Late 2012) configuration in Figure 18, is a high-end surveying device for producing accurate, dense, and precise point clouds (see the following Sections 4.3.2, 4.3.3 and 4.3.4). It can be used to perform three-dimensional mapping for the detection, positioning, modeling, analysis, and monitoring of anthropogenic and natural phenomena and processes. The survey trajectory is measured by a tactical-

grade NovAtel SPAN GPS-IMU system with Honeywell RLG, and typically DGPS approach is exploited. Publication III describes the basic construct and functions of the platform, which is complemented with equipment updates, and more thorough analysis and discussion in Kukko (2009) and Kukko et al. (2009). What was unique at the time of ROAMER introduction (2006) was the use of a high-speed scanner with wide FOV and the possibility to adjust the scanning angle for different applications, an which remains unique approach and has been proven to be effective in practice (**V**; **VII**). The system is also easy to operate in terms of data recording facilities and ease of mounting on different platforms, which is shown by numerous study cases reported in **IV**; **VI**; **VII**; Kaasalainen et al. (2011a) and Zhu et al. (2011).

Figure 18. ROAMER system on a vehicle mount with additional imaging cluster of six Nikon D5100 cameras (Photo: H. Kaartinen, 2012).

The ROAMER integration platform was manufactured of hardened aluminum plates cut in shape and of profile tubes, whereas the scanner socket was stainless steel. Base plate size of the platform is approximately 63 cm in length and width. The scanner head could be tilted around a cross-track aligned axis fitted with high-quality bearing. The height of the scanner origin/mirror is approximately 97.5 cm above the base plate when the scanner is in upright position and 36−57 cm when a negative tilt position

is used. The scanner angles available are: -60º, -45º, -30º, -15º, 0º, 15º, 30º and 90º. The horizontal position (i.e., 0º) provides for simultaneous localization and mapping (SLAM) applications. The total weight of the instrumentation and the platform is approximately 40 kg. The system elevation can be increased 0.5 m or 1.5 m with extensions, as shown in Figure 18 and Figure 30. When mounted on a vehicle the 50 cm stand is typically used to allow better scan angles to the ground and to reduce shadowing.

Table 10 summarizes the current ROAMER equipment and the main data acquisition parameters that are operator-selectable to adapt the data acquisition to different tasks. It is to be noticed that the scanner head has been updated from 880HE80 (2006–2008) to Photon 80 (2008–2009) and later to Photon 120 (since 2010) for improved performance in ranging and scan frequency.

Table 10. ROAMER MLS system equipment and characteristics (2012, **IV**).

FARO Photon 120 scanner ▪ 122000–976 000 pts/s, user selectable ▪ 320° maximum field of view ▪ 3–61 Hz scan frequency , user selectable
NovAtel SPAN GPS-IMU ▪ NovAtel DL-4plus receiver and GPS-702 antenna, ▪ L1 and L2 frequencies ▪ Honeywell HG1700 AG11 tactical-grade RLG IMU ▪ Gyro bias 1.0 deg/h ▪ Random walk 0.125 deg/$\sqrt{h}$ ▪ Data rate 100 Hz
Data recording ▪ Panasonic CF-29 ▪ Scanner operations and recording ▪ Panasonic CF-19 ▪ Navigation system operation and recording
Bi-trigger synchronization ▪ In-house built electronics ▪ Scanning start-stop ▪ Delivers scanner triggers to receiver log pins (1=>2) ▪ Camera triggering x4

The ROAMER system is a DC-powered unit that can operate on battery power for several hours at a time, or when mounted on a vehicle the vehicle's DC system can be used as its power source for continuous operation. The data recording computers are rugged laptops—one for navigation and the other for storing the laser scanning data.

The current laser scanning unit in ROAMER is a FARO Photon 120 that uses a 785 nm laser with a power of 20 mW (Laser class 3R). The laser beam diameter at the beam exit point of the scanner is 3.3 mm and the beam spreads with a 0.16 mrad divergence angle. This results in a laser footprint with a diameter of 20 mm at 100 m distance from the scanner. Combining this with precise range

measurements enables detailed 3D measurements of objects. The highest available angular resolution with a scanning frequency of 48 Hz is 0.3 mrad (0.018°) with PRF of 976 kHz. Using 61 Hz scanning frequency, the corresponding value is 0.8 mrad (0.045°) with PRF of 488 kHz. Ultimately, the point distribution on the object surface depends on platform velocity, surface orientation, scanning angle, and the object's distance from the scanner.

The GPS-IMU unit of the SPAN system produces time dependent/critical information on the position and body attitude at up to 100 Hz frequency. The SPAN system uses the GPS time, and the data acquisition sub-systems need to be coupled tightly with that time frame for exact georeferencing. In order to be able to reconstruct a rigid and correct transformation between the data acquisition systems and the body frame, and especially to get correct attitude and position readings at the exact time single measurement was taken place, a timing mechanism was needed.

A triggering device was designed for the ROAMER to resolve the unmatched signal frequency between the output of the LS and the input capability of the SPAN system. The synchronizer applies bi-frequency divider to separate the LS induced timing pulses into two pulse streams for the timing event logger by sending the pulses into the two channels of the SPAN system receiver. Simultaneously, the synchronizer chip applies a quad-frequency divider, i.e., the synchronization signal frequency from the scanner is further lowered to generate pulses to trigger the cameras. The GPS-IMU and timing data are used in the georeferencing phase to interpolate the trajectory of the system to a data rate provided by the LS to give instantaneous position and attitude of the system for each laser point measured.

The first-generation imaging sensors for ROAMER included two AVT Oscar cameras (Kukko, 2009), which were operated in the first field tests and in the fluvial studies conducted in 2008, as reported in **VI**. These cameras were later replaced with the Pike model cameras from the same manufacturer. The current (October 2013) solution for image data capture is to use six Nikon D5100 cameras with Samyang AE 14 mm lenses to provide a wide-angle field of view for each camera, as well as back- and forward-looking images from both sides. Two of the cameras are oriented upwards so that their FOVs slightly overlap at the zenith.

By upgrading the scanner unit several times, the data needs in different projects and studies have been continually met (**IV**, **V**, **VI** and **VII**). The system performance has been improved by continuing with the development of data acquisition, calibration, preprocessing and analysis processes and updates of the hardware during the course of the past years.

4.3.2 Testing of the real-time GPS-IMU system

In **III** the fundamental performance of the NovAtel SPAN GPS-IMU applied to the ROAMER system was tested using a real-time setup with Differential GPS corrections supplied by a reference station over a GPRS connection. To measure the performance of the SPAN system in a realistic setting, data were collected while driving a route of 18 km, during which the vehicle passed under 4 bridges and multiple areas covered by forest that offered the possibility to test the solution under full satellite outages. Figure 19 shows the trajectory travelled during the test as calculated using the GPS-INS filter. Table 11 shows the quantified position error during the test for both GPS and GPS-IMU solutions.

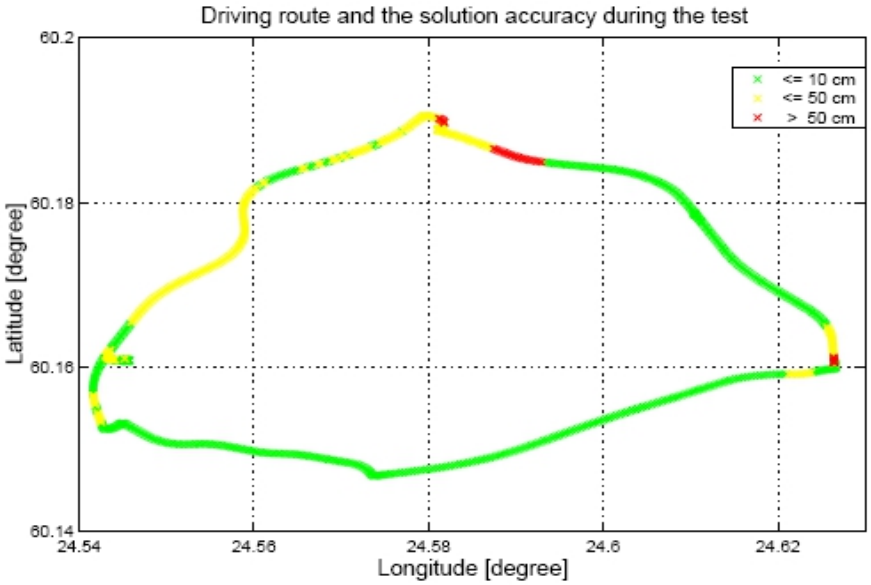

Figure 19. Driving route and the solution 3D accuracy during the test (from **III**).

Table 11. Position Accuracy during the drive test.

Solution type	Positional Error (m)			
	Horizontal		Vertical	
	RMSE	Max	RMSE	Max
GPS-only	3.765	61.980	4.046	57.102
GPS-IMU	0.232	1.043	0.124	0.650

Due to the shadowing caused by the forests and the bridges during the test, as well as the instability of the GPRS connection, the availability of a GPS-only solution was limited. Table 12 shows the solution availability for the GPS-only and GPS/INS filters, confirming that the addition of inertial data results in a more reliable positioning solution. Under the conditions of this test, the GPS-only solution could be

computed for 82.6 percent of the time elapsed. The SPAN-integrated GPS-IMU solution gave 100 % availability, and 60.4 % availability was achieved for the GPS-only RTK solution.

Table 12. Availability of the positioning solution during the drive test.

Solution type	Number of epochs	Percentage of solution
GPS-only	925	82,6 %
RTK-fixed (GPS-only)	677	60,4 %
GPS-IMU	1120	100 %

4.3.3 Benchmarking ROAMER

ROAMER performance was validated using the Espoonlahti urban MLS test field within the EuroSDR MLS benchmarking test, along with several commercial MLSs, such as StreetMapper, Optech Lynx and Riegl VMX-250, and FGI's low-cost Sensei MLS system.

ROAMER data

The data capture for benchmarking analysis was performed with 49 Hz scan frequency and 122 kHz PRF. ROAMER was the only system in this comparison that utilized a laser scanner with a continuous wave laser and PS distance measurements. The beam size of ROAMER's FARO 880HE80 LS scanner was also the smallest of those provided by the systems in the test. The data comprises two independent runs driven clockwise and counter-clockwise around the test field.

The direct georeferencing of ROAMER point clouds were computed using Waypoint Inertial Explorer™ GPS-IMU post-processing software for trajectory solution, combined with a bespoke georeferencing program to couple the laser points to the trajectory. The GPS reference station data were acquired from the Finnish VRS network. After georeferencing, "dark points" were deleted (to reduce noise and erroneous points) by filtering out points with intensity values of less than 800 (whole data set ranged from 0–2047). Isolated points (to reduce random stray noise) were deleted by filtering out points that had less than 50 points within a 2 m radius around them. (**V**).

Accuracy analysis

Two point clouds were produced from the original data using two different set of calibration parameters, and analyzed for ROAMER. In the first one, the georeferencing of the point cloud was computed using the calibration values between the instruments determined only in laboratory calibration. The laboratory calibration was based on measuring the physical offsets and rotations between the scanner, the IMU and the GPS antenna (see Kukko (2009) for the principles). For the second attempt, the laboratory calibration was fine-tuned using field data, i.e., by utilizing the MLS data acquired by driving the same location in two directions and using some control targets and road

objects. The fine-tuned calibration values were applied in re-computing the data to produce the second set of point clouds for the analysis. (**V**).

Figure 20 summarizes the planimetric data quality of the MLSs that participated in the test expressed by RMSE value. ROAMER data outperforms the other studied systems by 30–50 % lesser STD with the fine-tuned calibration (ROAMER II). In contrast, the elevation data accuracy characterized by standard deviation (STD) in Figure 21 shows worse performance of a similar magnitude in comparison to the VMX-250 and StreetMapper data. This was found to be due in part to some systematic roll trend still remaining in the data (**V**). Tables Table **13** and Table **14** show also the number of data points used for error value computations in each case, as well the minimum and maximum values of error.

Table 13. The planimetric accuracy values, in cm, for the tested MLS systems. Driving directions counter-clockwise CCW and clockwise CW. N is the number of reference points.

	ROAMER I		ROAMER II		RIEGL I		RIEGL II		StreetMapper		Optech Lynx	
	CCW	CW	CCW	CW	CCW	CW	CCW	CW	CCW	CW	CCW	CW
N	124	120	136	120	169	178	193	192	190	177	160	160
Mean	3.4	3.5	2.2	1.8	2.3	1.5	1.6	2.0	1.7	1.8	3.2	3.7
Min.	0.4	0.5	0.2	0.3	0.1	0.0	0.1	0.0	0.0	0.2	0.1	0.3
Max.	8.7	11.8	6.7	5.1	11.7	11.7	11.5	10.6	9.4.	9.7	12.3	13.2
STD	1.8	2.2	1.1	0.9	1.7	1.3	1.4	1.5	1.5	1.3	1.8	2.3
RMSE	3.9	4.2	2.5	2.0	2.8	2.0	2.2	2.5	2.2	2.2	3.7	4.3

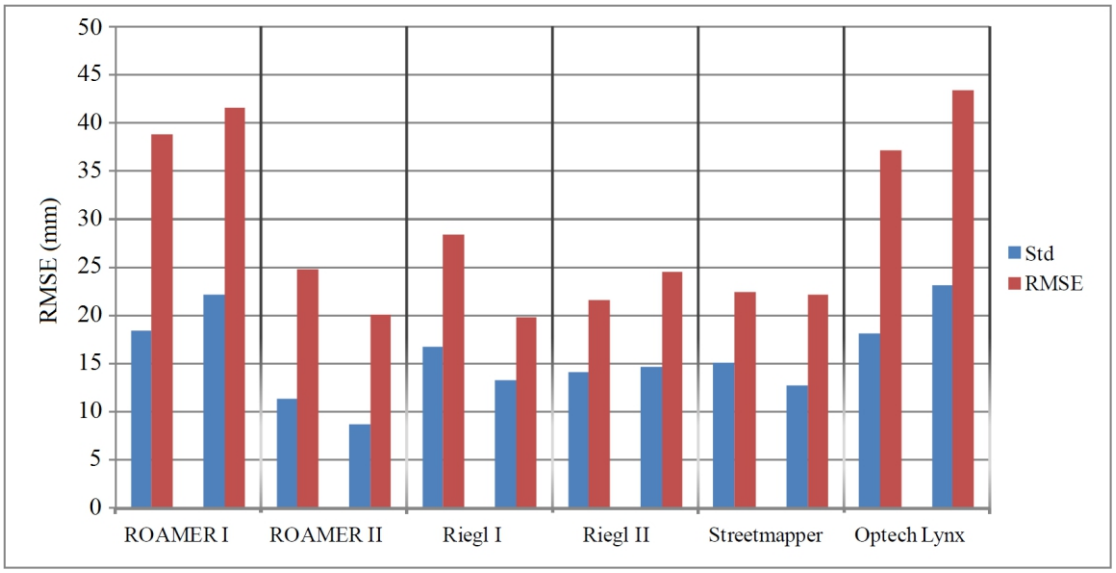

Figure 20. RMSE of the planimetric check points of the tested MLS systems in two driving directions. The left column stands for counter-clockwise, CCW, and the one on the right for clockwise, CW, direction (from **V**).

Table 14. The elevation accuracy values, in cm, for the tested MLS systems. Driving directions: counter-clockwise CCW and clockwise CW. N is the number of reference points.

	ROAMER I		ROAMER II		Sensei		RIEGL I		RIEGL II		StreetMapper		Optech Lynx	
	CCW	CW	CCW	CW	CCW	CW	CCW	CW	CCW	CW	CCW	CW	CCW	CW
N	2936	2946	2819	2816	1418	1450	1566	1600	1585	1585	2970	2549	2693	2527
Min.	-12.9	-17.1	-6.8	-7.5	-11.1	-10.1	-5.7	-5.3	-4.6	-5.7	-5.0	-5.0	-7.1	-6.4
Max.	10.4	12.6	6.0	5.0	14.3	15.0	6.1	4.1	6.5	5.2	5.4	5.1	8.1	9.1
STD	3.9	3.9	2.0	2.0	3.3	2.9	1.2	1.3	1.2	1.5	1.6	1.6	2.7	2.6

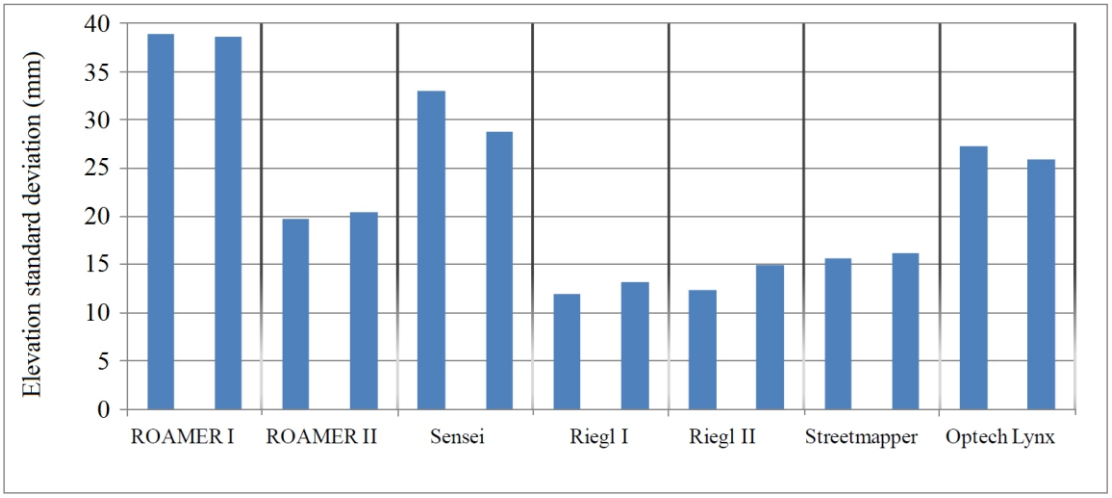

Figure 21. STD of the elevation check points for the tested MLS systems for the two driving directions. The left column stands for counter-clockwise, CCW, and the column on the right for clockwise, CW, direction (from **V**).

From a usability point of view, the along-track scan line density of ROAMER data could have been better, especially when considering the initial object modeling initiative of the project. It could have been increased by applying lower speed in the data acquisition. Should the data be collected now with the current scanner version, which provides higher maximum scan frequency and PRF, the situation would be better in this regard as well.

4.3.4 ROAMER in geomorphological studies

For the beginning of a series of geomorphological field campaigns using MLS, ROAMER was adapted for laser scanning as BoMMS, and the campaign was undertaken on the Pulmankijoki River in August 2008 (**VI,** the latest acquisition on the same site in September 2013). In total, a 6 km long trajectory of the reach was scanned in less than 90 minutes, including the northern part of Pulmankijärvi Lake, resulting in a dataset which comprises 75,000 scanning profiles. Additional data were acquired with static TLS on every point bar of the reach. The TLS scanning took about 8 h. An accuracy assessment

was performed on the data acquired with the BoMMS, and its application for fluvial geomorphology was demonstrated.

The total data coverage of the BoMMS was approximately 0.7 km^2, and it was achieved within 85 min. In addition, system preparation for the first time took about 2 h. One of the mapped river bends was selected for a detailed investigation. The BoMMS scans were conducted from approximately 1.5 m above the river surface, indicating that as the point-bars were virtually flat, the incidence angle of the laser beam increased rapidly with the distance. Thus, the BoMMS data had a number of obscured (or shadowed) areas on top of the point-bar, an area typically located at the inner bends of a meandering river, as well as in the chute channels and opposite sides (laser profiles) of the dunes. The BoMMS scanning profiles showed an along-track spacing of ~0.1 m, while the along-profile spacing varied, depending on the distance between the scanner and the scanned object. This allowed accurate calculation of the point-bar volume above water surface, as well as acquiring detailed point-bar topography on a scale of tens of meters. Volume of the point bar above the water surface at test site A was calculated to be around 9500 m^3 (See **VI** for details).

The BoMMS and static TLS data were compared by cropping an area from one bank, which was 10 m wide and 160 m in length (for location, see Figure 1B in **VI**). A TIN (triangulated irregular network) surface was created using the BoMMS data points. The height deviations between the TLS points and the BoMMS surface were computed and an accuracy assessment was undertaken. Elevations for 80 % of the TLS points were with 0.02 m of the respective BoMMS elevations, and 96% were with 0.05 m. Only 0.05 % of the dataset showed a height difference greater than 0.12 m. The overall standard deviation for the height differences was 0.027 cm. It should be emphasized here that the data used was not adjusted in any way. Some systematic elevation difference was found between static TLS and BoMMS data mainly due to different measuring geometry.

In the 2009 data campaign (**VII**), the ROAMER system was mounted on a cart (CartMMS) and used to complete the mapping for the upper parts of the point bars not reached from the boat. Better data coverage was pursued especially for intensive change detection of five point bars. The applicable operating range of ROAMER varied between 20 and 70 m in the 2009 BoMMS collection, depending on visibility. The scanner was mounted in a vertical orientation when on the boat, and was tilted -60° from the horizontal in the cart application. In the 2009 BoMMS, the enhanced support structure for ROAMER allowed for measurements from a position that was 1 m higher (i.e., 2.5 m from the water) than in 2008 (i.e., 1.5 m from the water), in order to help measure the point bars with a better geometry, and was also used in the CartMMS. This modification increased the data coverage of the measurements on flat point bar terrain, where the observation range of laser beams was approximately five to ten meters longer in 2009 than in 2008. On the non-vegetated point bars, the ground point density was 100–

1,000 points/m^2. The ground point density was much lower (1–30 points/m^2) on the river banks, where the low vegetation was dense and reduced the number of hits returning from bare ground.

Leica HDS6000 terrestrial laser scanner was used to provide reference data for the MLS data verification. The HDS6000 data was acquired with a 'High' resolution setting, providing a point spacing of 6 mm on an orthogonal target at 10 m distance from the scanner. Scan stations were positioned using VRS-GPS. A single 145 mm sphere target was used in order to provide an orientation for each of the TLS scans. The sphere target was periodically moved so that its distance to the scanner remained reasonable relative to the scanning resolution in use, and its location was measured using VRS-GPS. For each scan, the sphere target was detected from the laser data, and a template sphere was matched to the selected points reflected from the target to find its center point. Subsequently, the TLS scans were transformed to global map coordinates, according to the measured scanner and sphere target locations. As a result, the precision of the reference point clouds was better than 1 cm.

Accuracy of the BoMMS and CartMMS for elevation modeling was tested by comparing the DEMs created with the three MMS datasets (2008 BoMMS, 2009 BoMMS, and 2009 CartMMS) with reference points collected using static TLS measurements (**VII**). To validate the data, the reference areas were selected from the three point bars and the neighboring river banks for a more detailed estimation of the DEM accuracy. The areas were close to the shoreline, and the distance from the boat trajectory was about 20–30 m. For the CartMMS data, test area distances varied between 2–20 m from the MLS trajectories. The point bars were used as a reference to check the quality of the DEMs, which were used for change detection. The river banks were selected for studying how well the ground surface could be mapped in densely vegetated areas.

For the 2008 data, the most accurate DEMs were obtained from the data from point bars, for which RMSE's ranged from 0.055 to 0.176 m, including bias ranging from -0.043 to 0.174 m. Thus, the main source of error was systematic in nature. Also a systematic heading error was found in the data analysis. For the river banks, the corresponding errors were 0.203–0.284 m and -0.225– -0.021 m. From the 2009 data, the accuracy of the CartMMS data (see **VII** for illustration) for the studied point bars had an RMSE between 0.040 and 0.053 m and a bias of -0.018 to 0.024 m. Using the boat-mounted MLS, the corresponding errors for the individual point bars were 0.104–0.122 m (RMSE) and -0.07.2–0.12 m (bias). For the river banks mapped with the boat-mounted BoMMS, an RMSE of 0.157–0.244 cm with a bias ranging from -0.065 to 0.082 m was obtained. It was found in the analysis that clear systematic errors existed in the BoMMS data sets for the study. The source of the error related to the GPS-IMU data and system calibration. After correcting for the systematic errors, an RMSE of 0.030, 0.023 and 0.076 m was obtained for the three study point bars in the 2009 campaign, while the corresponding figures for the 2008 data were 0.046, 0.029 and 0.036 m. (**VII**.)

4.4 AKHKA

4.4.1 System integration

A new approach for MLS was innovated and built to meet the challenges of mobility in marshlands and rugged terrains yet also be suitable also for narrow city passages and indoors. The AKHKA system was designed to be operable by one person as a backpack MLS solution. The backpack platform was expected to be ideal to provide the required mobility in such environments yet maintain the high performance 3D surveying capacity with the same sensors and navigation equipment as used in ROAMER (**IV**).

In AKHKA the scanner head is mounted directly under the IMU unit to allow robustness and ease of alignment yet adding only minimum weight to that of the sensor equipment itself. Thus the scanner points downwards roughly to an angle of approx.. 40 degrees, depending on the operator's pose during the survey. It provides cross-track profiles as shown in Figure 22.

Figure 22. The AKHKA system (Image: H. Kaartinen, 2012).

The AKHKA backpack MLS system was first used in 2011 for mapping of permafrost palsa landforms (palsas are low, often oval, frost heaves occurring in polar and sub-polar climates, which contain permanently frozen ice lenses.), but it was also used as part of the continuum of fluvial studies described earlier (**VI**;**VII**). The mapping performance of AKHKA is essentially equal to that of ROAMER, as the sensors are the same (see Table 10); only the integration platform differs.

Since its introduction, AKHKA has been successfully operated in numerous projects, the largest of which included 30 km of total trajectory completed in three days in March 2012 for topographic mapping a section of Rambla de la Viuda, mostly dry river bed in located in Valencia, Spain. For this particular study, the power unit was modified to provide more stable voltage for the scanner, which improved the synchronization performance and was also later adopted for the ROAMER. 61 Hz scan frequency and 488 kHz PRF were used for the data collections. The mobility of the backpack platform could outperform the vehicle MLS in many applications. Irregular terrain characteristics and fluvial features could be mapped comprehensively with only minor shadowing holes in the final data over the about 7 km long reach.

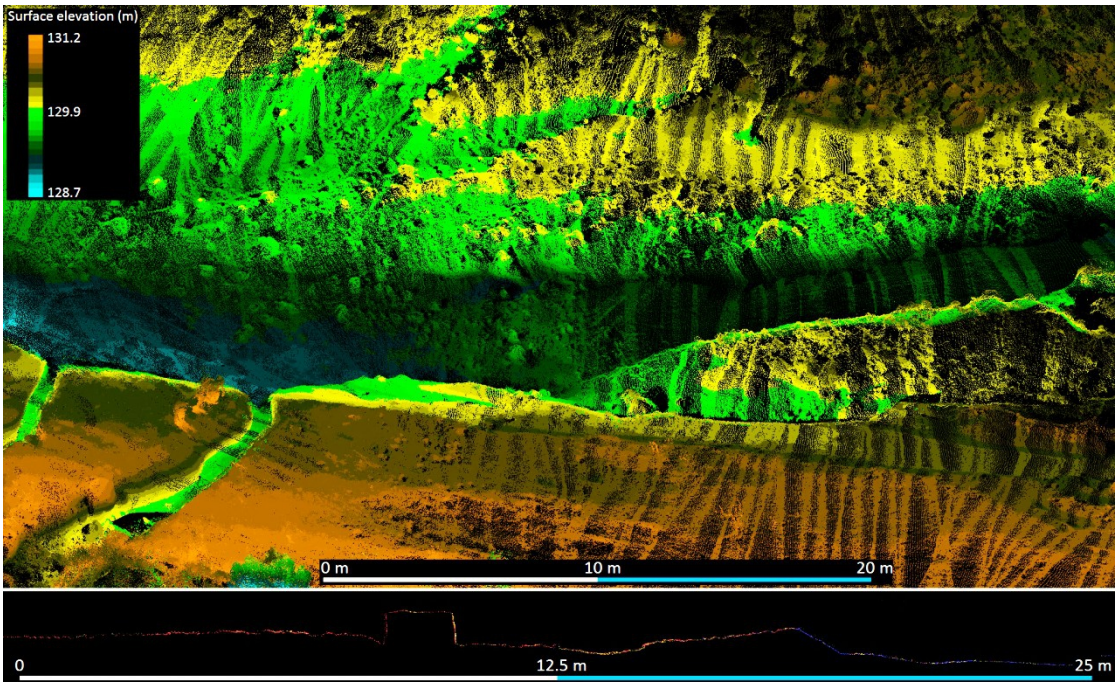

Figure 23. Microscale topographic data collected with AKHKA. Terrain elevations are represented as color tones, the lower part expresses a transect of data to illustrate the accuracy and level of detail.

4.4.2 In situ performance of AKHKA

As the AKHKA system was built for operative field use on environments usually lacking geometric objects such as lamp posts etc., the performance analysis was based on an in situ target geometry test. This test was done as part of development of a boresight misalignment calibration approach based on principles proposed in (Kukko, 2009), and was reported first in (**IV**). For such analysis a set of eight white and round sphere targets were mounted on top of the palsas and located using RTK-GPS. The MLS data collection was performed so that the targets could be detected from both sides of the trajectory nearly simultaneously, i.e., target gate, to be able to determine angular misalignments. The targets and the survey trajectory are plotted on top of the point cloud data in Figure 25.

The calibration of the data was based on system design as for the translations $\Delta\vec{X}^{s}_{GPS-IMU}$ (see Eg. 3). The sensor to body rotations R^{b}_{s} were considered to be the systematic part of the target gate misalignments found in the MLS data when compared to the RTK-GPS reference target locations. These rotational misalignments were determined using the proposed target gate approach (Section 3.2.6).

The internal precision of the AKHKA system was analyzed against the target spheres whose locations were extracted automatically from the point cloud data each time the spheres were detected in the field of view of the scanner. A model sphere 198.8 mm in diameter (SRS targets by ATS) was matched by least squares estimation to the point sets to solve the target center location each time the MLS passed it. The purple line in Figure 24 shows the survey trajectory, and the green lines connect the targets, indicated by the red dots, to the trajectory locations from where they were detected. Otherwise, the coloring in the figure indicates point elevation. After removal of the systematic errors (−0.003 in E, 0.006 in N, and 0.018 in h) found by comparing the coordinates of the sphere locations to the RTK-GPS, the RMSE for all the targets was 18 mm in the horizontal plane and 29 mm in elevation, or a total of 34 mm in three dimensions. These values correspond closely to the result for the ROAMER benchmarking case, showing even slightly better performance. However, shorter scanner-target distances may have an effect on this.

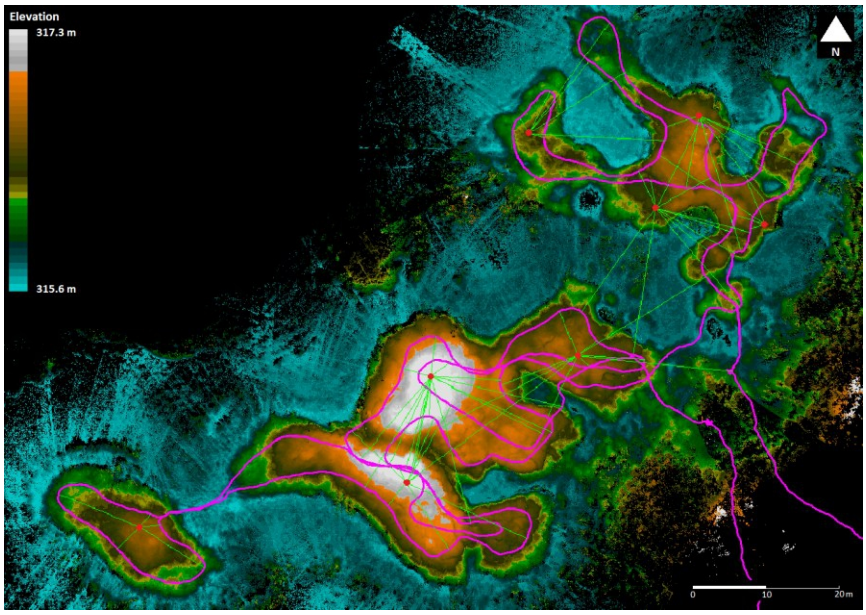

Figure 25. The field target arrangement for the calibration and geometric validation. Spherical targets (red dots) are connected with green lines to the trajectory (purple line) locations, from where they were seen by the scanner (from **IV**).

In this study, the target-to-scanner distance varied from 1 m to 20 m, being 9.7 m on average. In general, the error figures show good agreement internally, as well as in absolute terms, to the expected RTK-GPS accuracy levels of the target locations. The results are also consistent with the error estimation reported for the test field case with the ROAMER data. From the trajectory plot, it can be seen that the target gate approach was not fully exploited: the number of straight portal passes is less than what could have been achievable with the setting.

4.5 Applications

In this section the usability of the developed MLSs is demonstrated through results from different application scenarios, where they have been extensively used to collect 3D data point clouds for various modeling and monitoring tasks. The developed MLS systems (ROAMER and AKHKA) have been used in numerous small development projects, as well as in large area mapping projects in many fields of research, showing the feasibility but also the limitations of the developed systems. The applications scenarios are summarized from the publications included in this thesis, i.e., **IV**, **V**, **VI** and **VII**. Further discussion and references to other publications, as well as the latest, previously unpublished examples, are given later in Section 5.5, in order to show the full potential of MLS.

4.5.1 Urban assets and city models

The most prominent use of MLS is urban asset mapping, including roads, etc. In these environments, the usability of MLS outperforms any other methods in terms of mobility, safety, and the level of detail and coverage. For example, the data from Keilaniemi shown in Figure 26 was captured in approx. 2 hours including GPS-IMU initializations covering an area of roughly 1.4 × 1.1 km^2 including all the streets and drivable passages, such as parking lots and small alleys. In this case, 49 Hz vertical scanning at 122 kHz PRF was used to capture even 100 m tall building façades. A closer view of an office building in the area is illustrated in the bottom of Figure 26, where the level of detail in the data can be clearly seen. What is not covered with MLS data are the building roofs and other surfaces with parallel orientation to the laser plane. Such data contains the accurate dimensions and orientation of objects, and the high point density allows for interpretation of the objects visually and, more importantly, for automated processing of building model data.

Zhu et al. (2011) describes processing of ROAMER laser and image data from the Tapiola shopping district into a virtual model, as seen in Figure 27. There ROAMER was mounted on a trolley in order to map the pedestrian areas of the study site. Vertical 49 Hz scanning and 244 kHz PRF was used in this case, resulting in 162 data blocks, totaling around 340 million points. Slow movement of the platform resulted in high-density MLS data, which together with additional imagery provides an excellent tool for generating geometrically correct virtual reality models.

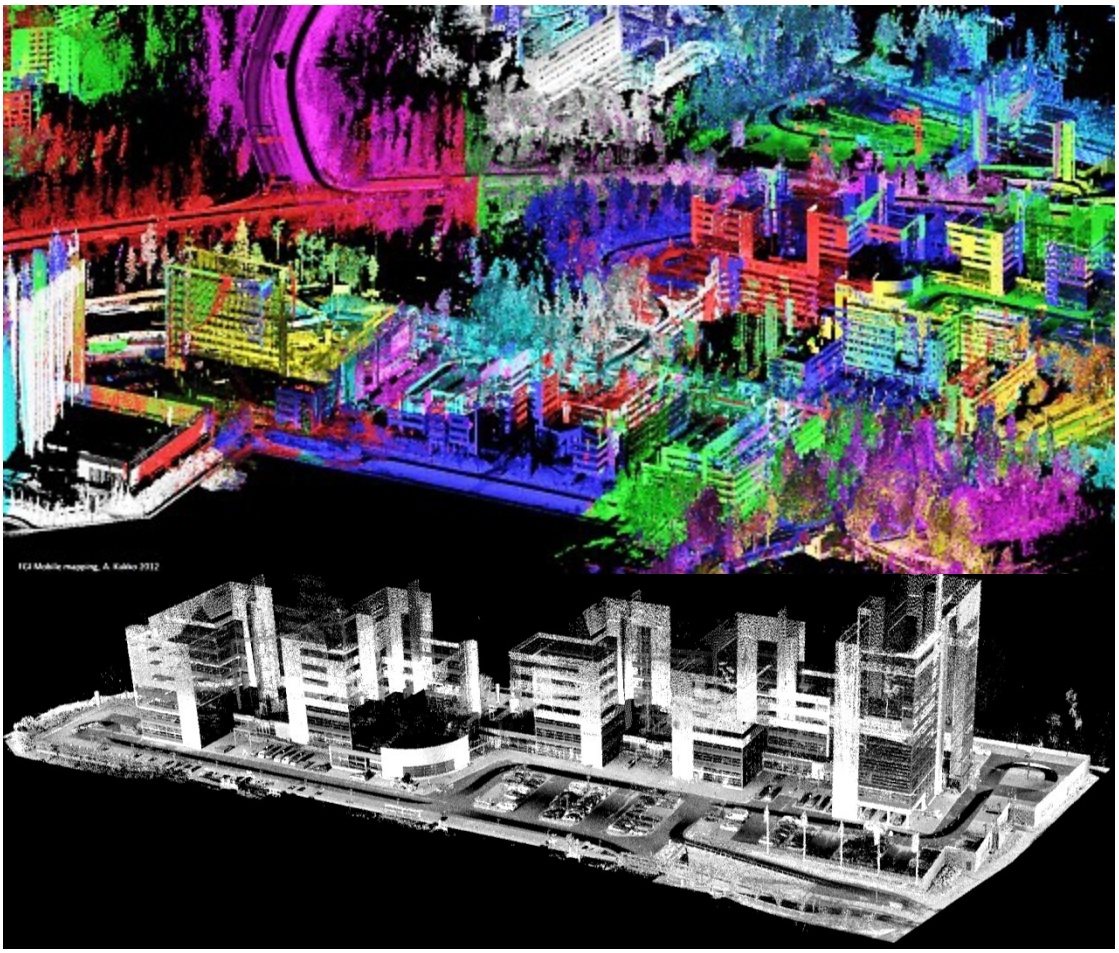

Figure 26. Top: ROAMER data from an urban scene. Different colors show the data block division, whereas the tone is from the intensity records. Bottom: An office building captured as a point cloud with intensity coloring.

By combining automated methods for geometry reconstruction and assistive software for texture mapping, photorealistic 3D models of the Tapiola area were produced. The results met the objectives of producing a model with reliable accuracy, good visual appearance, and small data size. The model was tested on a mobile phone platform for pedestrian navigation, allowing rapid rendering and continuous navigation, which were realized due to small model sizes. Despite the limited GPS signal availability in this urban area, the model accuracy was found to meet the navigation requirements. However, the adopted approach for complete model reconstruction is a combination of automated algorithms and manual operations and herefore the efficiency is relatively low. There are two main issues which have great influence on the efficiency of 3D model construction. First, the quality of the results from automated process affects the work load on manual correction. Second, texture preparation in its current state requires a lot of effort to clean the building textures for undesired object projections.

Use of this type of models is expected to expand in the fields of 3D pedestrian and indoor navigation, interactive marketing and information services, and also as part of geoinformation systems for emergency and maintenance services.

Figure 27. Interactive virtual model of Tapiola built using ROAMER MLS data (Image: A. Jaakkola, 2012).

Finally, Figure 28 shows a dataset collected with AKHKA of an old foundry parcel to be renovated and upgraded into a studio and apartments. In this case, the surroundings of the parcel and the building were mapped within a half an hour, using 49 Hz scan frequency and 244 kHz PRF. From such data different structures and dimensions can be extracted for architectural and structural planning, as well as manufacturing of building parts such as window frames.

In this particular case, the indoors of the building were mapped with the MLS as well in order for the system performance to be studied, but the data was later found not to have been recorded for an unknown reason. Most probably the cause was the Ethernet connection between the scanner and laptop used to record the data. Otherwise, from a practical point of view the acquisition with the backpack MLS was smooth.

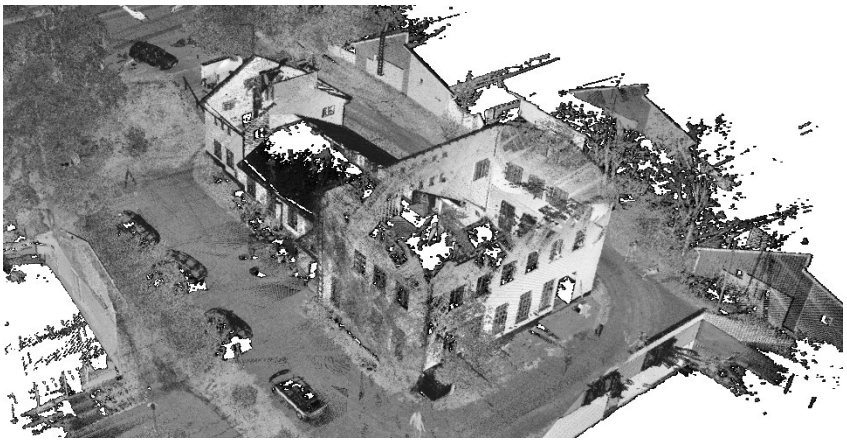

Figure 28. Point cloud data collected with AKHKA for urban renovation.

4.5.2 Road assets

In Jaakkola et al. (2008) the ROAMER data was used to derive road asset data using an automated process. Features included road paintings and curbs attached to the extracted road surfaces. The completeness and correctness of the produced model were assessed using ground reference data obtained using manual classification of the dataset. Based on the intensity image only, it is often unclear where the real road edge should be, and therefore part of the error could be caused by the ambiguousness of the line edges in the reference data. Some short line segments were completely missed because they were too short to be found by the applied feature-based classification algorithm. A zebra crossing and curbstones were identified as expected, and parking space lines were classified correctly where visible. More detailed analysis showed that correctness and completeness of about 80% or better were obtained using the data for the modeling for painted lines, zebra crossings and curbstones.

Lehtomäki et al. (2011) studied the detection of vertical poles from MLS data obtained with ROAMER in two suburban areas, which were scanned with driving speeds of 20 and 30 km/h and with scanning frequencies of 15 and 30 Hz respectively. The areas contained several hundred poles and tree trunks. For the range measurements, 122 kHz PRF and 320° FOV were used. An illustration of the detection capability is shown in Figure 29.

The detection rates were between 69 % and 78 % with targets closer than 30 m to the trajectory for the two test areas. A large portion of the missed targets, such as poles obscured inside vegetation and tree trunks inside branches, had points from objects around the pole or trunk that prevented the algorithm from detecting it, even if the pole or trunk was otherwise easily visible in the data. False detection rates were between 13 % and 19 % with targets closer than 30 m to the trajectory, corresponding to the test

areas. Most of the false detections came from different building structures. The cause for several false detections was the fact that walls perpendicular to the trajectory were not always visible in the data. The visibility could be improved if two or more scanners were used with appropriate configuration. This could also improve the visibility of poles and tree trunks in the data. (Lehtomäki et al., 2011).

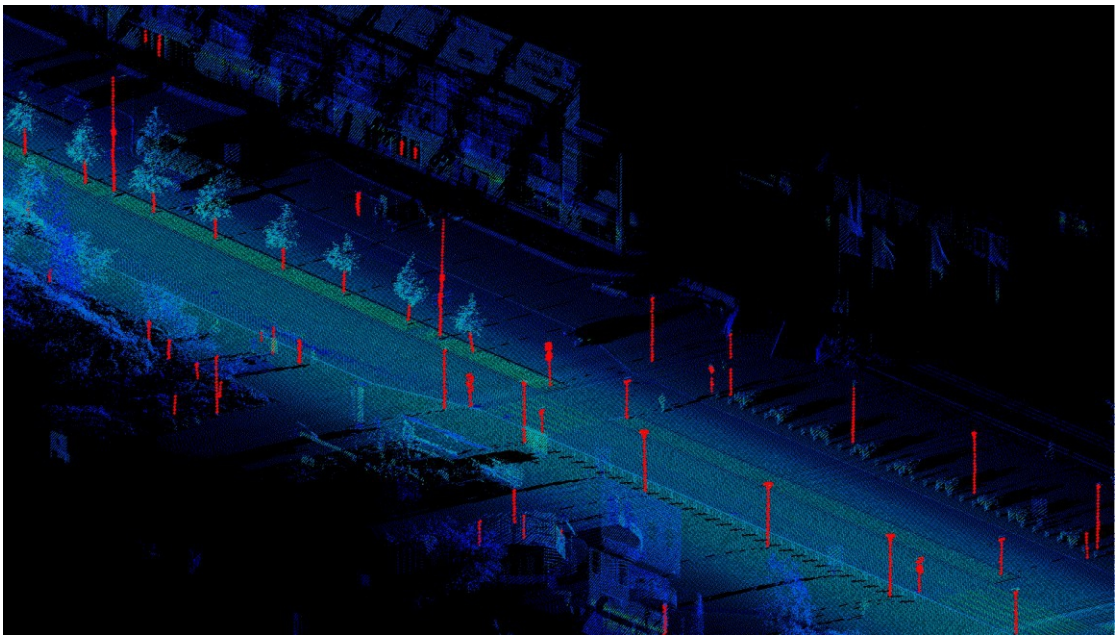

Figure 29. Extracted poles shown in red on top of the original point cloud (from Lehtomäki et al., 2011).

4.5.3 Topographic mapping for hydraulic modeling and geomorphology

In the boat installation, a.k.a. Boat Mobile Mapping System (BoMMS), the laser scanner was elevated approx. 2.5 m above the water surface by means of a stand, and vertical scanning was employed to yield adequate measurement geometry when considering the flat point bar areas. Combined with terrestrial laser scanning data (in the 2008 campaign), boat-mounted mobile laser scanning facilitated a new field mapping approach for fluvial studies (**VI**). The mobile mapping approach proved to be an extremely rapid method for surveying riverine topography, taking only 85 min to survey a reach approximately 6 km in length with typical profile density of 40/m.

In **VII** the use of multi-temporal MLS data on geomorphologic inventories to map changes in riverine topography was studied. A mobile laser scanner mounted on a boat and on a cart was used to detect the topography changes of a selected river reach over one flood cycle. Subsequently, the accuracy and feasibility of the methodology were evaluated.

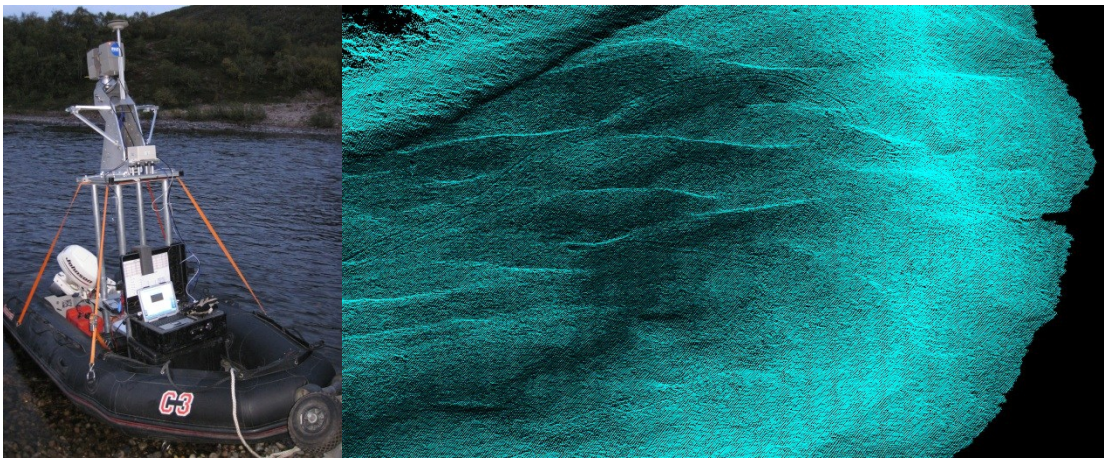

Figure 30. **(a)** A boat-mounted MLS for mapping of fluvial processes; (**b**) River point bar subject to flood erosion and deposition mapped using MLS. Geomorphologic features are easily detected from the dense point clouds.

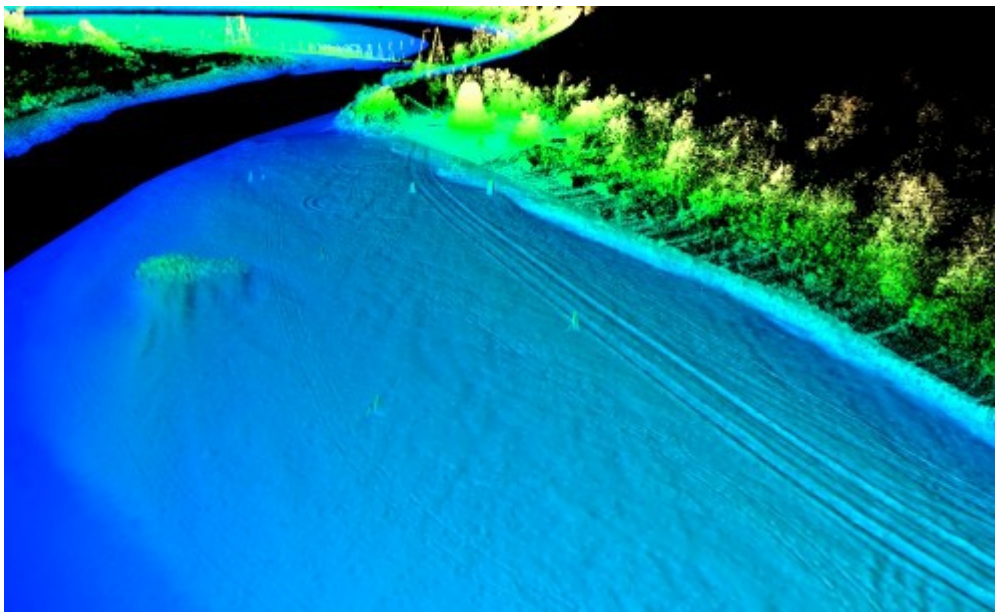

Figure 31. TIN model of a river scene generated from combination of boat and cart MLS data (**VI**).

The MLS data accuracy for the change detection was estimated by comparing the differences in MLS-derived DEMs obtained in 2008 and 2009 with the reference change model obtained with the terrestrial laser scanner data. The square of the sample correlation coefficient (R^2) between the elevation changes was found to be 0.93, and the standard deviation of error 3.4 cm. Volume analysis of the TLS data revealed that the volume of erosion within the study area in 2009 was 12.5 $m^{3,}$ while the deposition volume was 29.9 m^3. MLS data analysis showed similar morphological changes, and the corresponding

values were 11.5 m^3 for erosion and 32.5 m^3 for deposition (**VII**). The small bias in the results may have been caused by a slightly different spatial distribution of the point sets, especially in areas close to the water line, where the changes are more prominent. (**VII**).

The MLS-based change detection possibilities are further demonstrated in Figure 30, where the deposition and erosion areas on Point Bar 2 in the Pulmanki River between the years 2008 and 2009 are mapped. The deposition areas are marked in brown and red colors, whereas the blue tones indicate erosion. The size of the area was 3,100 m^2, and the level of statistically significant change (see e.g., Bransington, Langham and Rumsby 2003; Lane, Westaway and Hicks, 2003; Milan et al., 2011) for the MLS-based DEM of difference was 8.5 cm. The largest changes occurred near the shoreline (see Figure 32). This was also demonstrated with a cross-section over the change map (see illustration in **VII**).

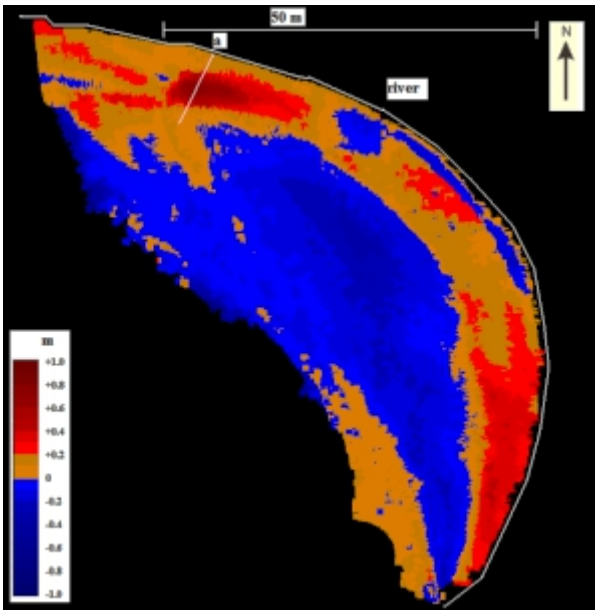

Figure 32. Deposition and erosion areas on Point Bar 2 between the years 2008 and 2009 (from **VII**).

4.5.4 Forestry

Forestry is seen as an important future area of application of MLS for collection of forest inventory data. For such an approach, the performance of MLS techniques have been studied and verified. This includes the performance of the GNSS-IMU system in forested environments but also the feasibility of the laser scanning of trees from a moving ground platform, such as an all-terrain vehicle or backpack. Under evaluation were the scanning geometries and point density, as well as the relative accuracy of the data. Initial investigations on such data collected with the ROAMER system in years 2010–2012 show

that GPS-IMU positioning was the greatest source for error (see Holopainen et al., 2011; Holopainen et al., 2013).

The orientation of the scanning plane has a prominent effect on tree trunk and canopy capture, but more thorough analysis is needed to better understand this relationship. It seems that a tilted plane in conjunction with abrupt movements of the platform, e.g., tight turns, causes problems for the completeness at close ranges, as seen in Figure 33. This can be overcome with vertical scanning, but only at a cost of reduced point density on trunk edges, due to the ratio of angular resolution and scan frequency, i.e., the line spacing gets more sparse at turns as a function of range. This means that tree trunks far away become easily missed. The effect if discussed more in Section 5.4. However, the situation could be improved with an increase in scan frequency, provided that the angular resolution within the profile is maintained by increasing the PRF as well. The relatively slow progress of the ATV on the forest floor in part reduces the effect of moderate scan frequency but also the fact that the platform seldom is vertically oriented when in motion. Abrupt turning of the vehicle causes the profile density to vary significantly in time, reducing the reliability of tree trunk detection. The experiments suggest that the scan plane should be tilted 10-20 degrees.

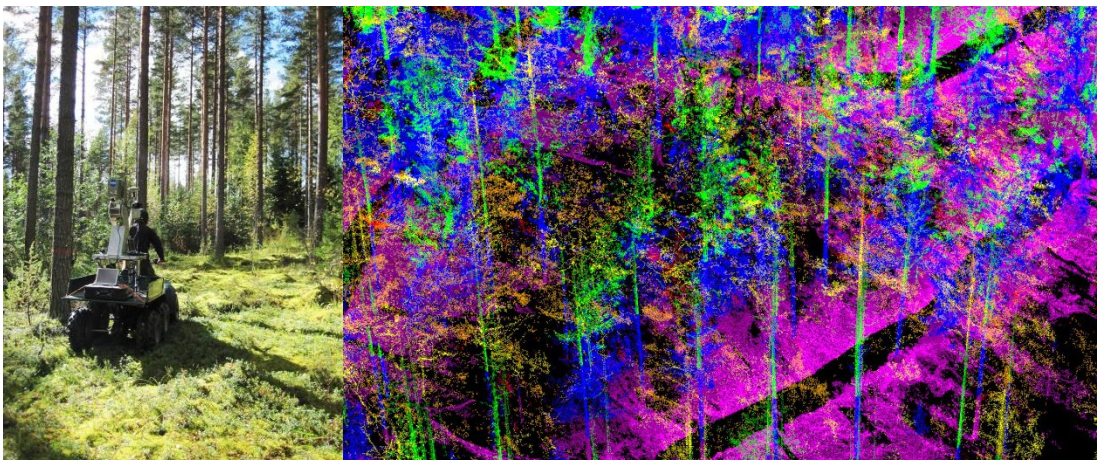

Figure 33. Forest data collection with ATV-mounted ROAMER with vertical scanning, and the resulting preprocessed data. Color tones show the point elevation.

ATV-mounted MLS works well in forests with modestly rugged terrain, which such vehicles are able to negotiate. This improves the usability of MLS in such environments, provided that the equipment is suitable for such operations. The ROAMER system seems to be operable for tree data collection at least in managed forests, where the understory is not too dense for ATV driving. The backpack-based platform might provide data in the near future for more dense forests, e.g., for plot-wise inventories.

4.5.5 Ground elevation modeling for precision agriculture

For certain applications the ground surface is the feature of specific interest. For mobile platforms this can be mapped easily when the ground is bare or the vegetation is sparse. Figure 35 shows an extract of a surface elevation model of an agricultural test field on a fairly flat terrain that is sloping towards a nearby river channel. The MLS data for the study was collected in May 2011 using a trolley platform with 49 Hz scan frequency at -45° scan angle and 244 kHz PRF. Figure 34 shows the original MLS data as a color-coded point cloud, and the scanner trajectory is plotted in white on top of the data. The GPS-IMU initialization and scanning of calibration targets are to be seen from the trajectory in the mid-right of the figure. Each of the 16 rectangular crop plots was covered with one scan line, making the maximum scan angle to be around 20°. With low and sparse crop shoots, the bare ground was easily visible, and the ground detection algorithm performed well in this case. Overlapping data from the target field could be used in calibrating the data for boresight misalignment.

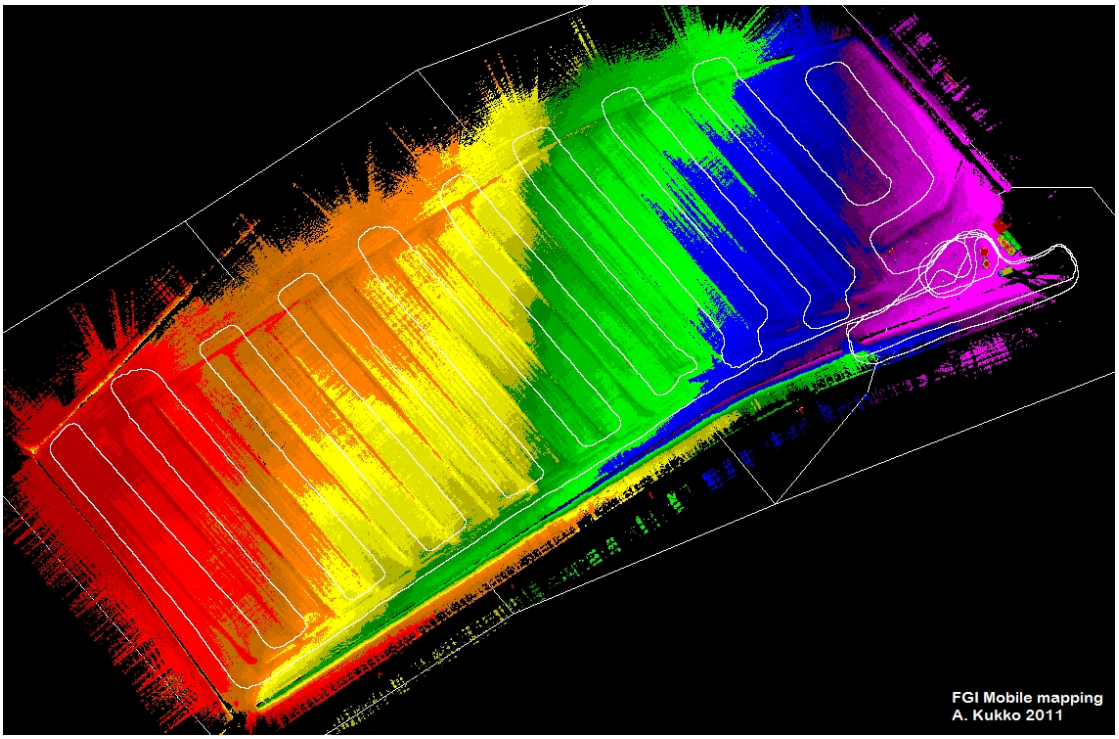

Figure 34. Every 10th point of the original MLS point cloud (elevation scale about 100–104 m) and the scanner trajectory (white line).

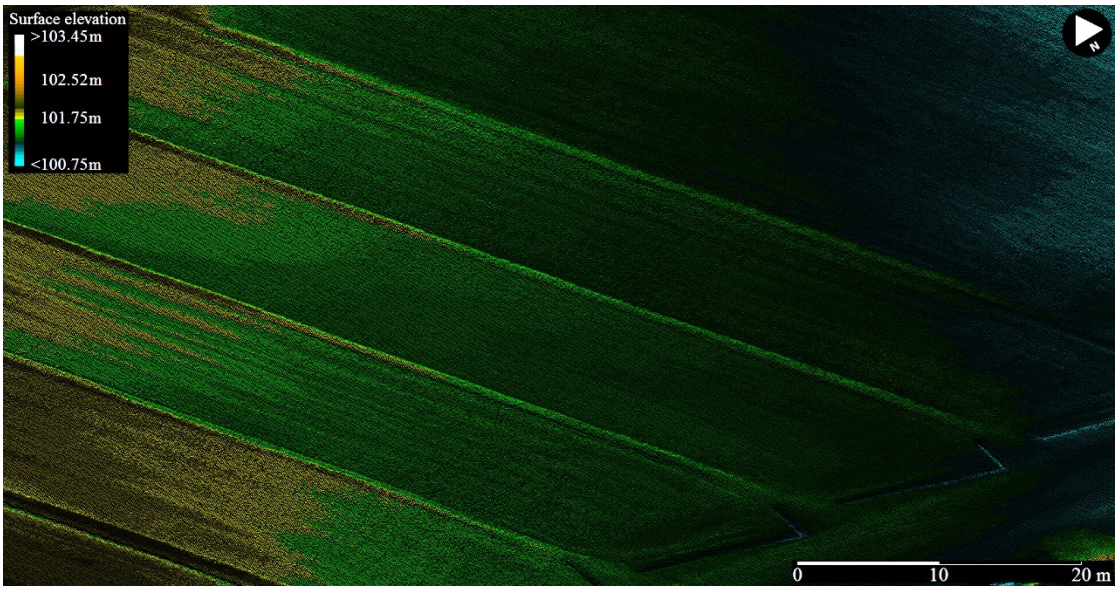

Figure 35. Crop land ground surface topography could be reproduced from the MLS point cloud with a high level of detail (an extract of DEM at 10 cm grid resolution).

4.5.6 Environmental and climate change research

Permafrost palsas and climate change

Palsas are low, frost heaves occurring in polar and sub-polar climates, which contain permanently frozen ice lenses. Palsas consist of an ice core with overlying soil, and often occur in groups. Palsas are characteristically found in areas with discontinuous permafrost, and in such areas they may be the only reliable surface evidence of permafrost. Palsas need large quantities of water for the formation of their ice lenses, and for this reason they occur particularly in bogs. The vegetation of a palsa may comprise low shrubs and lichen in addition to the sedges characterizing the peat. Also, the higher a palsa grows the dryer the peat covering the palsa becomes leading to more insulation which protects the inner core from melting.

The AKHKA backpack MLS system was deployed in June and September 2011 to map a palsa landform area in Vaisjeaggi bog in Utsjoki, Finland measuring of about 50 m × 100 min area. The study aimed attesting the system's operability in such environment and to analyze data feasibility to produce high-resolution multi-temporal DEMs. Such data products are often used for change analysis over long periods of time especially in climate change research. Figure 36 shows the point cloud obtained in June 2011 with coloring for elevation applied after processing. The scanner trajectory is illustrated on top of the point data as a purple line. The point density over the area of interest varied from 1,800 up to 50,000 pts/m^2, with the mean point density being 9,100 pts/m^2.

The geometric quality of the point cloud data was verified against eight spherical targets erected on top of the palsas and located by means of RTK-GPS. Three scans with a Leica HDS6100 were acquired for validation of the data, and these were geo-referenced using the spherical targets. The mean error between the RTK-GPS and TLS data was 15 mm with a standard deviation of 7 mm. The initial analysis of the ground elevation derivation using the AKHKA system was tested against the TLS reference scans. In order to be able to compare the appropriate data, 5 cm lowest hit point grids were computed from both the TLS and MLS data. The lowest hit points were further filtered for isolated points, requiring points to be closer than 6 cm to any of the other points, in order to reduce non-ground points from the analysis. The MLS data were also translated to correct for the systematic shifts found earlier (-0.003 in E, 0.006 in N, and 0.018 in h) for more adequate comparison.

As a result of the analysis, a systematic lowest hit ground elevation shift of 7 mm was found between the TLS and MLS datasets, and the average magnitude of the error was 14 mm. The standard deviation of the elevation error in the data comparison was 16 mm, and RMSE was 17 mm. This shows that the data quality is, in good agreement, considering the non-obstructed GPS visibility in this environment, with the results of the EuroSDR test for ROAMER.

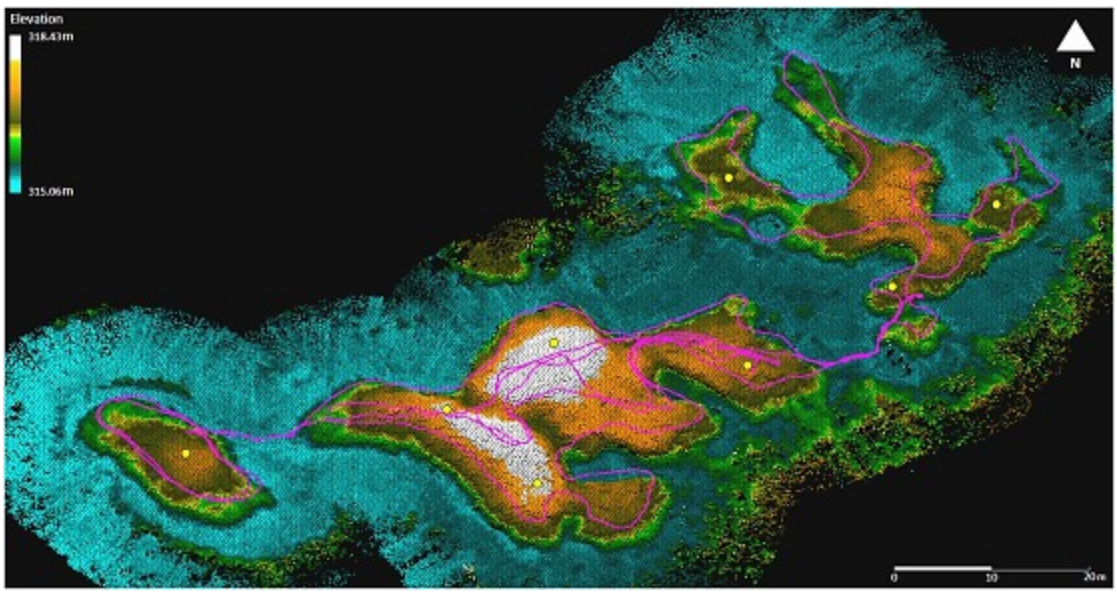

Figure 36. An elevation model with a 20 cm grid size of Vaisjeaggi permafrost palsa landform surveyed with the AKHKA backpack MLS in June 2011. The survey trajectory is represented by purple lines and the control spheres by yellow dots, (from **IV**).

Snow cover characterization

Based on the experience of two seasons during 2010–2011, applying MLS in seasonal snow research appears to be a practical solution and opens up new possibilities for snow surface characterization (see

e.g., Kaasalainen et al. 2011a; Kukko et al., 2013). Mobile laser scanning provides better possibilities for statistical analysis of the snow surface roughness and its impact on surface albedo than do traditional field methods, which are labor intensive and thus often limited in spatial coverage.

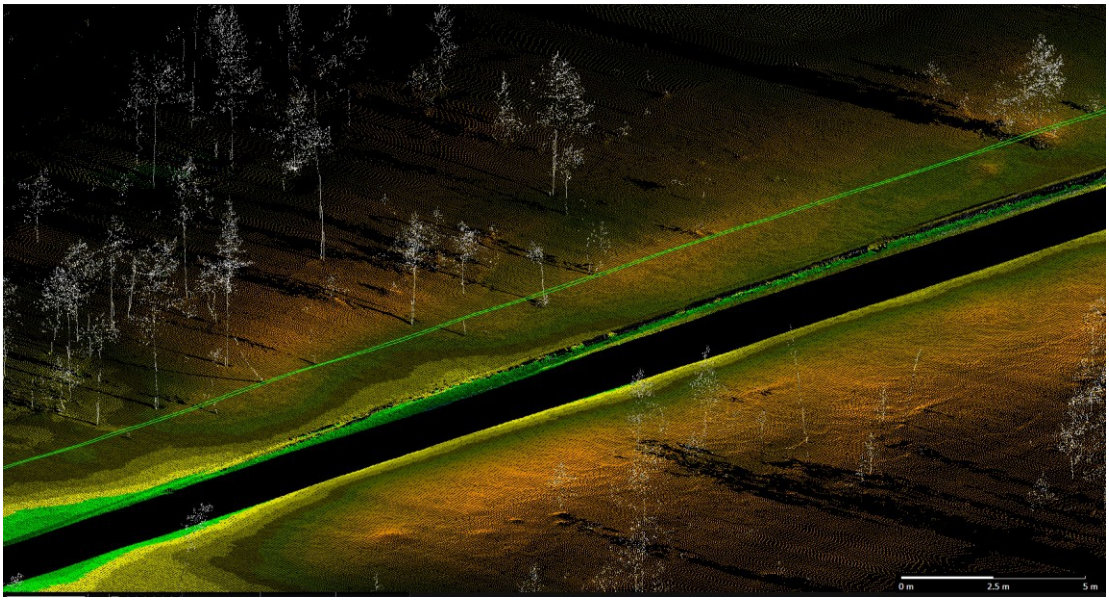

Figure 37. Snow surface and trees detected by classifying the MLS data. Snow surface is colored by point elevations, trees according to the data intensity. The green line shows the scanner trajectory.

Multi-temporal snow surface data enables one to study changes in snow depth (e.g. Kaasalainen et al. 2011a) and snow surface topography and roughness (Kukko et al., 2013). The MLS approach is capable of providing multi-scale data, ranging from millimeter to several meters in the vertical direction and from the centimeter scale to tens of meters (and even kilometers) in the horizontal direction. Horizontal scale is mainly restricted by profile spacing. The evaluation results show that surface shape and roughness modeling at the millimeter scale is possible with MLS data. The most limiting factor affecting the roughness computations is the profile spacing, which is a function of scanning frequency and platform speed. In on-going research, MLS data is being used for computing fine-scale surface roughness in connection with different ground sampling densities and sizes, ranging from centimeters to hundreds of meters (Kukko et al., 2013).

4.6 Summary

Chapter 4 reviews the results achieved in the separate publications of this thesis. The findings regarding the incidence angle effect were presented, and the implications to the development of LS simulator discussed. The simulator was evaluated for reliability with real data, and further used for MLS system

configuration simulations. The development and calibration of two distinct MLS systems were reported, and the feasibility of the systems for data acquisition in different application scenarios demonstrated with evaluations of accuracy performance.

5 DISCUSSION

5.1 Implications of incidence angle effect on LS

The results in **I** indicate that incidence angle effects have to be taken into account when correcting MLS intensities, or LS in general. In there, the incidence angle measurements were performed in a laboratory at close ranges. The decrease in brightness becomes more significant when the angle of incidence increases from 20° up to 70°. For comparison, Ruiz-Cortés and Dainty (2002) found a decrease in the backscatter peak as the angle of incidence increased. In case of MLS, the full incidence angle range from 0 to 90 degrees is often present in allover the obtained data. Compared to ALS, the intensity of MLS can be much more conveniently adjusted, since it is possible to use calibration targets together with MLS surveys, compared to ALS where there are usually no ground teams. Technologies used in Kaasalainen et al. (2005b), Ahokas et al. (2006) and Kaasalainen et al. (2009a) can then be applied in the context of the MLS. The knowledge gained in **I** can also be used to adjust the methods developed for ALS and TLS, as has been reported by Abed et al. (2012) and Krooks et al. (2013).

With correctly calibrated intensity data, it is expected to be able to derive more robust strip adjustment aiding for geometric correction of LS data but also more coherent spectral characterization of objects. This has been studied in the context of ALS and to some extent TLS (Kaasalainen el al., 2008b; Kaasalainen et al., 2011b), but in MLS scenarios this has not yet become a well-established practice. On the contrary, literature review shows that not much progress have been achieved using monochromatic intensity data for object classification. Such breakthrough is waiting for operational multi- and hyper-spectral laser scanners and data to emerge.

However, the hyperspectral measurements enabled investigation of the possible wavelength effects on intensity. The data showed that the intensity level dropped with an increase in the incidence angle, but the shapes of the spectra remained the same. This can also be seen in the 3D spectral images (Figures 5 and 6 in **I**) for linden (*tilia cordata*) leaf, crushed redbrick, and the sandblasting sand targets. There is little variation in the shape of the spectra, even though the intensity level changes as a function of the incidence angle. The results (i.e., the overall trends in intensity) obtained in laboratory measurements are in agreement with those measured with the FARO LS despite the wavelength difference between the instruments. This means that the brightness effects related to laser scanning can be simulated in the laboratory, and the results can be generalized for use in the interpretation of ALS brightness and surface data, as well as their calibration. Although wavelength effects are evident in the data (i.e., the spectra show variation in the brightness of each target in different wavelengths), the overall dependence of brightness on incidence angle is reproduced.

Despite the obvious lack of direct use at the moment, the proposed approach would incorporate the target brightness and roughness, incidence angle and range effects on the model of intensity records, as shown by Jutzi and Gross (2009), Gatsiolis (2011), Abed et al. (2012) and Ahokas (2013). The problem of insufficient level of precision was found already in a study case dealing with sampling of directional scattering from digital airborne HRSC-A images (Kukko et al., 2005). All these factors can be estimated more precisely from TLS and MLS data compared to ALS as target geometry can be reconstructed more precisely. The only limiting factor would be the point density, which may affect the practical range of the approach, and again, at large angles. Such calibration techniques may also allow development of data matching methods, which are demanded for quality modeling.

Beyond the intensity aspect, the incidence angle strongly affects the ranging accuracy of LS, as the shape of the detected echo of the transmitted pulse changes with the angle of incidence, unless proper signal processing algorithms are used, as discussed in Palojärvi (2003) and Thiel and Wehr (2004). It is also expected that the laser scanner data could be further utilized if such sources of variation are properly understood. Furthermore, incidence angle data are essential in improving the waveform generation based on real-world object data for a simulation models of laser scanning as proposed by (Kukko and Hyyppä, 2007; **II**). As systematic experimental data on incidence angle effects are still in sparse supply, the results apply directly to the optical studies of directional light scattering.

In the simulation study described in this thesis, a simple detector threshold was utilized to derive synthetic point data from the simulator generated waveforms. More advanced point discrimination schemes could be employed based on finite differences of numerical derivatives (e.g., the detection of local maxima or the zero crossings of the second derivative), or, more generally, the zero crossings of a linear combination of time-shifted versions of the signal (Wagner et al., 2004). One such approach is the constant fraction discriminator, which determines the zero crossings of the difference between an attenuated and a time-delayed version of the signal (Gedcke and McDonald, 1968). Some of the methods, like maximum, zero crossing and constant fraction, are invariant with respect to amplitude variations, and therefore, to a certain extent, changes in pulse width (Wagner et al., 2004). These methods are usually applied in waveform data processing to take advantage of better performance over the amplitude-dependent discrimination methods. The application and analysis of these more advanced methods in the processing of simulated waveform data are of sufficient interest to be further explored.

5.2 Simulations for LS system analysis

The expectations considering the applicability of simulation for MLS system analysis has been shown, e.g., by Cahalane (2013) and Yoo et al. (2009b), the latter with improved urban scene modeling

compared to the FGI simulator. The data acquired with a hypothetical construct of a mobile mapping platform, or an airborne system, gives an impression of the data properties and thus helps in determining the final construct of the sensor platform. It also provides data for system performance analysis and algorithm development for mapping and modeling purposes.

The proposed laser scanning simulator—and the synthetic waveform and point data it produces—provide a research platform for algorithm development, in order to improve object classification and recognition, and to develop automatic mapping tools for detection of buildings and other structures, as well as natural targets such as trees. Based on waveform analysis, it is clear that the pulse length affects the separation of individual scatterers that are close to one another. In addition, degradation in the ranging accuracy can be expected, due to spreading of the last echo peak. However, the echo peak power seems to slightly increase as the pulse length is extended. Shortening of the sampling interval, i.e., increasing the resolution of the waveform recording enhances the discrimination of close objects, similar to the effect of decreasing the pulse length. Furthermore, the number of recorded samples improves the achievable depth range of the sensor.

Using a simulator, the effects of different parameters (e.g., pulse width, power and shape, detector sensitivity, sampling interval, and target properties) on waveform detection can be studied, as repetitive simulations can be performed while the spatial (especially the trajectory component) and radiometric conditions remain unchanged. This leads to better understanding of the beam interaction with different target surfaces and provides insight into system behavior. The fact that waveform decomposition procedures could be tested and verified using simulated waveform data is also emphasized, since the measuring conditions are computationally traceable.

Since simulation makes it possible to acquire data from an unchanged object with different scanning geometries, it is possible to perform a thorough analysis of the effect of scanning geometry on the quality of laser products. This is usually not possible using real data. Different laser scanners have, in addition to the geometric characteristics, unique properties for pulse transmission and echo detection that lead to different views of the same object. Simulation provides an important insight into waveform data performance and analysis, as well as the possibility to verify the effect of system-specific properties on the resulting data. The related empirical data are insufficient for effective research and exploitation in mapping purposes at the moment. Simulated waveform data fills this gap as a research platform. Further development of the LiDAR simulation method will focus on more precise empirical scattering models of different natural and artificial surfaces.

Compared to the previous simulations described by Holmgren et al. (2003) and Lovell et al. (2005) for small-footprint laser-assisted forest inventory, the results achieved with the proposed simulator and

simulations were promising. Simulation of scanning LiDAR provides a method for studying application-dependent parameters that optimally fulfill the demands of different LiDAR-based mapping tasks. This kind of approach could be used to find relevant system-dependent differences affecting data quality and suitability for desired mapping purposes. Furthermore, the effects of positioning and scanner inaccuracies for point acquisition can be studied by varying the magnitude of these errors. Alternatively, the inaccuracies can be completely omitted, focusing only on LiDAR-dependent sources of uncertainty in the data, as is the case with simulations presented in this thesis. In this way, greater understanding of the particular measurement technique and its properties is possible. Future LiDAR sensor types and concepts could be verified and demonstrated by simulation, and simulated data could be provided to generate awareness in the scientific and user communities and for development of data processing algorithms exploiting such data.

Within the context of MLS, it has been recently shown that simulation can be effectively used for analysis of scanner orientation and location effect on targets. Cahalane (2013) reported, using a simulation system, that high pulse repetition rate is preferable to a high mirror frequency for maximizing point density. Their simulator enables MLS to be configured to maximize point density for specific targets.

Analogous to ALS, the characteristics of the obtained point cloud, e.g., density, point pattern, and distribution, depend largely on the sensor arrangement on the MLS platform, and the sensor properties, such as point measurement rate, scan frequency, and wavelength (**II**; **IV**; Kukko, 2009; Yoo et al., 2010; Cahalane, Mc Elhinney and McCarthy, 2010). Different layouts and approaches have been analyzed by simulations (Yoo et al., 2009ab; Kukko and Hyyppä, 2009) and implemented and reviewed in numerous papers, e.g., (**III**; **IV**; **V**; **VI**; **VII**; El-Sheimy, 2005; Gräfe, 2007ab; Hesse and Kutterer, 2007; Kukko et al., 2009; Petrie, 2010; Yoo et al., 2010;). Some of these systems use only one type of sensors for data acquisition, but more and more systems are becoming equipped with multiple sensors. Barber, Mills and Smith-Voysey (2008) have updated the list of operative MMSs originally presented in Ellum and el-Sheimy (2002) up to year 2007. Since then, several commercial systems with LiDAR as the prime sensor have emerged (see also Tables Table **1** and Table **2**), and the number is increasing.

5.3 Influence of sensor parameters on data characteristics

There are some principal factors defining the performance of an MLS system. These include the performance of the scanner, sensor geometry and the field of view of the scanner. The most prominent components are the general arrangement of the laser sensors on the platform, scan frequency and angular resolution, which together affect greatly on the data characteristics, in addition to the obvious surface topographic effects. Figure 38 plots the relation of angular resolution to ground distance for a

sensor standing 2.5 meters above a flat ground surface. The point separation increases rapidly with the distance from the scanner. In reality, small irregularities in the ground topography have local effects on the point distribution; larger surface roughness causes increasing shadowing with large beam angles. This has an effect on ground determination in particular from the MLS data but also influences façade detail detection from tall buildings as well. The effect could be reduced to some extent by increasing the sensor elevation, but there are obvious limitations to this in practice. From Equation 11 (plotted in Figure 38), it can be determined that the practical range for 1 meter point separation is limited to about 20 meters for a 5 mrad system but extends to 60 meters for a 0.65 mrad system. In practice, vegetation and other environmental features further limit the visibility of the ground surface at large beam angles.

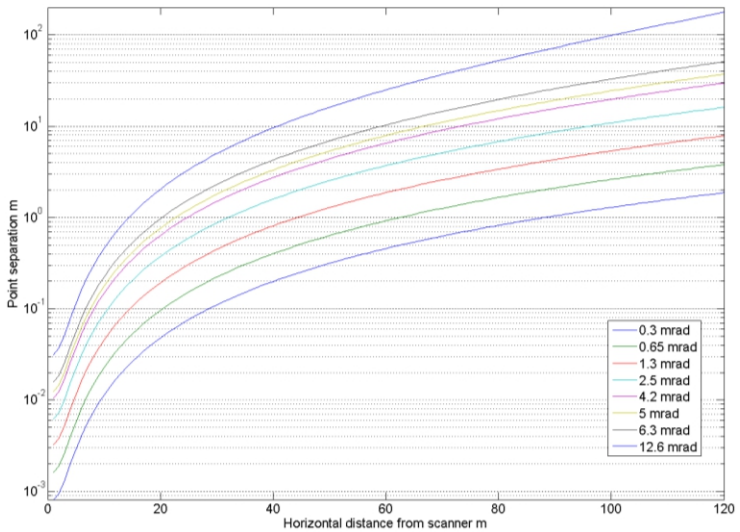

Figure 38. Ground distance effect on point separation at some sample angular resolutions. Sensor elevation at 2.5 meters above ground; applies also to a vertical wall at equal distance.

The effect on point distribution due to turning of the vehicle is more prominent for vertical scanning. Vehicle turning increases the profile spacing especially on the outer side of bends, thus reducing the ability to detect objects with vertical characteristics, such as trees. This effect, however, depends largely on the scan frequency provided by the scanner, as well as the rate of turning and range from the scanner (Equation 13). All in all, a higher scan frequency improves the data usability in both scanner configurations.

The scan frequency determines the MLS data coverage and distribution, especially at high platform velocities. The higher the frequency, the faster the survey can be completed while maintaining similar point density. This, however, requires that the point rate increases with the scan frequency so that the angular resolution within the scan line can be maintained. Figure 39 shows the effect of platform velocity on the scan line separation (see Equation 9). Figure 40 shows the effects of PRF and scan

frequency on angular resolution (see Equation 10). For highly detailed modeling, 5000 points per profile (i.e. 1 mrad angular resolution) requires 1 million pts/s at 200 Hz scan frequency. This is not possible with HSToF scanners, and even the scan frequencies provided by the current UHSPSs typically cannot reach that high (Z+F Profiler 9012 has a 200 Hz scan frequency, but no MLS has been built using it yet). In this regard, however, the UHSPS scanners have a slight advantage due to higher PRF capability, as the platform velocity can be adjusted according to the data specifications to compensate for the scan frequency deficit.

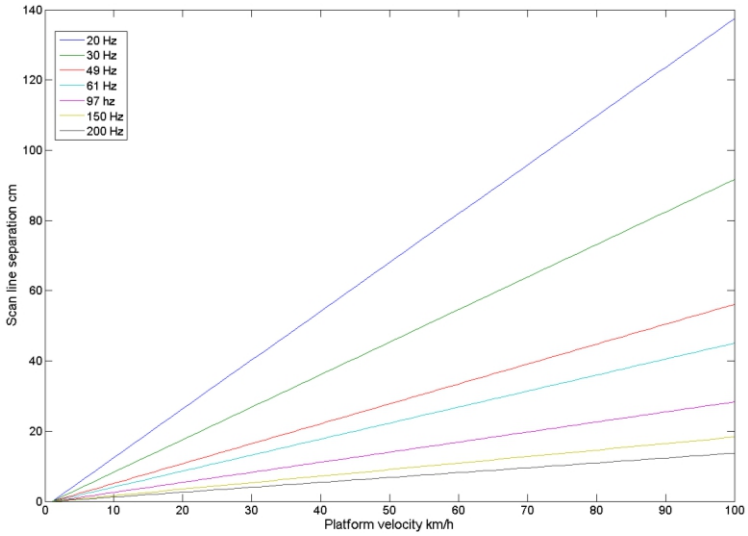

Figure 39. Platform velocity influence on scan line separation at selected scan frequencies.

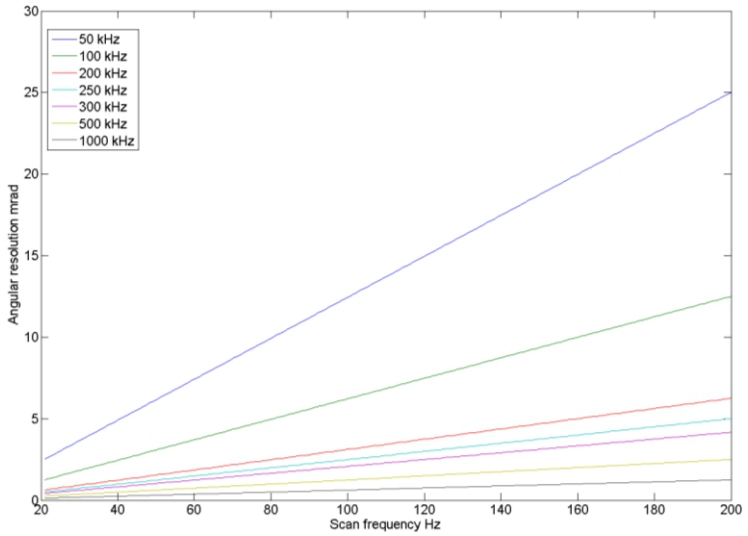

Figure 40. Angular resolution as function of scan frequency for some typical MLS sensor PRFs.

The FOV of the scanner affects the point coverage. For example, using a TLS with the ROAMER system has a shortcoming; the scanner base occludes a 40-degree portion of the full 360-degree scanning angle. In a tilted position, the base shadow thus prevents measurements of objects above the scanner within the occlusion angle at single pass, and at vertical position the road surface cannot be captured completely. To give an idea about the occlusion problem, at 4 m above the scanner the base shadow is approximately 2.9 m wide. While minimal, it is worth considering in the mission planning. To reduce such effects, full FOV scanners can be used, or the occluded areas can be covered using additional sensors.

5.4 MLS sensor configuration effects

In addition to the scanner parameters, the sensor layout or arrangement on the MLS platform has a great influence on the geometric characteristics of the acquired data. For single scanner systems, such as ROAMER and AKHKA, the possibilities in changing the layout are somewhat limited. What can be done is to adjust the scan plane, depending on the data needed, as has been proven by the ROAMER applications, and is also suggested by simulation studies by Yoo et al. (2009a) and Cahalane (2013).

The FOV and orientation of the scanner head on MLS platform affects the data distribution and coverage. The vertical scanner position can be used when structures above the scanner, e.g., bridges, tunnel roofs, and portals for traffic signs, have to be included in the model (assuming less than a full 360° FOV, the case with ROAMER). This position is also applicable in measurements of the building façades and other similar structures, though many of them can be captured as well at any of the tilted positions, bearing in mind the possible shadowing effects.

Tilted scanner positions are used in the seamless extraction of points from road and ground surfaces. A tilted scanning plane also produces multiple hits even from narrow pole structures usually present on both sides of the road, e.g., traffic signs, light poles and bridge pillars. This is due to the high scan frequency, high angular resolution, and the fact that the wide FOV of the scanner makes it possible to acquire multiple hits of the same object from several sequential profiles as the MLS unit passes by, as illustrated in (Kukko, 2009). Such an approach allows higher platform speeds than when using vertical profile orientation, which could miss narrow vertical structures completely. With multiple point arcs, the positioning and modeling of the object become more reliable.

A further advantage of using the tilted scanning plane is the capability of capturing vertical and horizontal edges with equal, angular resolution dependent precision. Such objects include corners of buildings and driveways, window and doorframes in the building façades, etc. Moreover, at a building corner the laser swath illuminates portions of two façades of the building, and thus data points are

measured from both walls. This helps in locating the building corners from the point cloud data more reliably. The same applies to the window frames on a more detailed scale. Given the same scan frequency, angular resolution and velocity, a tilted scanning system provides more localization information about the object in the along-track direction than vertical scanning.

A disadvantage of using tilted scanning plane is the partial occlusion of surfaces (e.g., façades) if there is variation in the façade depth, as the scanner sees some of the objects in the forward FOV, and some in the back FOV. The dual-pass procedure is nonetheless generally recommended for data acquisition with single scanner systems for accuracy assessment purposes, which mitigates this problem. On the contrary, systems operating with a vertical scanning plane do not have similar shadowing behavior in the data acquisition, but wall surfaces parallel to the scanning plane cannot be measured. It is estimated that platform velocity and scan frequency have also greater effects on the data pattern, i.e., point distribution, for systems with a vertical scanning plane (Kukko, 2009; Yoo et al., 2009a).

To overcome each individual shortcomings of a single scanner MLS, many of the commercial MLS systems have been equipped with multiple laser units. With multi-scanner MLS the need for multi-pass surveys is reduced, due to improved data coverage and diminishing of the shadowing effects. Multi-scanner systems also may result in more even and complete point distribution on the object surfaces, as each of the scanners sees them from a different viewpoint. The most common approach is to have two scanners mounted with scan planes at right angles to each other and tilted forward (e.g., StreetMapper 360, Riegl VMX-250, Optech Lynx). In this configuration, the reoccurrence distance S of an object seen by the first scanner into the FOV of the second depends on the object distance R from the MLS trajectory, added with the base line B between the scanners on the platform, thus S=B+2R, as illustrated in Figure 41. So, B defines the minimum shadow size caused by an occluding object. Moreover, the selection of sensor height influences the extent of shadowing – the higher, the better.

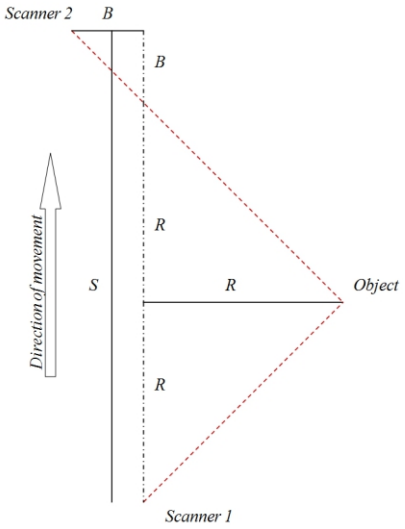

Figure 41. Relation of the object distance and reoccurrence for dual scanner MLS.

For tall building façades (above 50 m), the sensor parameter analysis can conclude that detailed modeling requires extremely high angular resolutions. For example, 10 cm maximum point separation on a 120 m high façade requires angular resolution of approx. 0.015 mrad, bearing in mind that increasing the scanner distance from the façade improves the situation, within the scanner ranging capability of course. It is nevertheless quite typical in an urban context to have relatively short scanner-to-target ranges, e.g., 10–20 meters. At 20 m horizontal façade distance from the scanner, a 0.2 mrad system could produce 15 cm point separation figures at a vertical wall surface 120 m above the sensor.

Scan plane angle determines the point pattern on the ground and on objects situated on both sides of the trajectory. With a vertical cross-track scanning plane the tall building façades can be reached even in narrow streets with tight corners. A tilted scan plane, e.g., 45 degrees, needs more straight roads to reach objects high above. This can, however, be compensated by employing additional scanner(s) to the system with a drawback of increased equipment and system calibration costs. The disadvantages of the vertical scan plane are the decreased detection rates, making it easier to miss objects like poles and localization of building corners, which can be more reliably determined from data acquired with a tilted scan plane.

5.5 MLS data characteristics and usability

Vehicle-borne laser scanning offers a huge potential for different surveying tasks, mainly due to the mobility and use of high-resolution, high precision active sensor technology (**IV**), but also as it provides a data archive allowing revisiting and mapping objects in the site without an additional survey. The last five–six years have shown mobile laser scanning to be a suitable method of acquiring and

characterizing information vital for road and urban infrastructure management (Gräfe, 2007a; Jaakkola et al., 2008; Lehtomäki et al, 2010; Ibrahim and Lichti, 2012), as well as for mapping and quantifying many other anthropogenic and physical aspects of the world (**IV**;**V**;**VI**;**VII**; Barber and Mills, 2007; Jochem, Höfle and Rutzinger, 2011; Holopainen et al., 2011; Kaasalainen et al. 2011a; Kasvi et al., 2012). MLS has been applied, e.g., to automated extraction and modeling of buildings (Manandhar and Shibasaki, 2002; Zhao and Shibasaki, 2003ab; Früh, Jain and Zakhor, 2005; Rutzinger et al., 2011a; Zhu et al., 2011). MLS is a suitable method also for modeling of trees (Zhao and Shibasaki, 2003a; Jaakkola et al., 2010; Pu et al., 2011; Puttonen et al., 2011; Rutzinger et al., 2011b), and for automated detection and measurement of poles in urban and road scenery (Brenner, 2009; Golovinskiy, Kim and Funkhouser, 2009; Lehtomäki et al., 2010; Lehtomäki et al., 2011; Pu et al., 2011; Yokoyama et al. 2011). Ground topography has long been a field of interest for MLS in its different applications (Zhao and Shibasaki, 2003; Goulette et al., 2006; Yu, et al., 2007; Jaakkola et al., 2008; Mc Elhinney et al., 2010; Ibrahim and Lichti, 2012). Also, studies on topographic surveys for geomorphology and change detection in fluvial environments have been carried out using MLS (**VI**; **VII)**. More recent publications utilizing the proposed MLS technology in deriving surface roughness parameters for hydraulic modeling is presented in Wang et al., (2013), whereas Vaaja et al., (2013) further extends the performance investigations of the ROAMER and AKHKA in mapping of fluvial environments. Saarinen et al., (2013) investigated the feasibility of vegetation classification using MLS data.

Vehicle-mounted MLS street data typically include intensity data, which can be used to automatically extract road markings, e.g., zebra crossings, and geometric information about buildings, pavement, pedestrian structures, islands, manholes, curbs, poles, signs and pylons (**IV**). Intensity readings can be utilized in conjunction with the geometric data for automatic extraction of different target types from the point clouds (Jaakkola et al., 2008). Detection and inventory of utility poles, traffic signs and lamp posts are prime examples of utilizing MLS in urban infrastructure maintenance, e.g., (Lehtomäki et al., 2010). MLS data can also provide up-to-date information on power lines and other open-air infrastructure, such as railway facilities, etc. These data can be utilized e.g., in creating realistic environments for road traffic simulations and illumination studies (**III**; Kosonen and Bargiela, 2000; Ekrias et al., 2008). Hammoudi et al. (2010) and Zhu et al. (2011) discuss the detection of street façades from MLS data, and El-Halawany et al., (2011) have investigated detection of road curb.

The imperfection in using MLS in urban environments is that the visibility of some objects is highly dependent on the scanner setup (e.g., **II**; **V**; Kukko, 2009; Yoo et al., 2009) but also obstruction of the objects in the scene. Thus, ground modeling, for example, often becomes impractical with a low angle of incidence at ranges beyond about 30 meters due to demands for high angular resolution. This could be compensated by adding more traverses over the area. Also, roof structures on high buildings are

often not fully covered with MLS data and so ALS or aerial images are needed to complete the models, if not backpack MLS or such are available. Another effect is that when using tilted scan planes, the visibility of high parts of building façades is a function of tilt angle and trajectory curvature.

In an urban context, the renovation of buildings and urban assets is an important field where MLS could in the future provide remarkable improvement in the inventory data output. Even though the vehicle MLS is expected to provide wide area coverage, there are plenty of cases where such operations are hindered by the surrounding structures, buildings, narrow streets and terrain. Limited spaces further weaken the vehicle maneuverability, thus impairing the data collection severely. For such environments and data needs, backpack MLS provides an effective solution.

The applications of MLS to environmental remote sensing have thus far focused on vegetation, erosion studies, and hydrology studies (Barber and Mills, 2007; **VI**; Alho et al., 2011). MLS systems are capable of faster and more efficient 3D data acquisition than stationary TLS, especially in cases where ground validation (e.g., small-scale details) is needed for purposes such as airborne experiments or when dealing with areas covered by Earth-observing satellites (see Kaasalainen, Kaartinen and Kukko, 2008a; Connor et al., 2009).

The first non-urban application of ROAMER was to install the system on a boat (**VI**), as was shown in Figure 30. Having a fast laser scanner enabled detailed riverine topographical data to be acquired for fluvial applications such as hydraulic modeling (Kasvi et al, 2012) and geomorphological change detection (**VII**). In addition to static modeling of riverine topography, there is a growing need to map changes in topography as the geomorphology and topography of the river channel and surrounding floodplain are affected by fluvial erosion and deposition processes, varying from constant grain-scale displacement to large-scale flood-related avulsions (Heritage and Milan, 2009; Cook and Merwade, 2009; Alho and Mäkinen, 2010). This approach also enables an effective survey angle for steep river banks, which is difficult to achieve when using airborne or stationary terrestrial scanning. The BoMMS system has been used in data acquisition for numerous studies involving hydraulic modeling and analysis of geomorphological processes since 2008 (e.g., **VI**; **VII**; Alho et al., 2011; Kasvi et al., 2012).

Environmental and geophysical studies have been lacking good quality 3D data for modeling and monitoring of natural processes. Paper **IV** describes the use of MLS in mapping of permafrost palsa landforms. To the best of the author's knowledge, AKHKA was a world-first and seems to be a very promising approach to high-performance MLS, although generally speaking backpack platforms have been introduced before for mobile imaging (e.g., Ellum and El-Sheimy, 2000). The backpack version expands the range of applicability of MLS technology by opening up new possibilities into research fields that have lacked detailed 3D surveying capability and spatial coverage. The presented palsa study

is a good example of that. It is seen that such MLS systems possess good potential in speeding up and intensifying the collection of 3D survey data. Thereby, they will allow unprecedented, detailed analysis at remarkable point density with widening spatial coverage and data quality. Ease in mobilization of MLS systems allows better temporal resolution over the traditional surveying methods for change monitoring applications (**VI**; **VII**).

5.6 Future work

The next generations of ROAMER and AKHKA will have a new FOG-based IMU and multi-GNSS constellation receiver to facilitate more reliable positioning, especially in satellite limited areas, as the number of observable satellites is larger than that for a GPS-only system. Smaller laser scanning head than is currently in use will also be integrated in order to obtain increased scan frequency and easier operability especially for backpack-based mapping. Further, AKHKA (or an evolution version) will be benchmarked at the Espoonlahti test field as well, as these surroundings provide an ideal environment for such a study. This is expected to give an insight into practicality and usability of such MLS in urban area mapping, expanding the knowledge gained in the foundry case.

Due to the rapid development of laser scanning technology, the expected cost of systems like BoMMS are constantly becoming less expensive, promoting their increased use. More research is needed in the future to explore the full potential of MLS, combined with terrestrial and aerial LiDAR and UAV imagery. Based on the collected data, automatic algorithms for terrain extraction, vegetation analysis and surface roughness estimators require further development, as do those needed for semi-automatic change detection mapping of e.g., fluvial deposition.

There is a need for more thorough analysis concerning the use of MLS point clouds for the generation of digital elevation models of vegetated surfaces and the scan parameters in such a task in general. Also, a study on controlling and correcting the time-dependent variations in the trajectory, based on the retrieved target data, is a matter to be solved in the future. Such research contribution would concentrate on the further development of automatic data correction and field control schemes, as well as on object modeling and surface analysis methods.

It is also of great interest to study more thoroughly the GPS-IMU and multi-GNSS-IMU navigation performance in forested areas for better understanding and development for the use of MLS in operative forest management. MLS provides an indirect means to derive the trajectory errors from known object locations in forested (or, in general, GNSS occluded) environments. Such studies, in conjunction with the modeling aspects, could facilitate the use of MLS techniques for forest management with increased efficiency and objectivity. In order to optimize automated tree cutting,

MLS-derived individual tree level inventory and tree model data may provide a harvester with enhanced input, including detection of trees and detailed stem curve and volume.

As well trees in forestry data, a good alternative in urban scene for the target gate calibration would be pair of lamp posts, as they could provide precise localization and spatial extent (width and height) for accuracy, and moreover are automatically detectable from point clouds (Lehtomäki et al, 2011). They may also provide with a control and adjustment scheme for MLS data in general as poles are a typical road asset present almost everywhere. Such approach is yet a subject for a future study.

For densely vegetated surfaces, ground detection is expected to be more challenging than in the study cases presented in **IV**; **VI** and **VII**. Based on experience, it is predicted that the beam angle has a great influence on the result; thus the longer the beam needs to penetrate through vegetation, the more probable it is that the ground detection becomes fallacious. This necessitates the need for a systematic study to validate and to differentiate a variety of ranging techniques as they may perform differently for such a task.

Future MLS applications will have important roles to play in various development and modeling tasks in the vast fields of civil and transportation engineering, archaeology and geomatics, as well as in the monitoring and understanding of processes in different disciplines of natural sciences; e.g., cryosphere (an example of which is the monitoring of seasonal snow coverage) and glaciology, geophysics, hydrology, silviculture, and agriculture.

6 SUMMARY AND CONCLUSIONS

6.1 Incidence angle effects

The incidence angle effect is the most prominent for angle larger than 20 degrees, and the effect must be taken into account in interpretation of laser scanning data with steep slopes that affect topographic ALS and more frequently on MLS data with rapidly changing geometries (e.g., vertical walls and platform movements).

Before the study conducted in **I** there had been little of information of the effect available in the field of remote sensing, and particularly for laser scanning applications, on what role the incidence angle plays in the intensity calibration. It was demonstrated that the incidence angle effects are consistent at different wavelengths. The decrease in target brightness was found to be significant mostly at incidence angles larger than 30°. These angles may have minor relevance in ALS-based radiometric calibration measurements, due to lack of precision, but they are more prominent to be taken into account in the interpretation of ALS or TLS and MLS data where steep slopes and vertical surfaces are present in the target area. It also seems that the target brightness has an effect on the magnitude of the decrease. The knowledge gained in paper **I** of the incidence angle dependence of TLS/MLS data can be used to adjust the methods developed for ALS to correct MLS intensities.

6.2 Simulations

A simulation approach for attaining MLS data was introduced and tested. The simulation method combines both spatial and radiometric components of a laser scanner to produce realistic waveform and point cloud data for system performance analysis and for algorithm development for LiDAR data processing and mapping purposes. The waveform data generated by the simulator was based on the spatial discretization of the laser beam to a bundle of rays, Gaussian pulse power approximation and TEM00 intensity pattern model, computation of object intersections for each sub-beam, and the interaction of the sub-beams with the target surface scatterers.

Simulation provides a possibility, together with experimental data, for demonstrating the effects of different factors on a LS measurement. Integrating simulation into an implementation of sensor geometry and platform trajectory models provides a useful approach for verification and comparison of different LS systems and for analysis of LS measurement itself. It is also clear that simulation of this kind is an important adjunct to analytical error modeling and estimation.

6.3 MLS systems and performance

The research and development carried out concerning mobile laser scanning systems resulted in two distinct MLSs: ROAMER and AKHKA. The ROAMER system is a robust but adjustable vehicle-mounted multi-modal system, backed up with camera equipment, whereas AKHKA is a compact personal surveying system. Both systems use the same scanner and GPS-IMU instrumentation connected to each other with a synchronization system developed in studies for this thesis; only the integration platform differs. The fact that the same instrumentation can be used in completely different platforms proves that the initial objective of versatility was successfully achieved. Both platforms have been applied to 3D mapping of objects and scenes in different fields of research as was shown by application results.

When introduced in 2011 in environmental and fluvial contexts, the AKHKA backpack MLS was a completely new type of platform providing high-performance LiDAR mapping of environments where it is difficult, if not impossible, to operate with any ground-vehicle-based MLS. The AKHKA system enables exceedingly high point densities to be achieved with an absolute accuracy level of 20 mm. AKHKA was a world-first, and provides a promising approach to high-performance MLS data acquisition. It widens the range of applications of mobile laser scanning technology and enables new insights into research fields that have thus far lacked detailed 3D surveying systems with sufficient coverage, e.g., terrain modeling, urban mapping, precision forestry, hydrology and research focusing on fine-scale geophysical processes.

The EuroSDR project (**V**) provided a permanent test field for verifying and comparing the performance of different mobile laser scanning systems. The test field can also be utilized in data processing development and testing, for example, when devising new algorithms for automatic feature extraction. In this particular study, the geometric accuracy of an MLS-derived point cloud in good GNSS conditions was found to be within 1–2 cm. The relative accuracy can be even higher, when for example individual scanning lines are considered. The commonly accepted requirement for reference data is that the accuracy should be at least one order of magnitude better than the property to be evaluated. It is clear that this requirement is hard, if not impossible, to fulfill in practice. Robust test field data can nonetheless be used to validate the performance of MLS systems in varying measurement conditions, and a permanent test field is the only way to compare different systems reliably with minimal bias.

The performance of the developed MLS systems based on the analyses of results achieved on a permanent MLS test field and in situ target field studies show that the presented MLS systems can produce dense point cloud data for object reconstruction with absolute accuracy at the cm level (horizontal RMSE 23 mm for ROAMER and 17 mm for AKHKA), both in regards to plan and

elevation. The relative precision of the data was estimated to be around 12 mm. To achieve this, internal calibration of the system must be carried out with careful experimental setting and data analysis. Furthermore, in the DGPS real-time positioning test the tactical grade GPS-IMU system was proven to be suitable for MLS use, providing sufficiently accurate (better than 10 cm) positioning.

The benchmarking result further indicates that system calibration has a major impact on MLS performance. By implementing a field calibration scheme, i.e., using test field TLS data in estimating the angular bore-sight parameters of ROAMER, accuracy could be improved considerably. When compared to the first point cloud data computed without improvements from the field calibration, the standard deviations of both elevation and planimetric errors were diminished by half. Errors in the relative orientation of the instruments lead directly to errors in the measured point clouds, which cause problems in continued manipulation of the data, e.g., in extraction and modeling of objects and change detection. For multi-temporal studies, the possibility of positional discrepancies should be taken into account to ensure reliable analysis. Yet even at the level achieved in the study, the advantages of incorporating MLS techniques represent a huge leap in change analysis applications in many fields.

The target gate approach for calibration of MLS provides promising results. It is easy to set up in the field, and regular-shaped spherical targets are easy to detect from the point data regardless of the direction of observation, and detection could be automatized. The target model (ATS SRS) used in the studies was found to be suitable and allowed for accurate RTK-GPS measurements for the target center coordinates.

6.4 Fluvial application remarks

Within the fluvial context, a new approach based on boat-mounted mobile laser scanning was described and demonstrated to derive detailed micro-scale topographical data (on a scale from millimeters to meters) for fluvial studies. The study proved that high-density point clouds allow for effective sampling of detailed river environment topography, despite the fact that the scanner elevation, scan frequency and ranging capability were found to be somewhat limited at the time. Combined with static TLS data acquisition, boat-mounted mobile laser scanning enabled a totally new field mapping approach for fluvial studies, e.g., post-flood depositions could be mapped directly after a flood event without an extensive time lag. The demonstration carried out in the study proposed the following conclusions and possibilities:

- BoMMS allows a faster survey of riverine topography than traditional TLS scanning. In the study, the whole reach of 6 km was surveyed within 85 min. TLS scanning of only the five point-bars took ~8 h. Test site A in the study was surveyed ~30 times faster with MLS than with TLS. Furthermore,

MLS allows scanning angles from the channel to the banks that are not possible to achieve with TLS.

- The accuracy obtained with the BoMMS system was significantly higher than that typically obtained from ALS, and large areas can be covered cost-efficiently. When compared to the surface topography reference from static TLS, the standard deviation of boat-based mobile laser scanning data was 2.7 cm.

- Since a boat-based laser scanning approach can be used to derive accurate characterization of the topography and as a rapid and cost-effective measurement technique (less expensive than ALS), it is expected to be especially useful for multi-temporal studies of rivers, allowing topographic change detection.

The feasibility of using MLS to map changes in riverine topography was studied in two different years with boat- and cart-mounted ROAMER to record the topography of point bars and river banks before and after the effect of erosion or deposition. In five out of six test sites an RMSE of the elevation level with better than 5 cm accuracy was obtained. This, however, required a systematic elevation error to be calibrated out of the data.

Data with steeper scanning angles to the ground surface in particular were found to provide better accuracy than those of gentle angles. The data acquisition procedure was improved in the 2009 campaign by increasing the mapping system support structure height by 1 m. The results obtained indicate that MLS can provide accurate and precise change information over large areas. However, data needs to be controlled for systematic errors, as they significantly affect volumes derived from surface analysis.

6.5 Concluding remarks

The hypothesis in this study was that, by applying tactical grade GPS-IMU and an ultra-high-speed phase-shift laser scanner, a high-end mobile laser scanning system could be developed and used for proactive promotion of the particular technology, including data processing methods and applications, to industry, the scientific community and society. Appropriate calibration methods and data processing chain could provide accurate and high-resolution three-dimensional data for mapping and modeling applications in different fields of urban, industrial and road environment development, transportation planning, civil engineering, precision forestry and agriculture, as well as for modeling of geophysical entities and environmental research.

The aim of the study was to develop novel mobile laser scanning systems, analyze their performance and develop new applications. The aim was accomplished by implementing the objectives for development of systems, processes and quality analysis as follows:

1. The experimental setup for measuring the incidence angle effect on LS data was presented in publication **I**. The incidence angle was found to be a source of decrease in backscattering power at angles larger than 20 degrees, and should therefor taken into account when manipulating intensity data e.g., for classification purposes.
2. Laser scanning simulator was presented and evaluated in publication **II**. The simulator was exploited for analysis of MLS system configurations to fulfill the objective of
3. Design and development of ROAMER and AKHKA integration platforms, which were introduced in **III** and **IV**. Sensor integration was tested through multitude of evaluations and field tests reported in publications **III**–**VII**. Development of practical solutions for data georeferencing were performed and described. Publication **IV** discusses the development and testing of geometric calibration of the systems, which contribution is complemented in the Section 3.2 of this thesis. The applied calibration procedure could improve the attained data accuracy remarkable in the ROAMER benchmarking, and the backpack AKHKA data shows very good error figures as for being a human-borne mapping system.
4. Quality analysis of the data acquired with the developed systems were carried out especially in publications **IV** and **V**, but publications **VI** and **VII** carry out some application relevant performance analysis and system testing and presented a new application scenario for MLS. The performance of the systems was found to be on cm level, and data rates and acquisition efficacy were found satisfactory for the applications reported, even though the scan frequency was the most critical factor, especially for the data collected with the first scanner version.

The results achieved in the studies and the wide adoption of the technology for different applications confirmed the hypothesis.

Numerous authors have reported use of mobile scanners on different platforms, yet no single group of authors has reported an undertaking of the scope and variability provided by ROAMER and AKHKA. It has been shown through the application examples presented in this thesis that when using an MLS system equipped with a high-performance laser scanner and sufficient navigation capacity, it is possible to produce centimeter accuracy 3D point cloud data meeting application-specific needs in terms of data quality, density, and coverage. The benefits of using MLS data for producing high-resolution 3D models are clear, as has been demonstrated.

Considering MLS data acquisition compared to data acquired when using a stationary TLS, MLS provides high efficiency and a precise way of generating dense point clouds and its mobility makes it more suitable for surveying and modeling of large areas. Versatile design with an easy-to-adjust approach together with light data recording facilities is the key to the versatility of the proposed equipment. This also reduces the need of permanent modifications for the vehicle used for the mapping thus reducing the system cost and increasing availability and affordability of the proposed MLS systems for customers.

Based on the experiences gained in the separate studies of this thesis, it is evident that the proposed MLS approaches have the potential to speed up and improve the collection of 3D survey data and thereby widen spatial coverage with reassuring results as regards to point density and quality. With MLS the data capture can be performed with less effort and more safely, e.g., in road environment compared with traditional methods, greatly improving the data output rate. High-performance multi-purpose MLS systems with a moderate price tag may prove to be attractive for companies in need for accurate and up to date 3D surveying data.

The advantages of MLS for producing high-resolution 3D surveys are obvious, thus most of the ground-based mapping applications could benefit from this technology. Nevertheless, for attaining reliable mapping result, appropriate field calibration and control schemes are a necessity, especially in satellite obstructed environments. Application of the MLS techniques is diverse, and the awareness and use of MLS is growing rapidly worldwide.

REFERENCES

Abed, F.M.; Mills, J.P.; Miller, P.E., Echo Amplitude Normalization of Full-Waveform Airborne Laser Scanning Data Based on Robust Incidence Angle Estimation. IEEE Transactions on Geoscience and Remote Sensing **2012**, .50, 7, 2910–2918.

Ahokas, E. Aspects of accuracy, scanning angle optimization, and intensity calibration related to nationwide laser scanning. Publications of the Finnish Geodetic Institute **2013**, 150, 124 p.

Ahokas, E.; Kaasalainen, S.; Hyyppä, J.; Suomalainen, J. Calibration of the Optech ALTM 3100 laser scanner intensity data using brightness targets. International Archives of Photogrammetry, Remote Sensing, and Spatial Information Sciences **2006**, 36, 1.

Alho, P.; Mäkinen, J. Hydraulic parameter estimations of a 2-D model validated with sedimentological findings in the point-bar environment. Hydrological Processes **2010**, 24, 2578–2593.

Alho, P.; Vaaja, M.; Kukko, A.; Kasvi, E.; Kurkela, M.; Hyyppä, J.; Hyyppä, H.; Kaartinen, H. Mobile laser scanning in fluvial geomorphology: Mapping and change detection of point bars. Zeitschrift für Geomorphologie **2011**, 55, 31–50.

Amoureus, L.; Bomers, M.P.H.; Fuser, R.; Tosatto, M. Integration of lidar and terrestrial mobile mapping technology for the creation of a comprehensive road cadastre. The 5th International Symposium on Mobile Mapping Technology, Pradua, Italy, 29–31 May **2007**.

Anderson, J.; Martina, M.; Smith, M-L.; Dubayah, R.; Hofton, M.; Hyde, P.; Peterson, B.; Blair, J.; Knox, R. The use of waveform lidar to measure northern temperate mixed conifer and deciduous forest structure in New Hampshire, Remote Sensing of Environment **2006**, 105, 3, 248–261.

Artuso, R.; Bovet, S.; Streilein, A. Practical methods for the verification of countrywide terrain and surface models. ISPRS WG III/3 Workshop "3-D reconstruction from airborne laser scanner and InSAR data," Dresden, Germany, 08–10 October 2003, International Archives of Photogrammetry, Remote Sensing and Spatial Information Sciences **2003**, 34, 3/W13, 14–19.

Aschoff, T.; Thies, M.; Spiecker, H. Describing forest stands using terrestrial laser-scanning, Proceedings of the XXth ISPRS Congress: Geo-Imagery Bridging Continents, 12–23 July, Istanbul, Turkey, **2004**, 237–241.

Axelsson, P. DEM Generation from laser scanner data using adaptive TIN models. International Archives of Photogrammetry and Remote Sensing **2000**, 33, B4, 110–117.

Balsa-Barreiro, J.; Avariento, J.P.; Lerma, J. Airborne light detection and ranging (LiDAR) point density analysis. Scientific Research and Essays **2012**, 7, 33, 3010–3019.

Baltsavias, E. Airborne laser scanning: basic relations and formulas. ISPRS Journal of Photogrammetry and Remote Sensing **1999**, 54, 2/3, 199–214.

Barber, D.; Mills, J. Vehicle based waveform laser scanning in a coastal environment. The 5th International Symposium on Mobile Mapping Technology, Pradua, Italy, 29.–31. May, **2007**.

Barber, D.; Mills, J.; Smith-Voysey, S. Geometric validation of a ground-based mobile laser scanning system. ISPRS Journal of Photogrammetry & Remote Sensing **2008**, 63, 128–141.

Beinat, A.; Crosilla, F. Generalised Procrustes Analysis for Size and Shape 3-D Object Reconstructions. 5th Conference on Optical 3-D Measurement Techniques, Wien 1.–4. October, **2001**, 345–353.

Biber, P.; Fleck, S.; Strasser, W. A Probabilistic Framework for Robust and Accurate Matching of Point Clouds. Pattern Recognition, Lecture Notes in Computer Science **2004**, 3175, 280-487.

Bilker, M.; Kaartinen, H. The quality of real-time Kinematic (RTK) GPS positioning. Reports of the Finnish Geodetic Institute **2001**, 1, 1–25.

Blair, J.; Rabine, D.; Hofton, M. The Laser Vegetation Imaging Sensor: A medium-altitude, digitization only, airborne laser altimeter for mapping vegetation and topography, ISPRS Journal of Photogrammetry and Remote Sensing **1999**, 54, 115–122.

Boyd, D.; Hill, R. Validation of airborne lidar intensity values from a forested landscape using hymap data: preliminary analyses. International Archives of Photogrammetry, Remote Sensing, and Spatial Information Sciences **2007**, 36, 3/W52, 71–76.

Bransington, J.; Langham, J.; Rumsby, B. Methodological sensitivity of morphometric estimates of coarse fluvial sediment transport. Geomorphology **2003**, 53, 299-316.

Brenner, A.; Zwally, J.; Bentley, C.; Csathó, B.; Harding, D.; Hofton, M.; Minster, J.-B.; Roberts, L.A.; Saba, J.; Thomas, R.; Yi, D. Derivation of Range and Range Distributions from Laser Pulse Waveform Analysis for Surface Elevations, Roughness, Slope, and Vegetation Heights, Geoscience Laser Altimeter System (GLAS) Algorithm Theoretical Basis Document , Version 3.0, NASA Goddard Space Flight Center, **2000**, 93 p.

Brenner, C. Building reconstruction from laser scanning and images, Proceedings of ITC Workshop on Data Quality in Earth Observation Techniques, Enschede, The Netherlands, **2003**.

Brenner, C. Building reconstruction from images and laser scanning, International Journal of Applied Earth Observation and Geoinformation **2005**, 6, 3–4, 187–198.

Brenner, C.; Ripperda, N. Extraction of facades using rjMCMC and constraint equations, In: PCV'06, Photogrammetric Computer Vision, W. Förstner, R. Steffen (Eds.), ISPRS Comm. III Symposium, IAPRS Vol. XXXVI, Part 3, 20.–22. Sept., Bonn, **2006**, 155–160.

Brenner, C. Extraction of Features from Mobile Laser Scanning Data for Future Driver Assistance Systems. In Proceedings of the 12th Agile Conference, Hannover, Germany, **2009**.

Briese, C.; Höfle, B.; Lehner, H.; Wagner, W.; Pfennigbauer, M.; Ullrich, A. Calibration of full-waveform airborne laser scanning data for object classification. Proceeding of the SPIE– International Society for Optical Engineering, **2008**, 6950, p. 69500H.

Bufton, J.L. Laser altimetry measurements from aircraft and spacecraft. Proceedings of the IEEE, **1989**, 77, 3, 463–477.

Cahalane, C.; Mc Elhinney, C.; McCarthy, T. Mobile Mapping System Performance–An Analysis of the Effect of Laser Scanner Configuration and Vehicle Velocity on Scan. In Proceedings of the European Lidar Mapping Forum, The Hague, The Netherlands, 30th November–1st December, **2010**, 1–10.

Cahalane, C. Calculating and Assessing Mobile Mapping System Point Density for Roadside Infrastructure Surveys. PhD Thesis, National University of Ireland, Maynooth, Ireland, **2013**.

Carabajal, C.; Harding, D. Evaluation of geoscience laser altimeter system (GLAS) waveforms for vegetated landscapes using airborne laser altimeter scanning data. International Archives of Photogrammetry, Remote Sensing and Spatial Information Sciences **2001**, 34, 3/W4, 125–128.

Clarke, K. Mobile mapping and geographic information systems. Cartography and Geographic Information Science **2004**, 31, 3, 131–136.

Connor, L.; Laxon, S.; Ridout, A.; Krabill, W.; McAdoo, D. Comparison of Envisat radar and airborne laser altimeter measurements over Arctic sea ice. Remote Sensing of Environment **2009**, 113, 563–570.

Cook, A.; Merwade, V. Effect of topographic data, geometric configuration and modeling approach on flood inundation mapping. Journal of Hydrology **2009**, 377, 131–142.

Coren, F.; Sterzai, P. Radiometric correction in laser scanning. International Journal of Remote Sensing **2006**, 27, 3097–3104.

Cramer, M.; Stallmann D.; Haala, N. Direct georeferencing using gps/inertial exterior orientations for Photogrammetric applications. International Archives of Photogrammetry, Remote Sensing, and Spatial Information Sciences **2000**, 32/B, 198–205.

DMA. Department of Defense World Geodetic System 1984: Its definition and relationship with local geodetic systems. DMA Technical Report 8350.2, **1987**.

Dorninger, P.; Pfeifer, N. A Comprehensive Automated 3D Approach for Building Extraction, Reconstruction, and Regularization from Airborne Laser Scanning Point Clouds. Sensors **2008**, 8, 7323–7343.

Ekrias, A.; Eloholma, M.; Halonen, L.; Song, X.-J.; Zhang, X.; Wen, Y. Road lighting and headlights: Luminance measurements and automobile lighting simulations. Building and Environment **2008**, 43, 530–536.

El-Halawany, S.; Moussa, A.; Lichti, D.D.; El-Sheimy, N. Detection of road curb from mobile terrestrial laser scanner point cloud. In: Lichti, D.D.; Habib, A.F. (Eds.) ISPRS Workshop Laser Scanning, Calgary, Canada, 29–31 August, International Archives of Photogrammetry, Remote Sensing and Spatial Information Sciences **2011**, 38,-5/W12, 109-114.

Ellis, J.; Caillard, P.; Dogariu, A. Off-diagonal Mueller matrix elements in backscattering from highly diffusive media. Journal of the Optical Society of America A **2002**, 19, 43–48.

Ellum, C.; El-sheimy, N. The development of a backpack mobile mapping system. International Archives of Photogrammetry, Remote Sensing and Spatial Information Sciences **2000**, 33, 184–191.

Ellum, C.; El-Sheimy, N. Land-based mobile mapping systems. Photogrammetric Engineering and Remote Sensing **2002**, 68, 1, 13–17 (and 28).

El-Sheimy, N. An Overview of Mobile Mapping Systems. FIG Working Week 2005 and GSDI-8, Cairo, Egypt April 16-21, **2005**, on-line publication, 24 p.

Flood, M.; Gutelius, B. Commercial implications of topographic terrain mapping using scanning airborne laser radar. Photogrammetric Engineering and Remote Sensing **1997**, 63, 4, 327–329, 363–366.

Früh, C.; Jain, S.; Zakhor, A. Data Processing Algorithms for Generating Textured 3D Building Façade Meshes from Laser Scans and Camera Images. International Journal of Computer Vision **2005**, 61, 159–184.

Garvin, J.; Blair, J.; Bufton, J.; Harding, D. The Shuttle Laser Altimeter (SLA-01) Experiment: Topographic Remote Sensing of Planet Earth. Eos, Transactions American Geophysical Union **1996**, 77, 7, 239 p.

Gatsiolis, D. Dynamic range-based intensity normalization for airborne, discrete return lidar data of forest canopies. Photogrammetric Engineering & Remote Sensing **2011**, 77, 3, 251–259.

Gedcke, D.; McDonald, W. Design of the constant fraction of pulse height trigger for optimum time resolution. Nuclear Instruments and Methods **1968**, 58, 253–260.

Golovinskiy, A.; Kim, V.; Funkhouser, T. Shape-Based Recognition of 3D Point Clouds in Urban Environments. In Proceedings of the IEEE 12th International Conference on Computer Vision, Kyoto, Japan, **2009**, 2154–2161.

Gomes-Pereira, L.; Janssen L. Suitability of laser data for DTM generation: A case study in the context of road planning and design. ISPRS Journal of Photogrammetry and Remote Sensing **1999**, 54, 244–253.

Goodwin, N.; Coops, N.; Culvenor, D. Development of a simulation model to predict LiDAR interception in forested environments, Remote Sensing of Environment **2007**, 111, 481–492.

Goulette, F.; Nashashibi, F.; Abuhadrous, I.; Ammoun, S.; Laurgeau, C. An integrated on-board laser range sensing system for on-the-way city and road modelling. In: ISPRS Commission I Symposium, "From Sensors to Imagery". Paris, 3-5.7.2006. Internationa Archives of Photogrammetry, Remote Sensing and Spatial Information Sciences **2006**, 36, 1B.

Grejner-Brzezinska D. Direct Exterior Orientation of Airborne Imagery with GPS/INS System: Performance Analysis. Navigation **1999**, 46, 4, 261–270.

Grejner-Brzezinska, D.; Toth, C. Driving the line: multi-sensor monitoring for mobile mapping. GPSWorld **2003**, 14, 3, 16–22.

Grimes, J.G. Global Positioning System Standard Positioning Service Performance Standard, 4th edition, **2008,** 160 p.

Grün, A.; Zhang L. Automatic DTM Generation from TLS data. In: Grün, A.; Kahman, H. (Eds.), Optical 3-D Measurement Techniques VI **2003**, 1, 93–105.

Gräfe, G. High precision kinematic surveying with laser scanners. Journal of Applied Geodesy **2007**a. 1, 4, 185–199.

Gräfe, G. Kinematic surveying with static accuracy. In: Grün, A.; Kahmen, H. (Eds.) 8th Conference on Optical 3-D Measurement Techniques **2007**b, July 9–12, 2007 - ETH Zurich, Switzerland.

Haala, N.; Brenner, C.; Anders, K.-H. 3D urban GIS from laser altimeter and 2D map data, International Archives of Photogrammetry, Remote Sensing and Spatial Information Sciences **1998**, 32, 3/1, 339–346.

Habib, A.; Morgan, M.; Lee, Y. Integrating data from terrestrial mobile mapping systems and aerial imagery for change detection purposes. The 3rd International Symposium on Mobile Mapping Technology, Cairo, Egypt, **2001**.

Hammoudi, K.; Dornaika, F.; Soheilian, B.; Paparoditis. N. Extracting Wire-frame Models of Street Façades from 3D Point Clouds and the Corresponding Cadastral Map. International Archives of Photogrammetry, Remote Sensing and Spatial Information Sciences **2010**, 38, 3A, 91–96.

Hansen, W. v. Robust automatic marker-free registration of terrestrial scan data. In: Förstner, W.; Richard, S. (Eds.) Proceedings of Photogrammetric Computer Vision **2006**, 36, 105–110.

Harding, D.; Lefsky, M.; Parker, G.; Blair, J. Laser altimeter canopy height profiles. Methods and validation for closed-canopy, broadleaf forests, Remote Sensing of Environment **2001**, 76, 3, 283–297.

Henning, J.G.; Radtke, P.J. Detailed stem measurements of standing trees from ground-based scanning lidar, Forest Science **2006**, 52, 67–80.

Heritage, G.; Milan, D. Terrestrial laser scanning of grain roughness in a gravel-bed river. Geomorphology **2009**, 113, 4–11.

Hesse, C.; Kutterer, H. A mobile mapping system using kinematic terrestrial laser scanning (KTLS) for image acquisition. In: Grün, A.; Kahmen, H. (Eds.) 8th Conference on Optical 3-D Measurement Techniques, ETH Zurich, Switzerland, 9.–12. July, **2007**.

Hollaus, M.; Wagner, W.; Maier, B.; Schadauer, K. Airbone laser scanning of forest stem volume in a mountainous environment. Sensors **2007**, 7, 1559–1577.

Holmgren, J.; Nilsson, M.; Olsson, H. Simulating the effects of lidar scanning angle for estimation of mean tree height and canopy closure, Canadian Journal of Remote Sensing **2003**, 29, 5, 623–632.

Holopainen, M.; Kankare, V.; Vastaranta, M.; Liang, X.; Lin, Y.; Vaaja, M.; Yu, X.; Hyyppä, J.; Hyyppä, H.; Kaartinen, H.; Kukko, A.; Tanhuanpää, T.; Alho, P. Tree mapping using airborne, terrestrial and mobile laser scanning - a case study in a heterogeneous urban forest. Urban Forestry & Urban Greening **2013**, DOI 10.1016/j.ufug.2013.06.002.

Holopainen, M.; Vastaranta, M.; Kankare, V.; Hyyppä, H.; Vaaja, M.; Hyyppä, J.; Liang, X.; Litkey, P.; Yu, X.; Kaartinen, H.; Kukko, A.; Kaasalainen, S.; Jaakkola, A. The use of ALS, TLS and VLS measurements in mapping and monitoring urban trees. In Stilla, U.; Gamba, P.; Juergens, C.; Maktav, D. (Eds.), Proceedings of the Joint Urban Remote Sensing Event JURSE 2011, **2011**, 29–32.

Hooijberg, M. Practical geodesy using computers. Springer, Berlin, Germany, **1997**.

Huising, E.; Gomes-Pereira, L. Errors and accuracy estimates of laser altimetry data acquired by various laser scanning systems for topographic applications, ISPRS Journal of Photogrammetry and Remote Sensing **1998**, 53, 5, 245–261.

Hunter, G.; Cox, C.; Kremer, J. Development of a commercial laser scanning mobile mapping system – StreetMapper. Second International Workshop The Future of Remote Sensing, Antwerp, 17.–18. October, **2006**.

Hyde, P.; Dubayah, R.; Peterson, B.; Blair, J.B.; Hofton, M. ; Hunsaker, C.; Knox, R.; Walker, W. Mapping forest structure for wildlife habitat analysis using waveform lidar: Validation on montane ecosystems, Remote Sensing of Environment **2005**, 96, 3–4, 427–437.

Hyyppä, J.; Kelle, O.; Lehikoinen, M.; Inkinen, M. A segmentation-based method to retrieve stem volume estimates from 3-D tree height models produced by laser scanners, IEEE Transactions on Geoscience and Remote Sensing **2001**, 39, 5, 969–975.

Hyyppä, J.; Hyyppä, H.; Leckie, D.; Gougeon, F.; Yu, X.; Maltamo, M. Review of methods of small-footprint airborne laser scanning for extracting forest inventory data in boreal forests. International Journal of Remote Sensing **2008**, 29, 5, 1339–1366.

Hyyppä, J.; Yu, X.; Hyyppä, H.; Vastaranta, M.; Holopainen, M.; Kukko, A.; Kaartinen, H.; Jaakkola, A.; Vaaja, M.; Koskinen, J.; Alho, P. Advances in Forest Inventory Using Airborne Laser Scanning. Remote Sensing **2012**, 4, 1190–1207.

Höfle, B.; Pfeifer, N. Correction of laser scanning intensity data: data and model-driven approaches. ISPRS Journal of Photogrammetry and Remote Sensing **2007**, 62, 6, 415–433.

Ibrahim, S.; Lichti, D. Curb-based street floor extraction from mobile terrestrial lidar point cloud. International Archives of the Photogrammetry, Remote Sensing and Spatial Information Sciences **2012**, 38, B5, 193–198.

Inside GNSS News. BeiDou, GLONASS, QZSS Report Development Plans. InsideGNSS, September 30, **2013**. URL: http://www.insidegnss.com/node/3735. Accessed: 31.10.2013.

Jaakkola, A.; Hyyppä, J.; Hyyppä, H.; Kukko, A. Retrieval algorithms for road surface modelling using laser-based mobile mapping. Sensors **2008**, 8, 5238–5249.

Jaakkola, A.; Hyyppä, J.; Kukko, A.; Yu, X.; Kaartinen, H.; Lehtomäki, M.; Lin, Y. A Low-Cost Multi-Sensoral Mobile Mapping System and Its Feasibility for Tree Measurements. ISPRS Journal of Photogrammetry and Remote Sensing **2010**, 65, 514–522.

Jochem, A.; Höfle, B.; Rutzinger, M. Extraction of Vertical Walls from Mobile Laser Scanning Data for Solar Potential Assessment. Remote Sensing **2011**, 3, 650–667.

Joo, I.-H.; Hwang, T.-H.; Choi, K.-H. Updating geospatial database: An automatic approach combining photogrammetry and computer vision techniques. Lecture Notes in Computer Science **2005**, 3708, 324–331.

Jutzi, B.; Eberle, B.; Stilla, U. Estimation and measurement of backscattered signals from pulsed laser radar. Proceedings of SPIE, **2003**, 4885, 256–267.

Jutzi, B.; Gross, H. Normalization of LiDAR intensity data based on range and surface incidence angle. Int. Arch. Photogramm. Remote Sens. Spat. Inf. Sci. **2009**, 38, 213–218.

Jutzi, B.; Neulist, J.;Stilla, U. High-resolution waveform acquisition and analysis for pulsed laser. In Heipke, C.; Jacobsen, K.; Gerke, M. (Eds.), High-Resolution Earth Imaging for Geospatial Information, International Archives of Photogrammetry, Remote Sensing, and Spatial Information Sciences **2005**, 36, 1/W3, CD-ROM.

Kaartinen, H. Benchmarking of airborne laser scanning based feature extraction methods and mobile laser scanning system performance based on high-quality test fields. Publications of the Finnish Geodetic Institute **2013**, 152, 346 p.

Kaartinen, H.; Hyyppä, J. EuroSDR-Project Commission III "Evaluation of Building Extraction," Final Report, EuroSDR - European Spatial Data Research, Official Publication **2006**, 50, 9–77.

Kaartinen, H.; Hyyppä, J. EuroSDR/ISPRS Project Commission II, Tree Extraction, Final Report. European Spatial Data Research Official Publication **2008**, 53, 60 p.

Kaartinen, H.; Hyyppä, J.; Yu, X.; Vastaranta, M.; Hyyppä, H.; Kukko, A.; Holopainen, M.; Heipke, C.; Hirschmugl, M.; Morsdorf, F.; Næsset, E.; Pitkänen, J.; Popescu, S.; Solberg, S.; Wolf, B.M.; Wu, J.-C. An International Comparison of Individual Tree Detection and Extraction Using Airborne Laser Scanning. Remote Sensing **2012**, 4, 950–974.

Kaasalainen, S.; Ahokas, E.; Hyyppä, J.; Suomalainen, J. Study of surface brightness from backscattered laser intensity: calibration of laser data. IEEE Transactions on Geoscience and Remote Sensing **2005**a, 2, 255–259.

Kaasalainen, S.; Peltoniemi, J.; Näränen, J.; Suomalainen, J.; Stenman, F.; Kaasalainen, M. Small-angle goniometry for backscattering measurements in the broadband spectrum. Applied Optics **2005**b, 44, 1485–1490.

Kaasalainen, S.; Hyyppä, J.; Litkey, P.; Hyyppä, H.; Ahokas, E.; Kukko, A.; Kaartinen, H. Radiometric calibration of ALS intensity. In Proceedings of the ISPRS Workshop on Laser Scanning 2007 and SilviLaser 2007, International Archives of Photogrammetry, Remote Sensing, and Spatial Information Sciences **2007**a, 36, 3/W52, 201–205.

Kaasalainen, S.; Lindroos, T.; Hyyppä, J. Toward hyperspectral lidar—measurement of spectral backscatter intensity with a supercontinuum laser source. IEEE Transactions on Geoscience and Remote Sensing **2007**b, 4, 211–215.

Kaasalainen, S.; Kaartinen, H.; Kukko, A. Snow cover change detection with laser scanning range and brightness measurements. EARSeL eProceedings **2008**a, 7, 133–141.

Kaasalainen, S; Kukko, A.; Lindroos, T.; Litkey, P.; Kaartinen, H.; Hyyppä, J.; Ahokas, E. Brightness measurements and calibration with airborne and terrestrial laser scanners, IEEE Transactions on geosciences and remote sensing **2008**b, 46 (2), 528–534.

Kaasalainen, S.; Krooks, A.; Kukko, A.; Kaartinen, H. Radiometric Calibration of Terrestrial Laser Scanners with External Reference Targets. Remote Sensing **2009**a, 1, 3, 144-158.

Kaasalainen, S.; Vain, A.; Krooks, A.; Kukko, A. Topographic and distance effects in laser scanner intensity correction. In: Bretar F, Pierrot-Deseilligny M, Vosselman G (Eds) Laser scanning 2009, International Archives of Photogrammetry, Remote Sensing, and Spatial Information Sciences **2009**b, 38, 3/W8, 219–223.

Kaasalainen, S.; Kaartinen, H.; Kukko, A.; Anttila, K.; Krooks, A. Brief communication "Application of mobile laser scanning in snow cover profiling", The Cryosphere **2011**a, 5, 135–138. www.the-cryosphere.net/5/135/2011/.

Kaasalainen, S.; Jaakkola, A.; Kaasalainen, M.; Krooks, A.; Kukko, A. Analysis of Incidence Angle and Distance Effects on Terrestrial Laser Scanner Intensity: Search for Correction Methods. Remote Sensing **2011**b, 3, 2207–2221.

Kalman, R.E. A new approach to linear filtering and prediction problems. Journal of Basic Engineering **1960**, 82, 1, 35–45. doi:10.1115/1.3662552.

Karimi, H.; Khattak, A.; Hummer, J. Evaluation of mobile mapping systems for roadway data collection. Journal of Computing in Civil Engineering **2000**, 14, 3, 168–173.

Kasvi, E.; Vaaja, M.; Alho, P.; Hyyppä, H.; Hyyppä, J.; Kaartinen, H. and Kukko, A. Morphological changes on meander point bars associated with flow structure at different discharges. Earth Surface Processes and Landforms **2012**, doi: 10.1002/esp.3303.

Kikuta, H.; Iwata, K.; Nagata, R. Distance measurement by the wavelength shift of laser diode light. Applied Optics **1986**, 25, 17, 2976–2980.

King, A. Inertial Navigation – Forty Years of Evolution, GEC Review **1998**, 13, 3, 140–149.

Koetz, B.; Morsdorf, F.; Sun, G.; Ranson, K.; Itten, K.; Allgöwer, B. Inversion of a lidar waveform model for forest biophysical parameter estimation, IEEE Geoscience and Remote Sensing Letters **2006**, 3,1, 49–53.

Kosonen, I.; Bargiela, A. Simulation-based traffic information system. 7th World Congress on Intelligent Transport Systems. Turin, Italy, **2000**, 8 p.

Kremer, J.; Hunter, G. Performance of the StreetMapper Mobile LIDAR Mapping System in "Real World" Projects. In: Fritsch, D. (Ed.), Photogrammetric Week 2007, **2007**, 215–225.

Kraus, K.; Pfeifer, N. Determination of terrain models in wooded areas with airborne laser scanning data, ISPRS Journal of Photogrammetry and Remote Sensing **1998**, 53, 4, 193–203.

Krooks, A.; Kaasalainen, S.; Hakala, T.; Nevalainen, O. Correction of intensity incidence angle effect in terrestrial laser scanning. The 13th International Conference on LiDAR Applications for Assessing Forest Ecosystems, October 9-11, Beijing, China, **2013**.

Kukko, A., Road Environment Mapper - 3D data capturing with mobile mapping, Licentiate's thesis, Department of Surveying, Helsinki University of Technology, **2009**, 157 p.

Kukko, A.; Hyyppä, J.; Kuittinen, R. Use of HRSC-A for sampling bidirectional reflectance. ISPRS Journal of Photogrammetry and Remote Sensing **2005**, 59, 6, 323–341.

Kukko, A.; Hyyppä, J. Laser scanner simulator for system analysis and algorithm development: a case with forest measurements. International Archives of Photogrammetry, Remote Sensing, and Spatial Information Sciences **2007**, 36, 3/W52, 234–240.

Kukko, A.; Anttila, K.; Manninen T.; Kaasalainen, S.; Kaartinen, H. Snow surface roughness from mobile laser scanning data. Cold Regions Science and Technology **2013**, 96, 23-35.

Kukko, A.; Jaakkola, A.; Lehtomäki, M.; Kaartinen, H. Mobile mapping system and computing methods for modelling of road environment. Urban Remote Sensing Joint Event, Shanghai, 20.–22. May, **2009**, 1388–1393.

Landry, J.; Gray, J.; O'Toole, M.; Zhu, X. Incidence angle dependence of optical reflectivity difference from an ultrathin film on solid surface. Optics Letters **2006**, 31, 531–533.

Lane, S.; Westaway, R.; Hicks, D. Estimation of erosion and deposition volumes in a large, gravel-bed, braided river using synoptic remote sensing. Earth Surface Processes and Landforms **2003**, 28, 249–271.

Lefèvre, H. The Fiber-Optic Gyroscope. Artech House, Boston-London, **1993**, 313 p.

Lefèvre, H. Fundamentals of the Interferometric Fiber Optic Gyroscopes. Optical Review **1997**, 4, 1A, 20–27.

Lefsky, M.; Cohen, W.; Acker, S.; Parker, G.; Spies, T. Harding, D. Lidar remote sensing of biophysical properties of canopy structure of forests of Douglas-fir and western hemlock, Remote Sensing of Environment **1999**, 70, 339–361.

Lehner, H.; Briese, C. Radiometric calibration of Full-Waveform airborne laser scanning data based on natural surfaces, The International Archives of Photogrammetry, Remote Sensing and Spatial Information Sciences **2010**, 38, 7B, 360–365.

Lehtomäki, M.; Jaakkola, A.; Hyyppä, J.; Kukko, A.; Kaartinen, H. Detection of Vertical Pole-Like Objects in a Road Environment Using Vehicle-Based Laser Scanning Data. Remote Sensing **2010**, 2, 641–664.

Lehtomäki, M.; Jaakkola, A.; Hyyppä, J.; Kukko, A.; Kaartinen, H. Performance Analysis of a Pole and Tree Trunk Detection Method for Mobile Laser Scanning Data. International Archives of Photogrammetry, Remote Sensing and Spatial Information Sciences **2011**, 38, 5/W12.

Liang, X.; Hyyppä, J. Automatic Stem Mapping by Merging Several Terrestrial Laser Scans at the Feature and Decision Levels. Sensors **2013**, 2, 1614-1634.

Lin, Y.-C.; Mills, J.P. Factors influencing pulse width of small-footprint, full-waveform airborne laser scanning data, Photogrammetric Engineering & Remote Sensing **2009**, 75, 11, 49–59.

Lohani, B.; Mishra, R. Generating LiDAR data in laboratory: LiDAR simulator. International Archives of Photogrammetry, Remote Sensing and Spatial Information Sciences **2007**, 36, 3/W52, 264–269.

Lohr, U.; Eibert, M. The TopoSys Laser Scanner-System. In Fritsch, D. v.; Hobbie, D. (Eds.), Photogrammetrische Woche **1995**, 263–267.

Lovell, J.; Jupp, D.; Newnham, G. Coops, N.; Culvenor, D. Simulation study for finding optimal lidar acquisition parameters for forest height retrieval, Forest Ecology and Management **2005**, 214m, 398–412.

Maas, H.-G. The suitability of airborne laser scanner data for automatic 3D object reconstruction, In Baltsavias, E.; Gruen, A.; Van Gool, L. (Eds.), Automatic Extraction of Man- made Objects From Aerial and Space Images (III), Lisse, Balkema, **2001**.

Maas, H.-G.; Vosselman, G. Two algorithms for extracting building models from raw laser altimetry data, ISPRS Journal of Photogrammetry and Remote Sensing **1999**, 54, 2–3, 153–163.

Mallet, C.; Bretar, F. Full-waveform topographic lidar: State-of-the-art, ISPRS Journal of Photogrammetry and Remote Sensing **2009**, 64, 1, 1–16.

Manandhar, D.; Shibasaki, R. Vehicle-borne Laser Mapping System (VLMS) for 3-D Urban GIS Database. Proceedings of the 7th International Conference on Computers in Urban Planning and Urban Management, University of Hawaii at Manoa, USA, July 18–20, **2001**, CD-ROM.

Manandhar, D.; Shibasaki, R. Auto-extraction of urban features from vehicle-borne laser data. International Archives of Photogrammetry, Remote Sensing and Spatial Information Sciences **2002**, 34, 4, 6 p.

Manandhar, D.; Shibasaki, R. Accuracy assessment of mobile mapping system. Proceedings of the 24th Asian Conference on Remote Sensing, **2003**, 3 p.

Matikainen, L.; Hyyppä, J.; Hyyppä, H. Automatic detection of buildings from laser scanner data for map updating, International Archives of Photogrammetry, Remote Sensing and Spatial Information Sciences **2003**, 34, 3/W13, 218–224.

Mc Elhinney, C.; Kumar, P.; Cahalane, C.; McCarthy, T. Initial Results from European Road Safety Inspection (EuRSI) Mobile Mapping Project. Int. Arch. Photogramm. Remote Sens. **2010**, XXXVIII-5, 440–445.

Milan, D.; Heritage, G.; Large, A.; Fuller, I. Filtering spatial error from DEMs; implications for morphological change estimation. Geomorphology **2011**, 125, 160–171.

Mitra N. J.; Gelfand N.; Pottmann H.; Guibas L. Registration of point cloud data from a geometric optimization perspective. In: Eurographics Symposium on Geometry Processing **2004**, 23–32.

Montemerlo, M.; Thrun, S.; Dahlkamp, H.; Stavens, D.; Strohband, S. Winning the DARPA Grand Challenge with an AI Robot, Proceedings of the 21st National Conference on Artificial Intelligence AAAI-06, Boston, Massachusetts, 16–20 July, **2006**.

Mostafa, M.; Hutton, J.; Reid, B. GPS/IMU products – the Applanix approach, In Fritsch, D.; Spiller, R. (Eds.) Photogrammetric Week 01', Wichmann Verlag, Heidelberg, **2001**, 63–83.

Naesset, E. Determination of mean tree height of forest stands using airborne laser scanner data, ISPRS Journal of Photogrammetry and Remote Sensing **1997**, 52, 2, 49–56.

Naesset, E. Predicting forest stand characteristics with airborne scanning laser using a practical two-stage procedure and field data, Remote Sensing of Environment **2002**, 80, 88–99.

Napolitano, F. Fiber-optic gyroscopes key technological advantages, URL: http://www.ixsea.com/pdf/fog-key-advantages.pdf, **2010,** accessed 25.10.2013.

Nelson, R.; Krabill, W.; Maclean, G. Determining forest canopy characteristics using airborne laser data. Remote Sensing of Environment **1984**, 15, 201-212.

NIMA. Department of Defense World Geodetic System 1984: Its definition and relationship with local geodetic systems. NIMA Technical Report 8350.2, 3rd Edition, **2000**.

Ni-Meister, W.; Jupp, D.L.B.; Dubayah, R. Modeling lidar waveforms in heterogeneous and discrete canopies, IEEE Transactions on Geoscience and Remote Sensing **2001**, 39, 9, 1943–1958.

NovAtel, 2005. SPAN Technology User Manual, Revision 7, **2005**, 111 p.

Paschotta, R.; Encyclopedia of Laser Physics and Technology. URL: http://www.rp-photonics.com/index.html. Accessed: 27.2.2013.

Palojärvi, P. Integrated electronic and optoelectronic circuits and devices for pulsed time-of-flight laser rangefinding. Ph.D. dissertation, University of Oulu, **2003**, 56 p.

Parkinson, B. W.; Spilker, J.J. Jr. Global Positioning System: Theory and Applications, vols. 1 and 2, American Institute of Aeronautics, 370 L'Enfant Promenade, SW, Washington, DC, **1996**.

Persson, Å.; Holmgren, J.; Söderman, U. Detecting and measuring individual trees using an airborne laser scanner, Photogrammetric Engineering & Remote Sensing **2002**, 68, 9, 925–932.

Pesci, A.; Teza, G. Effects of surface irregularities on intensity data from laser scanning: an experimental approach. Annals of Geophysics **2008**, 51, 5/6, 839–848.

Petrie, G. An introduction to technology mobile mapping systems. GeoInformatics **2010**, 13, 32–43.

Petzold, B.; Reiss, P.; Stossel, W. Laser scanning - Surveying and mapping agencies are using a new technique for the derivation of digital terrain models, ISPRS Journal of Photogrammetry and Remote Sensing **1999**, 54, 1, 95–104.

Poutanen, M. GPS-paikanmääritys. in Finnish, Ursan julkaisuja **1999**, 64, 269 p.

Pu, S.; Rutzinger, M.; Vosselman, G.; Oude Elberink, S. Recognizing Basic Structures from Mobile Laser Scanning Data for Road Inventory Studies. ISPRS Journal of Photogrammetry and Remote Sensing **2011**, 66, 28–39.

Puente, I.; González-Jorge, H.; Arias, P.; Armesto. J. Land-based mobile laser scanning systems: a review. In: Lichti, D.D.; Habib, A.F. (Eds.) ISPRS Workshop Laser Scanning, Calgary, Canada, 29–31 August, International Archives of Photogrammetry, Remote Sensing, and Spatial Information Sciences **2011**, 38,-5/W12, 163-168.

Puttonen, E.; Jaakkola, A.; Litkey, P.; Hyyppä, J. Tree Classification with Fused Mobile Laser Scanning and Hyperspectral Data. Sensors **2011**, 11, 5158-5182.

Reulke, R.; Wehr, A. Mobile panoramic mapping using CCD-line camera and laser scanner with integrated position and orientation system. Proceedings of the ISPRS working group V/1, International Archives of Photogrammetry Remote Sensing And Spatial Information Sciences **2004**, 34.

Reutebuch, S.; McGaughey, R.; Andersen, H.-E.; Carson, W. Accuracy of a high resolution LIDAR-based terrain model under a conifer forest canopy, Canadian Journal of Remote Sensing **2003**, 29, 527–535.

Rottensteiner, F. Automatic generation of high-quality building models from lidar data, IEEE Computer Graphics and Applications **2003**, 23, 6, 42–50.

Rottensteiner, F.; Trinder, J.; Clode, S. Data acquisition for 3D city models from lidar - Extracting buildings and roads, Proceedings of the 25th IEEE International Geoscience and Remote Sensing Symposium, Seoul, South Korea, 25–29 July, **2005**, 521–524.

Ruiz-Cortés, V.; Dainty, J. Experimental light-scattering measurements for large-scale composite random rough surfaces. Journal of the Optical Society of America A **2002**, 19, 2043–2052.

Rutzinger, M.; Höfle, B.; Oude Elberink, S.; Vosselman, G. Feasibility of Façade Footprint Extraction from Mobile Laser Scanning Data. Photogrammetrie - Fernerkundung - Geoinformation **2011**a, 97–107.

Rutzinger, M.; Pratihast, A.K.; Oude Elberink, S.J.; Vosselman, G. Tree Modelling from Mobile Laser Scanning Data-Sets. The Photogrammetric Record **2011**b, 26, 361–372.

Rönnholm, P.; Hyyppä, J; Hyyppä, H.; Haggrén, H.; Yu, X.; Kaartinen, H. Calibration of laser-derived tree height estimates by means of photogrammetric techniques. Scandinavian Journal of Forest Research **2004**, 19, 6, 524–528.

Saarinen, N.; Vastaranta, M.; Vaaja, M.; Lotsari, E.; Jaakkola, A.; Kukko, A.; Kaartinen, H.; Holopainen, M.; Hyyppä, H.; Alho, P. Area-Based Approach for Mapping and Monitoring Riverine Vegetation Using Mobile Laser Scanning. Remote Sensing **2013**, 5, 5285-5303.

Sagnac, G. Sur la preuve de la réalité de l'éther lumineux par l'expérience de l'interférographe tournant [On the proof of the reality of the luminiferous aether by the experiment with a rotating interferometer], Comptes Rendus **1913**, 157, 1410–1413.

Schawlow, A; Townes, C. Infrared and Optical Masers. Physical Review **1958**, 112, 6, 1940–1949.

Schenk, T. Modeling and Analyzing Systematic Errors in Airborne Laser Scanners. Department of Civil and Environmental Engineering and Geodetic Science, The Ohio State University, Columbus, Ohio, Technical notes in photogrammetry **2001**, No. 19.

Schreier, H.; Lougheed, J.; Tucker, C.; Leckie, D. Automated measurements of terrain reflection and height variations using airborne infrared laser system. International Journal of Remote Sensing **1985**, 6, 1, 101–113.

Schwarz, K.; Chapman, W.; Cannon, M.; Gong, P. An Integrated INS/GPS Approach to the Georeferencing of Remotely Sensed Data. Photogrammetric Engineering and Remote Sensing **1993**, 59 11, 1667–1674.

Solodukhin, V.; Zhukov, A.; Mazhugin, I.; Bokova, T.; Plezhay, V. Possibilities of laser aerial forest profiles. Leningrad Forest Research Institute, **1978**, 31p.

Sun, G.; Ranson, K. Modeling lidar returns from forest canopies, IEEE Transactions on Geoscience and Remote Sensing **2000**, 38, 6, 2617–2626.

Talaya, J.; Bosch,; Alamús, R.; Bosch, E.; Serra, A.; Baron, A. GEOMÒBIL: The mobile mapping system from the ICC, Proceedings of 4th International Symposium on Mobile Mapping Technology (MMT'2004), Kinming, China, **2004**.

Tao, V. Mobile mapping technology for road network data acquisition. Journal of Geospatial Engineering **2001**, 2, 2, 1–13.

Tao, V.; Chapman, M.; Chaplin, B. Automated processing of mobile mapping image sequences. ISPRS Journal of Photogrammetry and Remote Sensing **2001**, 55, 5–6, 330–346.

Thiel K.-H.; Wehr, A. Performance capabilities of laser scanners—an overview and measurement principle analysis. International Archives of Photogrammetry, Remote Sensing, and Spatial Information Sciences **2004**, 36, 8/W2, 14–18.

Tsoulis, D. GPS/INS integration for direct georeferencing of airborne imaging sensors. International Summer School "Digital Recording and 3D Modeling", Aghios Nikolaos, Crete, Greece, 24-29 April, **2006**.

Vaaja, M.; Kukko, A.; Kaartinen, H.; Kurkela, M.; Kasvi, E.; Flener, C.; Hyyppä, H.; Hyyppä, J.; Alho, P. Evaluation of Data Processing and Quality of Boat-based Mobile Laser Scanning System. Sensors **2013**, 13, 12497-12515.

van Albada, M.; Lagendijk, A. Observation of weak localization of light in a random medium, Physical Review Letters **1985**, 55, 2692–2695.

Videen, G.; Bickel, W.; Iafelice, V.; Abromson, D. Experimental light-scattering Mueller matrix for a fiber on a reflecting optical surface as a function of incident angle. Journal of the Optical Society of America A 1992, 9, 312–315.

Vock, D.M.M.; Jungmichel, M. A low budget mobile laser scanning solution using on board sensors and field bus systems of today's consumer automobiles. In: Lichti, D.D.; Habib, A.F. (Eds.) ISPRS Workshop Laser Scanning, Calgary, Canada, 29–31 August, International Archives of Photogrammetry, Remote Sensing, and Spatial Information Sciences **2011**, 38,-5/W12,

Vosselman, G. Fusion of laser scanning data, maps and aerial photographs for building reconstruction, IEEE International Geoscience and Remote Sensing Symposium and the 24th Canadian Symposium on Remote Sensing, IGARSS'02, Toronto, Canada, June 24–28th, **2002**.

Vosselman, G.; Dijkman, S. 3D building model reconstruction from point clouds and ground plans, International Archives of the Photogrammetry, Remote Sensing and Spatial Information Sciences **2001**, 34, 3/W4, 37–44.

Vosselman, G.; Süveg, I. Map based building reconstruction from laser data and images, Automatic Extraction of Man-Made Objects from Aerial and Space Images (III), Ascona, Switzerland, Balkema Publishers, 11th–15th June, **2001**, 231–239.

Wagner, W.; Hyyppa, J.; Ullrich, A.; Lehner, H.; Briese, C.; Kaasalainen, S. Radiometric calibration of full-waveform small-footprint airborne laser scanners. The International Archives of Photogrammetry, Remote Sensing and Spatial Information Sciences **2008**, 37, B1, 163–168.

Wagner, W.; Ullrich, A.; Melzer, T.; Briese, C.; Kraus, K. From single-pulse to full-waveform airborne laser scanners: potential and practical challenges International Archives of Photogrammetry, Remote Sensing and Spatial Information Sciences **2004**, 35, B3, 201–206.

Wagner, W.; Ullrich, A.; Ducic, V.; Melzer, T.; Studnicka, N. Gaussian decomposition and calibration of a novel smallfootprint full-waveform digitising airborne laser scanner. ISPRS Journal of Photogrammetry and Remote Sensing **2006**, 60, 2, 100–112.

Walchko, K. Low cost inertial navigation: learning to integrate noise and find your way. Master's Thesis, University of Florida,, USA, **2002**, 80 p.

Wang, Y.; Liang, X.; Flener, C.; Kukko, A.; Kaartinen, H.; Kurkela, M.; Vaaja, M.; Hyyppä, H.; Alho, P. 3D Modeling of Coarse Fluvial Sediments Based on Mobile Laser Scanning Data. Remote Sensing **2013**, 5, 9, 4571-4592.

Wehr, A.; Lohr, U. Airborne laser scanning–an introduction and overview. ISPRS Journal of Photogrammetry and Remote Sensing **1999**, 54, 2–3, 68–82.

Wiersma, D.; van Albada, M.; van Tiggelen, B.; Lagendijk, A. Experimental evidence for recurrent multiple scattering events of light in disordered media. Physical Review Letters **1995**, 74, 4193–4196.

Yokoyama, H.; Date, H.; Kanai, S.; Takeda, H. Pole-Like Objects Recognition from Mobile Laser Scanning Data Using Smoothing and Principal Component Analysis. International Archives of Photogrammetry, Remote Sensing, and Spatial Information Sciences **2011**, 38, 5/W12.

Yoo, H.; Goulette, F.; Senpauroca, J.; Lepère, G. Comparative analysis based on simulation for the design of laser terrestrial mobile mapping systems, 6th International Symposium on Mobile Mapping Technology, Sao Paolo, **2009**a.

Yoo, H.; Goulette, F.; Senpauroca, J.; Lepère, G. Simulation based comparative analysis for the design of laser terrestrial mobile mapping systems. Boletim de Ciências Geodésicas **2009**b, 15, 5, 839–854.

Yoo, H.; Goulette, F.; Senpauroca, J.; Lepère, G. Analysis and improvement of laser terrestrial mobile mapping systems configurations. International Archives of Photogrammetry, Remote Sensing, and Spatial Information Sciences **2010**, 38, 633–638.

Yoon, G.; Roy, N.; Straight, R. Coherent backscattering in biological media: measurement and estimation of optical properties. Applied Optics **1993**, 32, 580–585.

Yu, X.; Hyyppä, J.; Kaartinen, H.; Maltamo, M. Automatic detection of harvested trees and determination of forest growth using airborne laser scanner. Remote Sensing of Environment **2004**, 90, 451–462.

Yu, S.; Sukumar, S.; Koschan, A.; Page, D.; Abidi, M. 3D Reconstruction of Road Surfaces Using an Integrated Multi-Sensory Approach. Optics and Lasers in Engineering **2007**, 45, 808–818.

Yu, X.; Hyyppä, J.; Kukko, A.; Maltamo, M.; Kaartinen, H. Change Detection Techniques for Canopy Height Growth Measurements Using Airborne Laser Scanner Data. Photogrammetric Engineering & Remote Sensing **2006**, 72, 12, 1339–1348.

Zhang, K.; Xiao, B. Current status of low-cost GPS and mobile mapping systems. Proceedings of the Malaysia Geoinformation and Surveying conference, Kuching, Malaysia, **2003**, 10 p.

Zhao, H.; Shibasaki, R. A vehicle-borne urban 3-D acquisition system using single-row laser range scanners. IEEE Transactions on Systems, Man and Cybernetics, part B: Cybernetics **2003**a, 33, 4, 658–666.

Zhao, H.; Shibasaki, R. Reconstructing a textured CAD model of an urban environment using vehicle-borne laser range scanners and line cameras. Machine Visions and Applications **2003**b, 14, 1, 35–41.

Zhao, H.; Shibasaki, R. Updating digital geographic database using vehicle-borne laser scanners and line cameras. Photogrammetric Engineering & Remote Sensing **2005**, 71, 4, 415–424.

Zhu, L.; Hyyppä, J.; Kukko, A.; Kaartinen, H.; Chen, R. Photorealistic Building Reconstruction from Mobile Laser Scanning Data. Remote Sensing **2011**, 3, 1406–1426.

Suomen Geodeettisen laitoksen julkaisut:
Veröffentlichungen des Finnischen Geodätischen Institutes:
Publications of the Finnish Geodetic Institute:

1. Y. VÄISÄLÄ: Tafeln für geodätische Berechnungen nach den Erddimensionen von Hayford. Helsinki 1923. 30 S.
2. Y. VÄISÄLÄ: Die Anwendung der Lichtinterferenz zu Längenmessungen auf grösseren Distanzen. Helsinki 1923. 22 S.
3. ILMARI BONSDORFF, Y. LEINBERG, W. HEISKANEN: Die Beobachtungsergebnisse der südfinnischen Triangulation in den Jahren 1920-1923. Helsinki 1924. 235 S.
4. W. HEISKANEN: Untersuchungen über Schwerkraft und Isostasie. Helsinki 1924. 96 S. 1 Karte.
5. W. HEISKANEN: Schwerkraft und isostatische Kompensation in Norwegen. Helsinki 1926. 33 S. 1 Karte.
6. W. HEISKANEN: Die Erddimensionen nach den europäischen Gradmessungen. Helsinki 1926. 26 S.
7. ILMARI BONSDORFF, V.R. ÖLANDER, Y. LEINBERG: Die Beobachtungsergebnisse der südfinnischen Triangulation in den Jahren 1924-1926. Helsinki 1927. 164 S. 1 Karte.
8. V.R. ÖLANDER: Ausgleichung einer Dreieckskette mit Laplaceschen Punkten. Helsinki 1927. 49 S. 1 Karte.
9. U. PESONEN: Relative Bestimmungen der Schwerkraft auf den Dreieckspunkten der südfinnischen Triangulation in den Jahren 1924-1925. Helsinki 1927. 129 S.
10. ILMARI BONSDORFF: Das Theorem von Clairaut und die Massenverteilung im Erdinnern. Helsinki 1929. 10 S.
11. ILMARI BONSDORFF, V.R. ÖLANDER, W. HEISKANEN, U. PESONEN: Die Beobachtungsergebnisse der Triangulationen in den Jahren 1926-1928. Helsinki 1929. 139 S. 1 Karte.
12. W. HEISKANEN: Über die Elliptizität des Erdäquators. Helsinki 1929. 18 S.
13. U. PESONEN: Relative Bestimmungen der Schwerkraft in Finnland in den Jahren 1926-1929. Helsinki 1930. 168 S. 1 Karte.
14. Y. VÄISÄLÄ: Anwendung der Lichtinterferenz bei Basismessungen. Helsinki 1930. 47 S.
15. M. FRANSSILA: Der Einfluss der den Pendel umgebenden Luft auf die Schwingungszeit beim v. Sterneckschen Pendelapparat. Helsinki 1931. 23 S.
16. Y. LEINBERG: Ergebnisse der astronomischen Ortsbestimmungen auf den finnischen Dreieckspunkten. Helsinki 1931. 162 S.
17. V.R. ÖLANDER: Über die Beziehung zwischen Lotabweichungen und Schwereanomalien sowie über das Lotabweichungssystem in Süd-Finnland. Helsinki 1931. 23 S.
18. PENTTI KALAJA, UUNO PESONEN, V.R. ÖLANDER, Y. LEINBERG: Beobachtungsergebnisse. Helsinki 1933. 240 S. 1 Karte.
19. R.A. HIRVONEN: The continental undulations of the geoid. Helsinki 1934. 89 pages. 1 map.
20. ILMARI BONSDORFF: Die Länge der Versuchsbasis von Helsinki und Längenveränderungen der Invardrähte 634-637. Helsinki 1934. 41 S.
21. V.R. ÖLANDER: Zwei Ausgleichungen des grossen südfinnischen Dreieckskranzes. Helsinki 1935. 66 S. 1 Karte.
22. U. PESONEN, V.R. ÖLANDER: Beobachtungsergebnisse. Winkelmessungen in den Jahren 1932-1935. Helsinki 1936. 148 S. 1 Karte.
23. R.A. HIRVONEN: Relative Bestimmungen der Schwerkraft in Finnland in den Jahren 1931, 1933 und 1935. Helsinki 1937. 151 S.
24. R.A. HIRVONEN: Bestimmung des Schwereunterschiedes Helsinki-Potsdam im Jahre 1935 und Katalog der finnischen Schwerestationen. Helsinki 1937. 36 S. 1 Karte.
25. T.J. KUKKAMÄKI: Über die nivellitische Refraktion. Helsinki 1938. 48 S.
26. Finnisches Geodätisches Institut 1918-1938. Helsinki 1939. 126 S. 2 Karten.
27. T.J. KUKKAMÄKI: Formeln und Tabellen zur Berechnung der nivellitischen Refraktion. Helsinki 1939. 18 S.
28. T.J. KUKKAMÄKI: Verbesserung der horizontalen Winkelmessungen wegen der Seitenrefraktion. Helsinki 1939. 18 S.
29. ILMARI BONSDORFF: Ergebnisse der astronomischen Ortsbestimmungen im Jahre 1933. Helsinki 1939. 47 S.
30. T. HONKASALO: Relative Bestimmungen der Schwerkraft in Finnland im Jahre 1937. Helsinki 1941. 78 S.
31. PENTTI KALAJA: Die Grundlinienmessungen des Geodätischen Institutes in den Jahren 1933-1939 nebst Untersuchungen über die Verwendung der Invardrähte. Helsinki 1942. 149 S.

32. U. PESONEN, V.R. ÖLANDER: Beobachtungsergebnisse. Winkelmessungen in den Jahren 1936-1940. Helsinki 1942. 165 S. 1 Karte.
33. PENTTI KALAJA: Astronomische Ortsbestimmungen in den Jahren 1935-1938. Helsinki 1944. 142 S.
34. V.R. ÖLANDER: Astronomische Azimutbestimmungen auf den Dreieckspunkten in den Jahren 1932-1938; Lotabweichungen und Geoidhöhen. Helsinki 1944. 107 S. 1 Karte.
35. U. PESONEN: Beobachtungsergebnisse. Winkelmessungen in den Jahren 1940-1947. Helsinki 1948. 165 S. 1 Karte.
36. Professori Ilmari Bonsdorffille hänen 70-vuotispäivänään omistettu juhlajulkaisu. Publication dedicated to Ilmari Bonsdorff on the occasion of his 70th anniversary. Helsinki 1949. 262 pages. 13 maps.
37. TAUNO HONKASALO: Measuring of the 864 m-long Nummela standard base line with the Väisälä light interference comparator and some investigations into invar wires. Helsinki 1950. 88 pages.
38. V.R. ÖLANDER: On the geoid in the Baltic area and the orientation of the Baltic Ring. Helsinki 1950. 26 pages.
39. W. HEISKANEN: On the world geodetic system. Helsinki 1951. 25 pages.
40. R.A. HIRVONEN: The motions of Moon and Sun at the solar eclipse of 1947 May 20th. Helsinki 1951. 36 pages.
41. PENTTI KALAJA: Catalogue of star pairs for northern latitudes from 55° to 70°for astronomic determination of latitudes by the Horrebow-Talcott method. Helsinki 1952. 191 pages.
42. ERKKI KÄÄRIÄINEN: On the recent uplift of the Earth's crust in Finland. Helsinki 1953. 106 pages. 1 map.
43. PENTTI KALAJA: Astronomische Ortsbestimmungen in den Jahren 1946-1948. Helsinki 1953. 146 S.
44. T.J. KUKKAMÄKI, R.A. HIRVONEN: The Finnish solar eclipse expeditions to the Gold Coast and Brazil 1947. Helsinki 1954. 71 pages.
45. JORMA KORHONEN: Einige Untersuchungen über die Einwirkung der Abrundungsfehler bei Gross-Ausgleichungen. Neu-Ausgleichung des südfinnischen Dreieckskranzes. Helsinki 1954. 138 S. 3 Karten.
46. Professori Weikko A. Heiskaselle hänen 60-vuotispäivänään omistettu juhlajulkaisu. Publication dedicated to Weikko A. Heiskanen on the occasion of his 60th anniversary. Helsinki 1955. 214 pages.
47. Y. VÄISÄLÄ: Bemerkungen zur Methode der Basismessung mit Hilfe der Lichtinterferenz. Helsinki 1955. 12 S.
48. U. PESONEN, TAUNO HONKASALO: Beobachtungsergebnisse der finnischen Triangulationen in den Jahren 1947-1952. Helsinki 1957. 91 S.
49. PENTTI KALAJA: Die Zeiten von Sonnenschein, Dämmerung und Dunkelheit in verschiedenen Breiten. Helsinki 1958. 63 S.
50. V.R. ÖLANDER: Astronomische Azimutbestimmungen auf den Dreieckspunkten in den Jahren 1938-1952. Helsinki 1958. 90 S. 1 Karte.
51. JORMA KORHONEN, V.R. ÖLANDER, ERKKI HYTÖNEN: The results of the base extension nets of the Finnish primary triangulation. Helsinki 1959. 57 pages. 5 appendices. 1 map.
52. V.R. ÖLANDER: Vergleichende Azimutbeobachtungen mit vier Instrumenten. Helsinki 1960. 48 pages.
53. Y. VÄISÄLÄ, L. OTERMA: Anwendung der astronomischen Triangulationsmethode. Helsinki 1960. 18 S.
54. V.R. ÖLANDER: Astronomical azimuth determinations on trigonometrical stations in the years 1955-1959. Helsinki 1961. 15 pages.
55. TAUNO HONKASALO: Gravity survey of Finland in years 1945-1960. Helsinki 1962. 35 pages. 3 maps.
56. ERKKI HYTÖNEN: Beobachtungsergebnisse der finnischen Triangulationen in den Jahren 1953-1962. Helsinki 1963. 59 S.
57. ERKKI KÄÄRIÄINEN: Suomen toisen tarkkavaaituksen kiintopisteluettelo I. Bench mark list I of the Second Levelling of Finland. Helsinki 1963. 164 pages. 2 maps.
58. ERKKI HYTÖNEN: Beobachtungsergebnisse der finnischen Triangulationen in den Jahren 1961-1962. Helsinki 1963. 32 S.
59. AIMO KIVINIEMI: The first order gravity net of Finland. Helsinki 1964. 45 pages.
60. V.R. ÖLANDER: General list of astronomical azimuths observed in 1920-1959 in the primary triangulation net. Helsinki 1965. 47 pages. 1 map.
61. ERKKI KÄÄRIÄINEN: The second levelling of Finland in 1935-1955. Helsinki 1966. 313 pages. 1 map.
62. JORMA KORHONEN: Horizontal angles in the first order triangulation of Finland in 1920-1962. Helsinki 1966. 112 pages. 1 map.
63. ERKKI HYTÖNEN: Measuring of the refraction in the Second Levelling of Finland. Helsinki 1967. 18 pages.

64. JORMA KORHONEN: Coordinates of the stations in the first order triangulation of Finland. Helsinki 1967. 42 pages. 1 map.
65. Geodeettinen laitos - The Finnish Geodetic Institute 1918-1968. Helsinki 1969. 147 pages. 4 maps.
66. JUHANI KAKKURI: Errors in the reduction of photographic plates for the stellar triangulation. Helsinki 1969. 14 pages.
67. PENTTI KALAJA, V.R. ÖLANDER: Astronomical determinations of latitude and longitude in 1949-1958. Helsinki 1970. 242 pages. 1 map.
68. ERKKI KÄÄRIÄINEN: Astronomical determinations of latitude and longitude in 1954-1960. Helsinki 1970. 95 pages. 1 map.
69. AIMO KIVINIEMI: Niinisalo calibration base line. Helsinki 1970. 36 pages. 1 sketch appendix.
70. TEUVO PARM: Zero-corrections for tellurometers of the Finnish Geodetic Institute. Helsinki 1970. 18 pages.
71. ERKKI KÄÄRIÄINEN: Astronomical determinations of latitude and longitude in 1961-1966. Helsinki 1971. 102 pages. 1 map.
72. JUHANI KAKKURI: Plate reduction for the stellar triangulation. Helsinki 1971. 38 pages.
73. V.R. ÖLANDER: Reduction of astronomical latitudes and longitudes 1922-1948 into FK4 and CIO systems. Helsinki 1972. 40 pages.
74. JUHANI KAKKURI AND KALEVI KALLIOMÄKI: Photoelectric time micrometer. Helsinki 1972. 53 pages.
75. ERKKI HYTÖNEN: Absolute gravity measurement with long wire pendulum. Helsinki 1972. 142 pages.
76. JUHANI KAKKURI: Stellar triangulation with balloon-borne beacons. Helsinki 1973. 48 pages.
77. JUSSI KÄÄRIÄINEN: Beobachtungsergebnisse der finnischen Winkelmessungen in den Jahren 1969-70. Helsinki 1974. 40 S.
78. AIMO KIVINIEMI: High precision measurements for studying the secular variation in gravity in Finland. Helsinki 1974. 64 pages.
79. TEUVO PARM: High precision traverse of Finland. Helsinki 1976. 64 pages.
80. R.A. HIRVONEN: Precise computation of the precession. Helsinki 1976. 25 pages.
81. MATTI OLLIKAINEN: Astronomical determinations of latitude and longitude in 1972-1975. Helsinki 1977. 90 pages. 1 map.
82. JUHANI KAKKURI AND JUSSI KÄÄRIÄINEN: The Second Levelling of Finland for the Aland archipelago. Helsinki 1977. 55 pages.
83. MIKKO TAKALO: Suomen Toisen tarkkavaaituksen kiintopisteluettelo II. Bench mark list II of the Second Levelling of Finland. Helsinki 1977. 150 sivua.
84. MATTI OLLIKAINEN: Astronomical azimuth determinations on triangulation stations in 1962-1970. Helsinki 1977. 47 pages. 1 map.
85. MARKKU HEIKKINEN: On the tide-generating forces. Helsinki 1978. 150 pages.
86. PEKKA LEHMUSKOSKI AND JAAKKO MÄKINEN: Gravity measurements on the ice of Bothnian Bay. Helsinki 1978. 27 pages.
87. T.J. KUKKAMÄKI: Väisälä interference comparator. Helsinki 1978. 49 pages.
88. JUSSI KÄÄRIÄINEN: Observing the Earth Tides with a long water-tube tiltmeter. Helsinki 1979. 74 pages.
89. Publication dedicated to T.J. Kukkamäki on the occasion of his 70th anniversary. Helsinki 1979. 184 pages.
90. B. DUCARME AND J. KÄÄRIÄINEN: The Finnish Tidal Gravity Registrations in Fennoscandia. Helsinki 1980. 43 pages.
91. AIMO KIVINIEMI: Gravity measurements in 1961-1978 and the results of the gravity survey of Finland in 1945-1978. Helsinki 1980. 18 pages. 3 maps.
92. LIISI OTERMA: Programme de latitude du tube zénithal visuel de l'observatoire Turku-Tuorla systéme amélioré de 1976. Helsinki 1981. 18 pages.
93. JUHANI KAKKURI, AIMO KIVINIEMI AND RAIMO KONTTINEN: Contributions from the Finnish Geodetic Institute to the Tectonic Plate Motion Studies in the Area between the Pamirs and Tien-Shan Mountains. Helsinki 1981. 34 pages.
94. JUSSI KÄÄRIÄINEN: Measurement of the Ekeberg baseline with invar wires. Helsinki 1981. 17 pages.
95. MATTI OLLIKAINEN: Astronomical determinations of latitude and longitude in 1976-1980. Helsinki 1982. 90 pages. 1 map.
96. RAIMO KONTTINEN: Observation results. Angle measurements in 1977-1978. Helsinki 1982. 29 pages.
97. G.P. ARNAUTOV, YE N. KALISH, A. KIVINIEMI, YU F. STUS, V.G. TARASIUK, S.N. SCHEGLOV: Determination of absolute gravity values in Finland using laser ballistic gravimeter. Helsinki 1982. 18 pages.

98. LEENA MIKKOLA (EDITOR): Mean height map of Finland. Helsinki 1983. 3 pages. 1 map.
99. MIKKO TAKALO AND JAAKKO MÄKINEN: The Second Levelling of Finland for Lapland. Helsinki 1983. 144 pages.
100. JUSSI KÄÄRIÄINEN: Baseline Measurements with invar wires in Finland 1958-1970. Helsinki 1984. 78 pages.
101. RAIMO KONTTINEN: Plate motion studies in Central Asia. Helsinki 1985. 31 pages.
102. RAIMO KONTTINEN: Observation results. Angle measurements in 1979-1983. Helsinki 1985. 30 pages.
103. J. KAKKURI, T.J. KUKKAMÄKI, J.-J. LEVALLOIS ET H. MORITZ: Le 250^{e} anniversaire de la mesure de l'arc du meridien en Laponie. Helsinki 1986. 60 pages.
104. G. ASCH, T. JAHR, G. JENTZSCH, A. KIVINIEMI AND J. KÄÄRIÄINEN: Measurements of Gravity Tides along the "Blue Road Geotraverse" in Fennoscandia. Helsinki 1987. 57 pages.
105. JUSSI KÄÄRIÄINEN, RAIMO KONTTINEN, LU QIANKUN AND DU ZONG YU: The Chang Yang Standard Baseline. Helsinki 1986. 36 pages.
106. E.W. GRAFAREND, H. KREMERS, J. KAKKURI AND M. VERMEER: Adjusting the SW Finland Triangular Network with the TAGNET 3-D operational geodesy software. Helsinki 1987. 60 pages.
107. MATTI OLLIKAINEN: Astronomical determinations of latitude and longitude in 1981-1983. Helsinki 1988. 37 pages.
108. MARKKU POUTANEN: Observation results. Angle measurements in 1967-1973. Helsinki 1988. 35 pages.
109. JUSSI KÄÄRIÄINEN, RAIMO KONTTINEN AND ZSUZSANNA NÉMETH: The Gödöllö Standard Baseline. Helsinki 1988. 66 pages.
110. JUSSI KÄÄRIÄINEN AND HANNU RUOTSALAINEN: Tilt measurements in the underground laboratory Lohja 2, Finland, in 1977-1987. Helsinki 1989. 37 pages.
111. MIKKO TAKALO: Lisäyksiä ja korjauksia Suomen tarkkavaaitusten linjastoon 1977-1989. Helsinki 1991. 98 sivua.
112. RAIMO KONTTINEN: Observation results. Angle measurements in the Pudasjärvi loop in 1973-1976. Helsinki 1991. 42 pages.
113. RAIMO KONTTINEN, JORMA JOKELA AND LI QUAN: The remeasurement of the Chang Yang Standard Baseline. Helsinki 1991. 40 pages.
114. JUSSI KÄÄRIÄINEN, RAIMO KONTTINEN AND MARKKU POUTANEN: Interference measurements of the Nummela Standard Baseline in 1977, 1983, 1984 and 1991. Helsinki 1992. 78 pages.
115. JUHANI KAKKURI (EDITOR): Geodesy and geophysics. Helsinki 1993. 200 pages.
116. JAAKKO MÄKINEN, HEIKKI VIRTANEN, QIU QI-XIAN AND GU LIANG-RONG: The Sino-Finnish absolute gravity campaign in 1990. Helsinki 1993. 49 pages.
117. RAIMO KONTTINEN: Observation results. Geodimeter observations in 1971-72, 1974-80 and 1984-85. Helsinki 1994. 58 pages.
118. RAIMO KONTTINEN: Observation results. Angle measurements in 1964-65, 1971, 1984 and 1986-87. Helsinki 1994. 67 pages.
119. JORMA JOKELA: The 1993 adjustment of the Finnish First-Order Terrestrial Triangulation. Helsinki 1994. 137 pages.
120. MARKKU POUTANEN (EDITOR): Interference measurements of the Taoyuan Standard Baseline. Helsinki 1995. 35 pages.
121. JORMA JOKELA: Interference measurements of the Chang Yang Standard Baseline in 1994. Kirkkonummi 1996. 32 pages.
122. OLLI JAAKKOLA: Quality and automatic generalization of land cover data. Kirkkonummi 1996. 39 pages.
123. MATTI OLLIKAINEN: Determination of orthometric heights using GPS levelling. Kirkkonummi 1997. 143 pages.
124. TIINA KILPELÄINEN: Multiple Representation and Generalization of Geo-Databases for Topographic Maps. Kirkkonummi 1997. 229 pages.
125. JUSSI KÄÄRIÄINEN AND JAAKKO MÄKINEN: The 1979-1996 gravity survey and the results of the gravity survey of Finland 1945-1996. Kirkkonummi 1997. 24 pages. 1 map.
126. ZHITONG WANG: Geoid and crustal structure in Fennoscandia. Kirkkonummi 1998. 118 pages.
127. JORMA JOKELA AND MARKKU POUTANEN: The Väisälä baselines in Finland. Kirkkonummi 1998. 61 pages.
128. MARKKU POUTANEN: Sea surface topography and vertical datums using space geodetic techniques. Kirkkonummi 2000. 158 pages

129. MATTI OLLIKAINEN, HANNU KOIVULA AND MARKKU POUTANEN: The Densification of the EUREF Network in Finland. Kirkkonummi 2000. 61 pages.
130. JORMA JOKELA, MARKKU POUTANEN, ZHAO JINGZHAN, PEI WEILI, HU ZHENYUAN AND ZHANG SHENGSHU: The Chengdu Standard Baseline. Kirkkonummi 2000. 46 pages.
131. JORMA JOKELA, MARKKU POUTANEN, ZSUZSANNA NÉMETH AND GÁBOR VIRÁG: Remeasurement of the Gödöllö Standard Baseline. Kirkkonummi 2001. 37 pages.
132. ANDRES RÜDJA: Geodetic Datums, Reference Systems and Geodetic Networks in Estonia. Kirkkonummi 2004. 311 pages.
133. HEIKKI VIRTANEN: Studies of Earth Dynamics with the Superconducting Gravimeter. Kirkkonummi 2006. 130 pages.
134. JUHA OKSANEN: Digital elevation model error in terrain analysis. Kirkkonummi 2006. 142 pages. 2 maps.
135. MATTI OLLIKAINEN: The EUVN-DA GPS campaign in Finland. Kirkkonummi 2006. 42 pages.
136. ANNU-MAARIA NIVALA: Usability perspectives for the design of interactive maps. Kirkkonummi 2007. 157 pages.
137. XIAOWEI YU: Methods and techniques for forest change detection and growth estimation using airborne laser scanning data. Kirkkonummi 2007. 132 pages.
138. LASSI LEHTO: Real-time content transformations in a WEB service-based delivery architecture for geographic information. Kirkkonummi 2007. 150 pages.
139. PEKKA LEHMUSKOSKI, VEIKKO SAARANEN, MIKKO TAKALO AND PAAVO ROUHIAINEN: Suomen Kolmannen tarkkavaaituksen kiintopisteluettelo. Bench Mark List of the Third Levelling of Finland. Kirkkonummi 2008. 220 pages.
140. EIJA HONKAVAARA: Calibrating digital photogrammetric airborne imaging systems using a test field. Kirkkonummi 2008. 139 pages.
141. MARKKU POUTANEN, EERO AHOKAS, YUWEI CHEN, JUHA OKSANEN, MARITA PORTIN, SARI RUUHELA, HELI SUURMÄKI (EDITORS): Geodeettinen laitos – Geodetiska Institutet – Finnish Geodetic Institute 1918–2008. Kirkkonummi 2008. 173 pages.
142. MIKA KARJALAINEN: Multidimensional SAR Satellite Images – a Mapping Perspective. Kirkkonummi 2010. 132 pages.
143. MAARIA NORDMAN: Improving GPS time series for geodynamic studies. Kirkkonummi 2010. 116 pages.
144. JORMA JOKELA AND PASI HÄKLI: Interference measurements of the Nummela Standard Baseline in 2005 and 2007. Kirkkonummi 2010. 85 pages.
145. EETU PUTTONEN: Tree Species Classification with Multiple Source Remote Sensing Data. Kirkkonummi 2012. 162 pages.
146. JUHA SUOMALAINEN: Empirical Studies on Multiangular, Hyperspectral, and Polarimetric Reflectance of Natural Surfaces. Kirkkonummi 2012. 144 pages.
147. LEENA MATIKAINEN: Object-based interpretation methods for mapping built-up areas. Kirkkonummi 2012. 210 pages.
148. LAURI MARKELIN: Radiometric calibration, validation and correction of multispectral photogrammetric imagery. Kirkkonummi 2013. 160 pages.
149. XINLIAN LIANG: Feasibility of Terrestrial Laser Scanning for Plotwise Forest Inventories. Kirkkonummi 2013. 150 pages.
150. EERO AHOKAS: Aspects of accuracy, scanning angle optimization, and intensity calibration related to nationwide laser scanning. Kirkkonummi 2013. 124 pages.
151. LAURA RUOTSALAINEN: Vision-Aided Pedestrian Navigation for Challenging GNSS Environments. Kirkkonummi 2013. 180 pages.
152. HARRI KAARTINEN: Benchmarking of airborne laser scanning based feature extraction methods and mobile laser scanning system performance based on high-quality test fields. Kirkkonummi 2013. 346 pages.
153. ANTERO KUKKO: Mobile Laser Scanning – System development, performance and applications. Kirkkonummi 2013. 247 pages.

Finnish Geodetic Institute
P.O. Box 15
FI-02431 Masala
Finland
http://www.fgi.fi